Identification of Inverted Formin 1 (FHDC1)-interacting proteins by BioID proximity-dependent labeling.

Andrea McRae

This thesis is submitted as a partial fulfillment of the M.Sc. program in Cellular and Molecular Medicine

February 2016

Department of Cellular and Molecular Medicine
Faculty of Medicine
University of Ottawa
Ottawa, Ontario
Canada

Abstract

The actin and microtubule cytoskeleton play critical roles in Golgi and cilia assembly. Inverted-Formin 1 (INF1) is a novel, microtubule-associated protein that regulates both actin and microtubule dynamics and affects Golgi and cilia assembly. A non-biased discovery based approach was used to investigate the interactome of INF1 using BioID in combination with stable isotopic labeling in cell culture (SILAC). A number of INF1-interacting proteins were identified and validated in co-IP experiments. The INF1 interaction domains were mapped using an extensive set of INF1 deletion and point mutation derivatives. Functional characterization of these interactions suggests a mechanism for the effects of INF1 on ciliogenesis.

The establishment and maintenance of cellular architecture requires the coordinated, dynamic regulation of actin and microtubule networks. Our data suggests that INF1 plays a crucial role in connecting these two cytoskeletal networks for the regulated assembly of the Golgi ribbon and the primary cilium.

Table of Contents

List of Tables

CHAPTER 2: MATERIALS AND METHODS

CHAPTER 3: RESULTS

List of Figures

CHAPTER 1: INTRODUCTION

CHAPTER 3: RESULTS

CHAPTER 4: DISCUSSION

List of Abbreviations

ADP……Adenosine diphosphate
AP……Affinity purification
AP/MS……Affinity purification/Mass spectrometry
ATP……Adenosine Triphosphate
ARF……ADP-ribosylation factor
ARL……ADP-ribosylation factor-related
ARP 2/3……Actin Related Proteins 2 and 3
BBS……Bardet-Biedl syndrome
BioAMP……ATP bound biotin
BioID……Biotin-ligase identification
BirA……Biotin-ligase
C2CD……C2 calcium-dependent domain containing
Cby……Chibby
Cc2d……Coiled-coil and C2 domain containing
CEP……Centrosome associated protein
CETN……Centrin
CP……Centrosomal protein
CPs……Capping proteins
CV……Ciliary vesicle
DA……Distal appendage
DAAM……Disheveled-associated activators of morphogenesis
DAD……Diaphanous autoinhibitory domain
DAPI……4‟,6-diamidino-2-phenylindole
DAV……Distal appendage vesicle
DBS……Donor bovine serum
DC……Daughter centriole
Dia……Diaphanous
DMEM……Dulbecco's modified eagle medium
DID……Diaphanous inhibitory domain
DZIP……DAZ interacting zinc finger protein
EB……End-binding protein
EHD……EH-domain containing
ENA……Enabled protein
ER……Endoplasmic reticulum
F-Actin……Filamentous actin
FBF……Fas binding factor
FBS……Fetal bovine serum
FH……Formin homology
FHOD……Formin homology domain-containing protein
FL……Full length
FMN……Formin
FRL……Formin related gene in leukocytes

G-Actin……Globular actin
GAP……GTPase-activation protein
GBD……GTPase binding domain
GDMT……Golgi-derived microtubules
GDP……Guanosine diphosphate
GEF……Guanine nucleotide exchange factor
GFP……Green fluorescent protein
GTP……Guanosine triphosphate
HDAC……Histone deacetylase
HEF……Human enhancer of filamentation
IFM……Immunofluorescence microscopy
IFT……Intraflagellar transport
INF……Inverted formin
IP……Immunoprecipitation
Kif……Kinesin family member
MAPs……Microtubule associated proteins
MC……Mother centriole
MT……Microtubules
MTBD……Microtubule binding domain
MTOC……Microtubule organizing center
MW……Molecular weight
ODF……Outer dense fiber
PBS……Phosphate buffer saline
PEI……Polethylenimine
PFN……Profilin
PIC……Protease inhibitor cocktail
PKD……Polycystic kidney disease
PLK……Polo-like kinase
POI……Protein of interest
PTM……Post-translational modifications
SAG……Smoothened agonist
SCLT……Sodium channel and clathrin linker
SDA……Sub-distal appendages
SILAC……Stable isotopic labeling of amino acids in cell culture
SmiFH2……Small molecule inhibitor of FH2 domain
SNAP……Synatosomal protein
SNARE……Soluble NSF attachment protein
TGN……*Trans*-Golgi network
TTBK……Tau tubulin kinase
TZ……Transition zone
VASP……Vasodilator-stimulated phosphoprotein

Acknowledgments

I am thankful for the continuous support, advice, and motivation from my thesis supervisor, Dr. John Copeland. I am grateful for the opportunity to work with a novel formin and exciting new protein labeling technique. Dr. Copeland's enthusiasm and scientific knowledge helped nurture my passion for cellular biology. I am grateful to Sarah Copeland and the INF1 team for their patience, expertise, and willingness to share valuable insight. The guidance and technical support of Dr. Laura Trinkle-Mulcahy was invaluable to accomplishing the BioID screen essential to my thesis. I appreciate the encouragement and advice from my committee member Dr. Steve Gee who helped me persevere through the challenges of experimental research. I am grateful to Christine Péladeau and Tara Crawford whose passion and insight maintained my sensibility and motivation. I owe many thanks to Virja Mehta and Jennifer Law of the Trinkle-Mulcahy lab for their scientific knowledge and fresh perspectives with each new experiment.

To my parents I am forever grateful for their support and encouragement to pursue a graduate degree in the sciences, an opportunity I would not have afforded or grown from otherwise. I am grateful to my brothers for their humor in times of frustration and for helping me balance hard work with healthy living.

Chapter 1: Introduction

1.1 The Cytoskeleton

The cytoskeleton is composed of intracellular filaments required for cell morphology, division, migration and intracellular transport (Chesarone et al., 2010). The cytoskeletal networks include intermediate filaments, microfilaments (actin filaments), and microtubules. Intermediate filaments stiffen under physical stress and are necessary for the mechanical strength of the cell (Goldman et al., 2008; Lowery et al., 2015). Intermediate filaments are cell- and tissue-type specific, but are generally grouped as keratins, vimentin and desmin, neurofilament proteins, and lamins (Fuchs and Weber, 1994).

Cell polarity, motility, and subcellular organization require close coordination of the actin and microtubule networks. To ensure that the two networks act in tandem an essential cross talk exists. This cross talk enables dynamic microtubules to regulate actin dynamics through modulation of Rho family GTPase activity, while actin stress fibers serve as tracks to guide dynamic microtubules to receptors at the cell cortex to facilitate microtubule stabilization (Nagae et al., 2013; Palazzo et al., 2001).

Actin filaments are ubiquitous among eukaryotic cells and are involved in regulating cell shape and cell migration. Actin filaments are generated from the polymerization of monomeric globular actin (G-actin). Actin nucleation occurs when G-actin dimers and trimers form a stable tetramer that initiates polymerization (Chesarone et al., 2010). The transient formation of G-actin dimers and trimers limits spontaneous nucleation and this barrier is overcome by nucleating factors such as the Arp2/3

complex, spire proteins, and formins. Upon nucleation, the actin filament elongates through preferential addition of ATP-bound G-actin to the fast growing 'barbed end' of the filament. Spontaneous hydrolysis of ATP results in destabilization and disassembly of the filament removing G-actin subunits from the slow growing 'pointed end'. Elongation may also be inhibited by association of capping proteins with the barbed end of the filament (Goley and Welch, 2006).

Microtubules are found throughout the cytoplasm and are involved in processes including intracellular transport, extracellular sensing, organelle positioning, as well as cell division and migration. Microtubules are composed of cylindrical polymers of tubulin formed by polymerization of soluble α-and-β-tubulin dimers in the presence of GTP arranged in a polarized head-to-tail orientation (Howard and Hyman, 2009). Standard MTs are arranged in a singlet ring composed of 13 protofilaments. Cilia are higher order structures comprised of doublet microtubules that contain a set of ten protofilaments adjacent to the singlet ring. The axoneme of primary cilia are made of nine outer doublet MTs while the centrioles at the base of the cilia have an additional set of ten protofilaments linked to the doublet, generating a triplet (Satir and Christensen, 2007). Post-translational modifications including acetylation, glutamylation, detyrosination, glycylation, and phosphorylation are required to form these and other complex MT structures (Hammond et al., 2008). Microtubule organizing centres (MTOCs), including the centrosome and the Golgi, nucleate and anchor growing MTs (Luders and Stearns, 2007; Wade and Hyman, 1997).

1.2 Formin Homology Proteins

Formin family proteins are a set of highly conserved cytoskeletal remodeling proteins that regulate both the actin and microtubule networks required for cell morphology, adhesion, division, polarity, and migration (Chesarone et al., 2010; Goode and Eck, 2007; Higgs, 2005; Thurston et al., 2012). Formins are defined by the formin homology domains 1 and 2 (FH1 and FH2). The FH1 and FH2 domains are located in the C-terminal of all formins except Inverted Formin 1 (INF1). The proline-rich FH1 domain contains a binding site for the G-actin binding protein, profilin (Chesarone et al., 2010). As profilin-bound actin monomers accumulate at the FH1 domain, the neighbouring FH2 domain nucleates and elongates unbranched actin filaments (Sagot et al., 2002). The current model of formin induced actin nucleation and elongation is dependent on FH2 dimerization with each half of the dimer binding one actin subunit (Figure 1.1). A new actin monomer is accepted when half of the dimer shifts to open its conformation while the other half binds to the most recently added actin subunit. The 'stair stepping' model continues to elongate the actin filament (Moseley et al., 2004). The ability of the FH2 dimer to remain associated with the growing barbed end of the actin filament while inserting G-actin protects the filament from heterodimeric capping proteins (CPs) that inhibit elongation (Cooper and Sept, 2008; Harris et al., 2004; Kovar et al., 2006; Pruyne et al., 2002; Schirenbeck et al., 2005; Zigmond et al., 2003).

The FH2 domain of some formins also regulate microtubule dynamics placing formins as cytoskeletal bridging factors that connect the actin cytoskeleton and microtubule network (Bartolini and Gundersen, 2010). The FH2 domain binds and

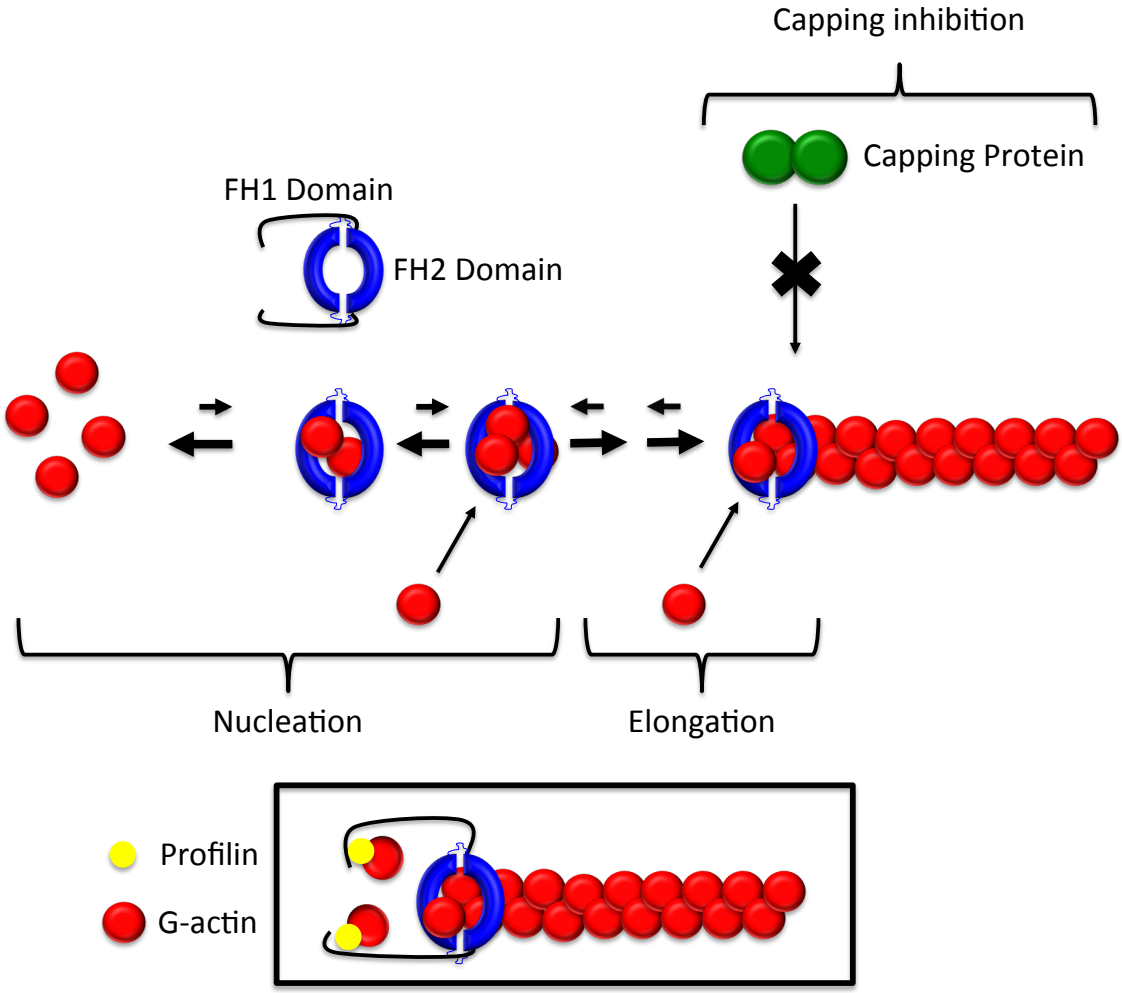

Adapted from Goode and Eck, Ann. Rev. Biochem, 2007

Figure 1.1. Formin induced actin nucleation and polymerization
The dimeric FH2 domains of formins function to 1) accelerate nucleation; 2) modulate elongation; and 3) inhibit barbed end capping by other proteins. The FH1 domain of formins has a high affinity for profilin bound actin monomers. Upon recruitment of profilin-actin monomers to the FH1 domain, the FH2 domain dimer participates in a "stair stepping" model to nucleate and elongate unbranched actin filaments.

stabilizes microtubules as detected by induction of microtubule post-translational modifications, acetylation and detyrosination. Microtubule acetylation and stabilization are induced by expression of isolated FH1 and FH2 functional domains of the majority of mammalian formins (Thurston et al., 2012).

There are fifteen mammalian formins that are divided into seven sub-families based on their regulatory domains: Diaphanous (Dia), formin-related proteins in leucocytes (FRL), disheveled-associated activators of morphogenesis (Daam), inverted formin (INF), formin homology domain-containing protein (FHOD), formin (FMN), and Delphilin (Figure 1.2). Within each sub-family a handful of genes encoding numerous splice variants may be present (Higgs, 2005). Many of the formins contain regions of homology, aside from the FH1 and FH2 domains, that regulate auto-inhibition. These domains include a C-terminal Diaphanous auto-regulatory domain (DAD) as well as an N-terminal GTP-binding domain (GBD), Diaphanous-inhibitory domain (DID), and a dimerization domain. The DAD can mediate auto-inhibition of FH2 domain activity via interaction with the N-terminal domains. Rho proteins are key regulators of numerous formin family members by binding to the GBD relieving DAD auto-inhibition permitting binding of formins to the barbed end of actin filaments (Higgs and Peterson, 2005).

1.3 INF1

Inverted Formin 1 (INF1) is a microtubule-associated formin family member. INF1 has a unique domain structure amongst the 15 mammalian formin proteins. INF1 contains N-terminal FH1 and FH2 domains followed by three domains of unknown

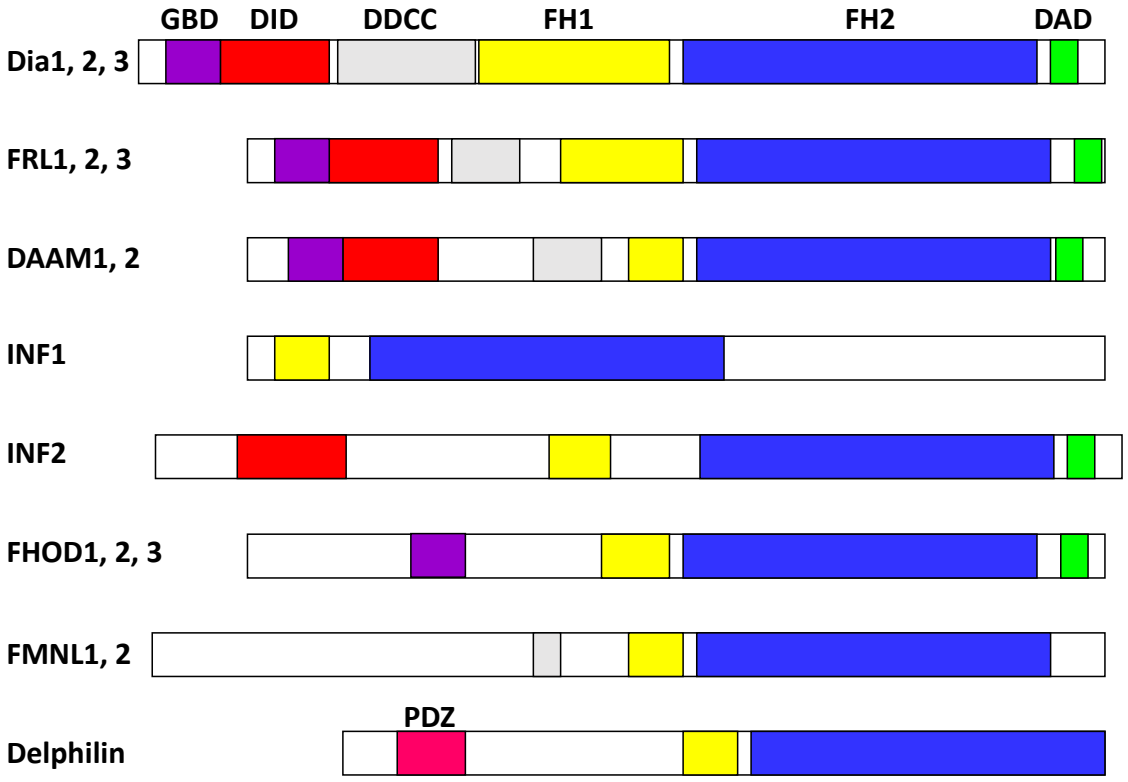

Figure 1.2. The mammalian formin domain structures.
Mammalian formins are distinguished by their FH1/FH2 domains and are divided into seven sub-families. The Dia, FRL, and DAAM sub-families are regulated by auto-inhibition via interaction between the DID and DAD as well as activation by Rho GTPase binding to the GBD. INF2 only contains the DID and DAD, while the FHOD sub-family is regulated by the GBD and DAD. The FMNL2 sub-family contains a DDCC domain while Delphilin contains a PDZ domain, and INF1 lacks auto-regulatory domains. DID, Diaphanous inhibitory domain; DAD, Diaphanous auto-regulatory domain; GBD, GTPase binding domain; DDCC, Dimerization domain-Coiled coil domain

function and a MT binding domain (MTBD) in the C-terminal. INF1 lacks the DID and DAD regulatory domains associated with formins and, unlike other formin family members, INF1 is not regulated by auto-inhibition (Young et al., 2008). INF1 regulates actin dynamics through its FH1/FH2 domains and is able to bind and stabilize MTs through its MTBD. The FH2 domain of INF1 is also involved in the stabilization of MTs (Figure 1.3) (Thurston et al., 2012). Throughout the cell there are two populations of microtubules: dynamic and stable. Stabilized MTs are marked by post-translational modifications including acetylation, polyglutamination, and detyrosination. INF1 over-expression increases cytoplasmic MT stabilization and tubulin acetylation, but not detyrosination, while endogenous INF1 is associated with the MT network (Young et al., 2008).

1.4 INF1 and Golgi

The Golgi consists of *cis*, *medial*, and *trans* cisternae (Papanikou and Glick, 2014). In mammalian cells the cisternae are tethered together generating a perinuclear ribbon that is required to establish cell polarity and normal subcellular organization (Yadav et al., 2009). Polarized cellular trafficking and normal cell motility require proper positioning and maintenance of the Golgi, an actin and MT-dependent process (Gurel et al., 2014). Perinuclear Golgi assembly is reliant on two cytoplasmic MT networks, one originating at the centrosome, and the other originating at the Golgi itself (Miller et al., 2009).

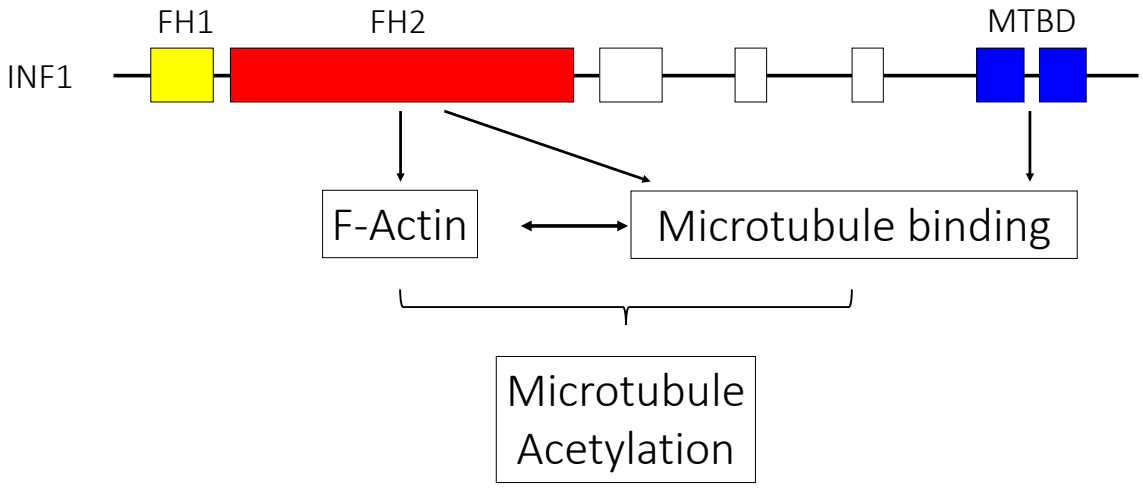

Figure 1.3. The functional domains of INF1.
INF1 is characterized by the C-terminal MTBD and N-terminal FH1, and FH2 domains. The FH1 and FH2 domains function as the actin regulatory motif, binding and polymerizing actin filaments. Microtubule stability is induced by the MTBD, and FH2 domain of INF1.

Endogenous INF1 preferentially associates with the Golgi-derived MT (GDMT) network to regulate the formation of the Golgi ribbon. Knockdown of INF1 expression results in defective Golgi assembly suggesting a role for INF1 in the function of the GDMT network. INF1 over-expression also results in defective Golgi assembly causing dispersal of the Golgi ribbon into functional mini stacks distributed throughout the cytoplasm. Over-expression of INF1 derivatives lacking either FH2 activity or the MTBD do not induce Golgi ribbon dispersal. These results suggest that INF1 coordination of actin and microtubule dynamics is required for normal perinuclear Golgi ribbon formation (Copeland et al., 2015).

1.5 INF1 and Cilia

Recent data from our laboratory suggests that formin activity is required for cilia assembly in mammalian cells. When quiescent NIH 3T3 fibroblasts are treated with a small molecule formin inhibitor, smiFH2, nearly all treated cells lose their cilia. The smiFH2 treatment targets the FH2 domain inhibiting formin activity suggesting that the FH2 domain of formins is essential for cilia assembly and maintenance (Copeland et al., manuscript in prep). Amongst the mammalian formin family, INF1 expression has a unique and dramatic effect on cilia assembly. In the majority (~75%) of quiescent NIH 3T3 cells over-expressing INF1, ciliogenesis is inhibited. In the small percentage of cells that do form cilia, however, the cilia are massively elongated. Epitope-tagged INF1 is clearly present in the cilia. The average cilia length is approximately 3μm in control cells. In contrast, in INF1 over-expressing cells the cilia have an average length of 15μm, with

a broad range of size, often exceeding 40µm. INF1-induced Golgi dispersion does not correlate with inhibition of cilia assembly as INF1 over-expressing cells with visibly dispersed Golgi still assemble elongated cilia (Copeland et al., manuscript in prep).

As with its effects on Golgi assembly, the effects of INF1 over-expression on cilia assembly are FH2-, and MTBD-dependent. Over-expression of a full-length INF1 derivative with an inactivating point mutation in the FH2 domain (FL INF1 I180A) had no significant effect on the percentage of cells forming cilia. The cilia that formed, in this case, were elongated, with an average length of 4.9µm, and a narrower distribution of size. Interestingly, the expression of the C-terminal derivative INF1 486C that contains the MTBD had similar effects on cilia number and length as expression of FL INF1 I180A. These results highlight that the effects of INF1 expression on cilia number and length are dependent on the MTBD and the FH2 domain. When INF1 over-expressing cells are treated with the actin-binding drug, Latrunculin B, the effects of INF1 on cilia elongation are reduced and the cilia shorten to the size of those observed in cells expressing FL INF1 I180A. These results suggest that INF1 inhibits disassembly in an F-actin/FH2-dependent manner (Copeland et al., manuscript in prep).

A balance between assembly and disassembly rates determines cilia length and disassembly of cilia can be induced in quiescent cells upon serum stimulation. INF1 expressing serum-stimulated cells showed inhibited cilia disassembly, and increased the length of the cilia. The over-expression of INF1 blocks serum-induced disassembly of the cilia suggesting that the INF1-induced elongated cilia result from inhibition of disassembly (Copeland et al., manuscript in prep).

1.6 The Primary Cilium

The primary cilium is an evolutionarily conserved non-motile structure that acts as the cell's antenna. This organelle is enriched with sensory receptors and signal transduction complexes that capture and relay extracellular and intracellular signals (Garcia-Gonzalo and Reiter, 2012). The primary cilia participates in mechanosensation, photoreception, and intracellular signaling required for tissue homeostasis, cell proliferation, and embryogenesis (Ishikawa and Marshall, 2011). Primary cilia are found on most mammalian cells and play an especially crucial role in the function of the epithelium of the kidney-collecting duct, in rod photoreceptors, olfactory receptors, as well as for the function of the sonic hedgehog and Wnt signaling pathways. In the kidney-collecting duct primary cilia detect fluid flow in the ducts and tubules as well as regulate cell division (Fliegauf et al., 2007; Pazour and Rosenbaum, 2002). In the retina, the membrane-associated sensory molecules in the cilia-modified outer segments of the rod photoreceptor cells detect light (Wheway et al., 2014). Olfactory cilia detect environmental chemicals sending signals to the brain for processing into sense and smell. Sonic hedgehog and Wnt signaling pathways regulate embryonic development through transduction of ciliary signals (Jenkins et al., 2009; Jones et al., 2008; Rohatgi et al., 2007).

1.7 Ciliopathies

Given the widespread distribution of cilia on virtually all cell-types throughout the human body, defective cilia affect the function and development of multiple tissues

resulting in a variety of syndromes collectively termed Ciliopathies. These include polycystic kidney disease (PKD), retinitis pigmentosa, Bardet-Biedl syndrome (BBS), Joubert syndrome, and Meckel syndrome, amongst others. Common clinical symptoms of Ciliopathies include obesity, blindness, cystic kidneys, as well as developmental defects such as polydactyly, and situs inversus (Nigg and Raff, 2009). Blindness is caused by retinitis pigmentosa resulting from photoreceptor cell degeneration that occurs when protein transport in the cilia is perturbed initiating apoptosis and eliminating defective cells from the retina (Crouse et al., 2014). Cystic kidneys result from an inability to assemble a cilia or defective ciliary signaling. This is due to mutations in either Polycystin-1 or Polycystin-2 that form a receptor-channel complex on the ciliary membrane crucial to kidney epithelial cell differentiation and proliferation (Fliegauf et al., 2007). Developmental defects often result from disrupted sonic hedgehog and Wnt signaling at the ciliary membrane, as well as protein transport within the cilia (Goetz and Anderson, 2010).

1.8 Cell Cycle Dependent Regulation of Ciliogenesis

Cilia assembly and disassembly are synchronized with the cell cycle. Cilia are not present in newly divided cells. During early G1 and G0 the mother centriole docks to the plasma membrane and assembles the primary cilium (Figure 1.4). As the cell cycle progresses the mother and daughter centrioles duplicate during S-phase to form new daughter centrioles with the mother centriole remaining at the base of the cilium (Pitaval et al., 2010). Prior to mitosis the cilium is resorbed through disassembly

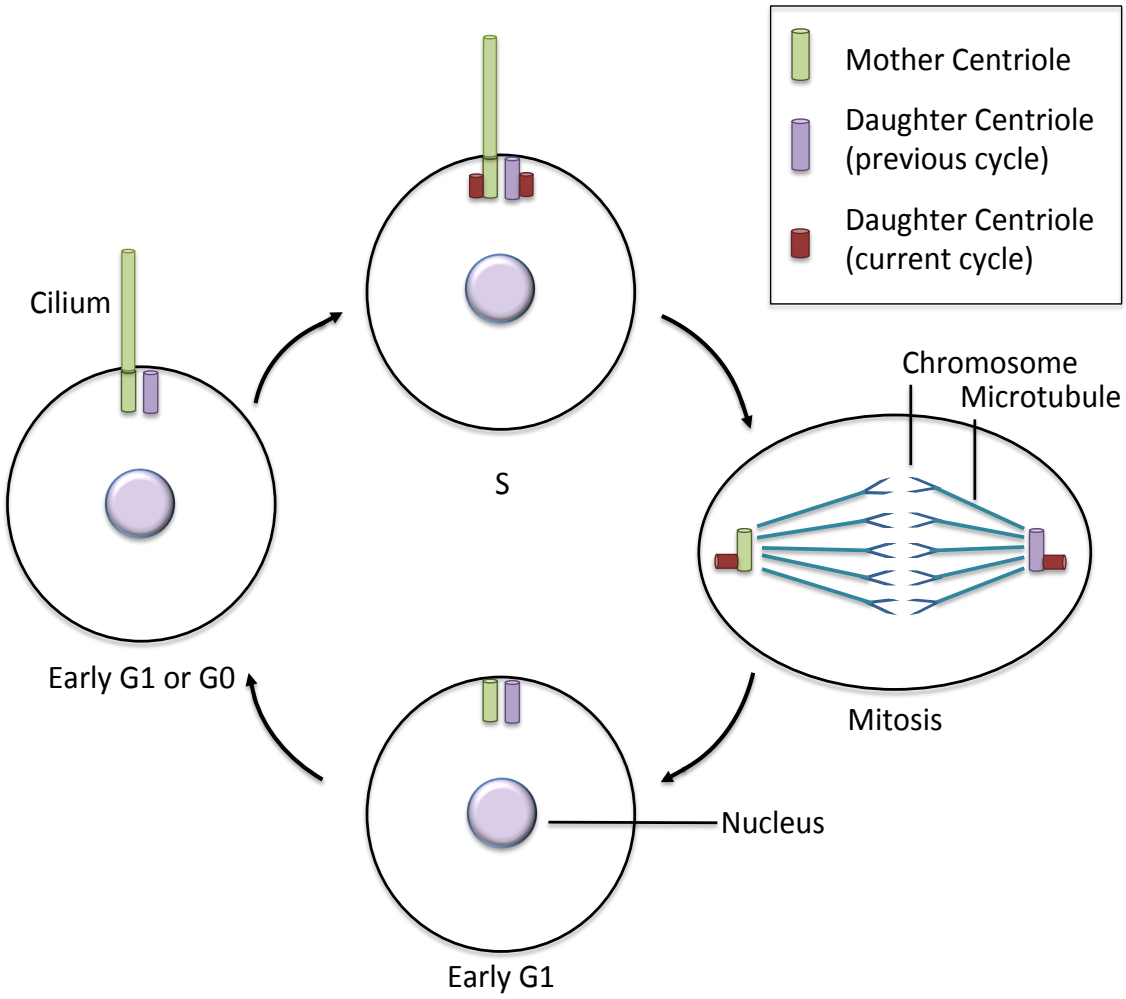

Adapted from Ishikawa and Marshall, Nature Mol Cell Bio, 2011

Figure 1.4. Cell cycle dependent regulation of ciliary assembly and disassembly. During early G1 and G0 the mother centriole migrates to the cell cortex and nucleates a cilium. The daughter centriole from the previous cycle generally does not form a cilium. During S phase the mother and daughter centrioles duplicate forming new daughter centrioles. In the majority of cells, the cilium is resorbed prior to mitosis to ensure proper detachment of the centriole pairs from the cortex and migration to the spindle poles.

at the ciliary tip, a process regulated by its own signal transduction pathway (Kinzel et al., 2010; Pan et al., 2004). The scaffolding protein human enhancer of filamentation 1 (HEF1), the basal body associated protein Pitchfork, and polo-like kinase 1 (PLK1) mediate ciliary resorption through interaction with Aurora A kinase (Kinzel et al., 2010; Lee et al., 2012; Pugacheva et al., 2007). Aurora A also decreases tubulin acetylation reducing microtubule stability by activating the tubulin deacetylase histone deacetylase 6 (HDAC6) (Hubbert et al., 2002; Pugacheva et al., 2007). Disassembly permits centriole pairs attached to the ciliary base to reposition to the cell interior and move to spindle poles where they help position the mitotic spindle (Pitaval et al., 2010).

1.9 Primary Cilium Structure

Primary cilia are microtubule-based organelles. A barrel-like core of nine outer microtubule doublets, termed the axoneme, protrudes from the basal body (Sui and Downing, 2006). The basal body is composed of a cylindrical structure of triplet microtubules derived from mitotic centrioles (Brown and Witman, 2014). Centrioles exist in pairs within the centrosome of cycling cells and consist of one mature mother centriole (MC) and one immature daughter centriole (DC). The MC is distinguished from the DC by the presence of the 9-bladed propeller-like distal and sub-distal appendages (Figure 1.5) (Paintrand et al., 1992). The MC functions in membrane tethering/docking, while the DC anchors arrays of cytoplasmic microtubules (Bornens, 2002; Ishikawa and Marshall, 2011). The sub-distal appendages (SDAs) of the MC also link to cytoplasmic microtubules and are essential for centriole anchoring. The distal appendages (DAs) fuse

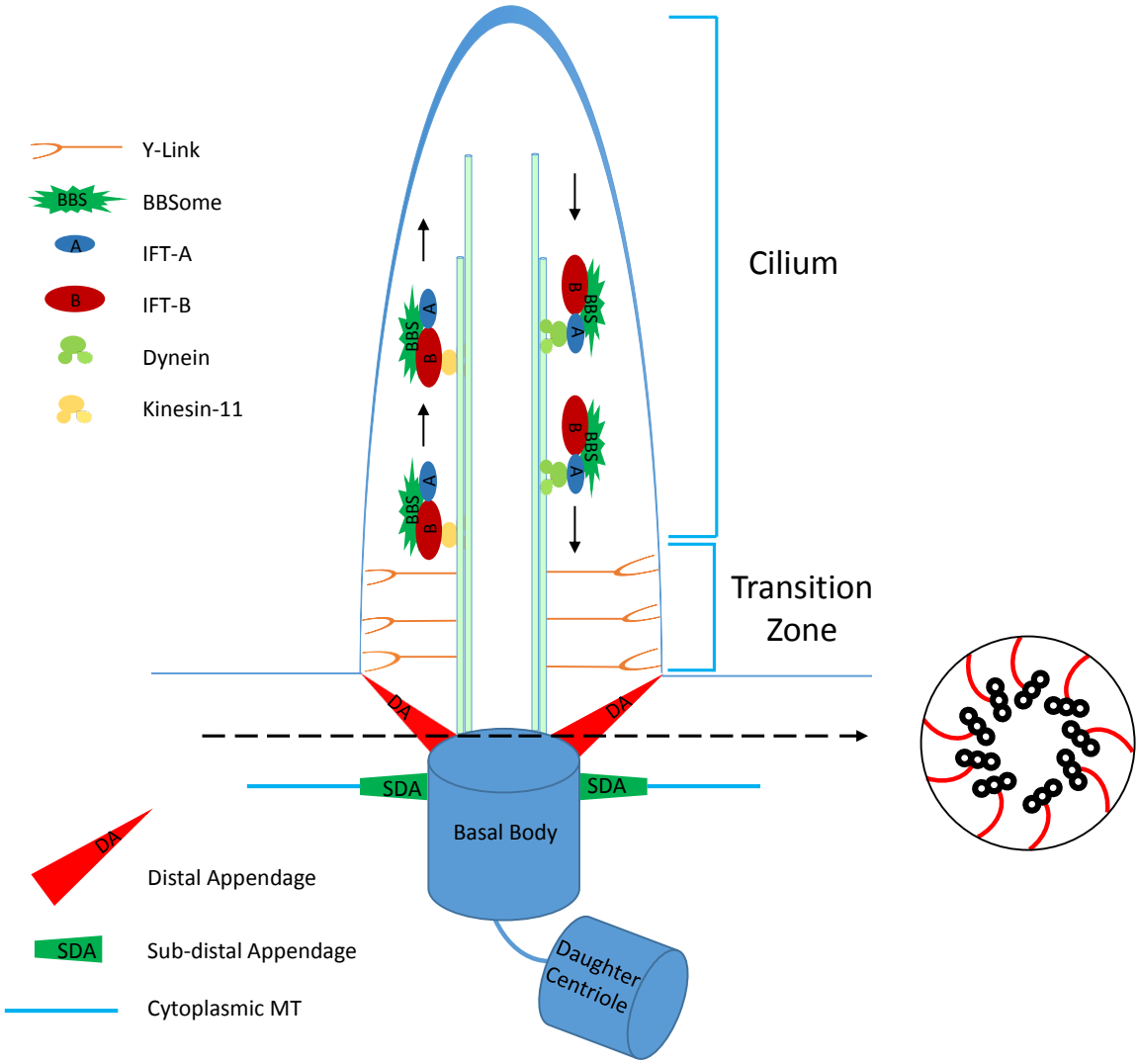

Adapted from Wei et al, Curr Opin Cell Biol, 2015

Figure 1.5. The structure of the primary cilium.
The core structure of the primary cilium, the axoneme, is MT-based, protrudes from the basal body, and is encapsuled by a ciliary membrane. The ciliary membrane contains receptors for intra- and inter-cellular signaling. The basal body contains distal appendages (transition fibers) that link to the ciliary membrane, and below are sub-distal appendages (basal feet) that anchor the basal body using cytoplasmic MTs. Distal to the transition fibers is the Transition Zone that contains Y-links connecting the axoneme to the ciliary membrane. IFT machinery, the BBSome and motor proteins are responsible for cilia extension, maintenance, and function. Cargos are thought to be transported into or out of the cilia by bi-directional IFT along the axoneme. MT, microtubule; DA, distal appendage; SDA, sub-distal appendages; IFT, intraflagellar transport.

to the ciliary membrane and there define the border between the plasma and ciliary membranes (Anderson, 1972; Bornens, 2002).

The ciliary membrane surrounds the axoneme and is a specialized extension of the plasma membrane containing the receptors and channels necessary for signal transduction (Bloodgood, 1992). At the base of the cilium in some mammalian cell-types a ciliary pocket is created by an invagination of the plasma membrane. This pocket serves as a docking site for actin filaments that may act on the positioning and function of the cilium (Molla-Herman et al., 2010). The ciliary membrane is connected to the axoneme by Y-link proteins. The region containing Y-link proteins between the basal body and axoneme is termed the Transition Zone (TZ) (Czarnecki and Shah, 2012; Garcia-Gonzalo and Reiter, 2012; Gilula and Satir, 1972). The TZ is proposed to act as a gate or pore that permits entry of targeted ciliary proteins into the cilium while excluding non-ciliary proteins (Craige et al., 2010; Garcia-Gonzalo et al., 2011; Williams et al., 2011).

Ciliary proteins and cargo are transported to the cilium base by intraciliary transport machinery, termed the Intraflagellar Transport (IFT) complex. Bidirectional movement of the IFT complexes along the axoneme beneath the membrane sheath enables axoneme elongation and maintenance. IFT is composed of two separable complexes, IFT-A and IFT-B, that together contain a specific set of IFT-particle proteins (Cole et al., 1998; Piperno and Mead, 1997). IFT-B is essential for assembly and maintenance of the cilia contributing to anterograde transport, while IFT-A is required for retrograde transport (Haycraft et al., 2003; Iomini et al., 2009).

1.10 IFT Regulation of Ciliogenesis

Ciliary proteins are sorted and packaged in the Golgi, then transported to the cilia by the BBSome and IFT complexes (Baker and Beales, 2009; Pedersen and Rosenbaum, 2008). The BBSome is a stable protein complex composed of seven Bardet-Beidl syndrome proteins and BBIP10 (Lechtreck et al., 2009; Loktev et al., 2008). The IFT complex transports the BBSome that traffics ciliary proteins from the plasma membrane to the ciliary base and into the ciliary compartment along the axoneme (Jin et al., 2010). Axoneme elongation requires the IFT complex to transport cytoplasmic dynein-2, receptor proteins, and axonemal subunits from the cytoplasm, through the ciliary gate, and along the axoneme to the site of assembly at the tip of the cilium (Hao et al., 2011; Johnson and Rosenbaum, 1992; Signor et al., 1999). The IFT-B complex utilizes the kinesin-11 plus-end directed motor protein complex for transportation to the ciliary tip (Pedersen and Rosenbaum, 2008). Upon arrival at the ciliary tip, axonemal and receptor proteins are released while kinesin-11 is inactivated and the minus-end directed motor, cytoplasmic dynein-2 is activated (Pan et al., 2006). Retrograde IFT transport along the axoneme towards the cell body is mediated by IFT-A and cytoplasmic dynein-2 to recycle ciliary turnover products such as inactive receptors sent to the cytoplasm for degradation (Mukhopadhyay et al., 2007).

Once the cilia reach a certain length they no longer elongate. Balancing continuous IFT driven ciliary assembly with axoneme disassembly, the mechanism of which is currently unknown, generates a steady state equilibrium length. The balance-point length control model suggests that the balance of assembly and disassembly is

itself determined by cilia length as the net rate of IFT cargo transport will decrease as the length of the cilium increases (Engel et al., 2009). Thus cilia length is self-regulated by the intrinsic rate of IFT delivery of axonemal subunits to the treadmilling tip (Dentler, 2005).

1.11 Primary Cilium Assembly

The assembly of the mammalian primary cilium occurs through an ordered pathway of distinct steps (Sorokin, 1968). The MC is transformed into the basal body with transition fibers (analogous to the distal appendages of the MC) and basal feet (analogous to the sub-distal appendages). Sequential recruitment of various structural and functional components assembles the transition fibers and basal feet, however, the exact timing and structural organization of this assembly remains largely unknown. Recent studies suggest that OFD1, ODF2, C2CD3, and DZIP1 prepare the distal end of the MC for formation of the DAs, however, these proteins are not thought to be DA structural components (Hunkapiller et al., 2011; Tateishi et al., 2013; Wang et al., 2013; Ye et al., 2014). Genuine DA functional components identified thus far include Cep164, Cep83 (Ccdc41), Cep89 (Ccdc123), SCLT1 (sodium channel and clathrin linker 1), and FBF1 (Fas binding factor 1). Cep83 has been reported to target Cep89 and SCLT1 to the distal appendages where SCLT1 in turn mediates recruitment of Cep164 and FBF1 (Joo et al., 2013; Sillibourne et al., 2011; Tanos et al., 2013). Assembly of both distal and sub-distal appendages in mouse cells requires ODF2, and DZIP1 (Ishikawa and Marshall, 2011; Tateishi et al., 2013; Wang et al., 2013). ODF2 recruits Ninein to the SDAs where it

works with Cc2d2a as a component of the SDAs (Graser et al., 2007; Kodani et al., 2013; Sillibourne et al., 2011).

The microtubule-associated protein, end-binding protein 1 (EB1), and the centrosomal protein Cep170, both localize to the SDA (Figure 1.6) (Guarguaglini et al., 2005; Louie et al., 2004). GST-pull-down assays and mass spectrometry analysis show that EB1 and Cep170 interact (Schroder et al., 2011). Cep170 organizes microtubules while EB1 links the minus-end of cytoplasmic microtubules to the basal body, thereby anchoring the cilia base and initiating ciliogenesis (Guarguaglini et al., 2005; Louie et al., 2004; Schroder et al., 2011).

The transition fibers form docking platforms for the distal appendage vesicles (DAVs), the precursors of the ciliary vesicle (CV). The vesicle membranes are stabilized by EHD1, while the t-SNARE Snap29 mediates the docking and fusion of the small DAVS into a single CV (Lu et al., 2015). As the CV is formed, Cep164 recruits TTBK2 to the transition fibers to remove the CP110 protein cap on the distal end of the basal body permitting the initiation of ciliogenesis and axoneme elongation (Cajanek and Nigg, 2014; Goetz et al., 2012). Cep164 also forms a complex with the coiled-coil protein, Chibby (Cby) at the transition fibers (Burke et al., 2014). The Cep164/Cby complex interacts with the Golgi-derived Rabin8/Rab8 protein complex to mediate further recruitment of Rab8 vesicles. These vesicles deliver new membrane to the elongating ciliary vesicle as the axoneme grows and forms the transition zone (Burke et al., 2014). The basal body-ciliary vesicle migrates to the cell cortex where the CV fuses to the

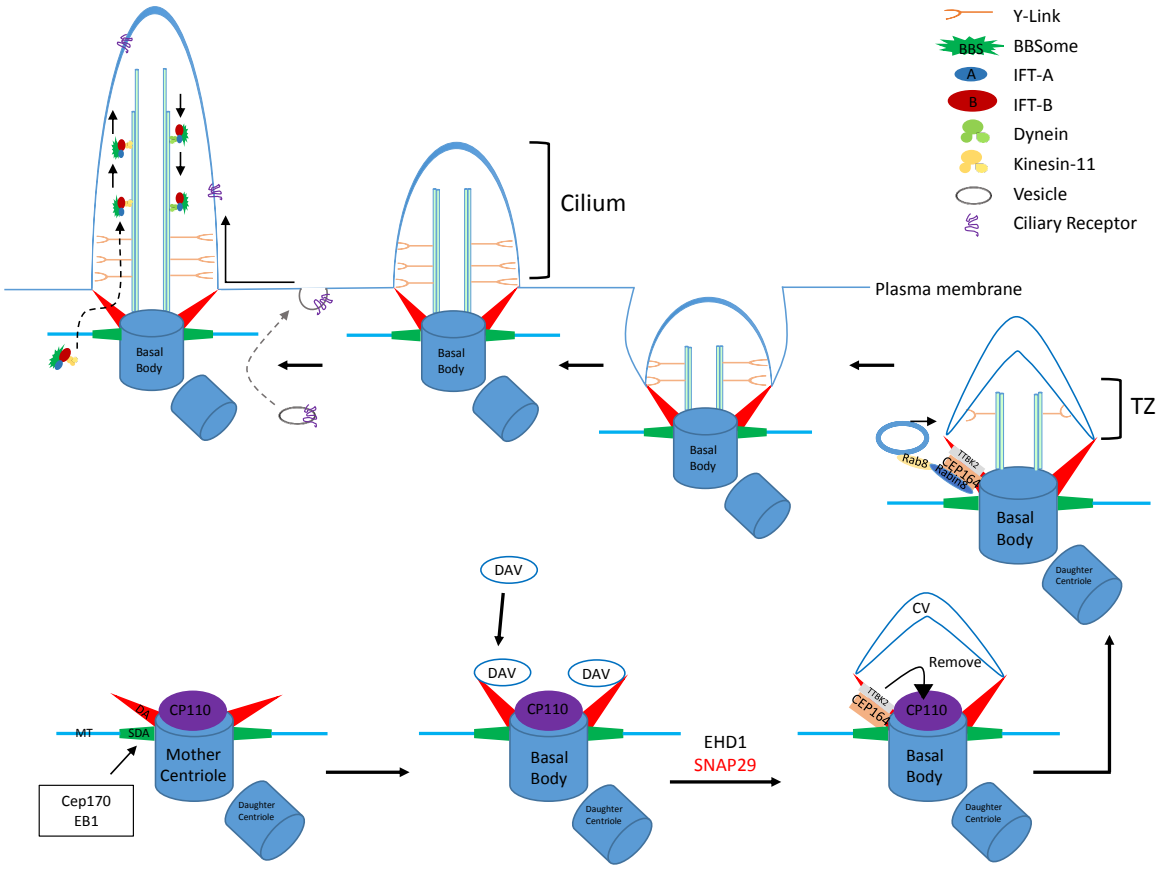

Adapted from Wei et al, Curr Opin Cell Biol, 2015

Figure 1.6. Assembling the primary cilium.
In some mammalian cell types, EB1 and Cep170 interact to ensure linking of MTs to the SDA to anchor the mother centriole. DAVs are then recruited to the DAs where EHD1 shapes and Snap29 fuses the membranes generating the CV. Cep164, located at the DA recruits TTBK2 to remove the CP110 cap permitting axoneme elongation. Cep164 also helps recruit Golgi-derived proteins, Rabin8 and Rab8 that migrate the basal body to the plasma membrane. The ciliary vesicle and plasma membrane fuse and the axoneme elongates further. Bidirectional IFT transport regulates and maintains axoneme extension. Polarized trafficking has been implicated in targeting ciliary cargo to the periciliary membrane. The cargo may enter the cilia through lateral diffusion. MT, microtubule; SDA; sub-distal appendages; DAV, distal appendage vesicle; DA, distal appendage; CV, ciliary vesicle

plasma membrane allowing further axoneme elongation and generation of the cilium on the cell surface (Sorokin, 1962).

1.12 The Golgi, Centrosome and Primary Cilia Connection

The assembly of the Golgi ribbon depends on both the centrosome and Golgi-derived MT networks (Miller et al., 2009; Rivero et al., 2009; Vinogradova et al., 2012). The integrity and re-orientation of the centrosome towards the leading edge of the cell are also dependent on its connection with the Golgi (Bisel et al., 2008; Kodani et al., 2009; Kodani and Sutterlin, 2009). A similar relationship is thought to be present between the Golgi, basal body, and cilia. Trafficking of ciliary components overcomes the logistical issue of the primary cilium lacking protein synthesis machinery. Components necessary for formation of the ciliary pocket and growth of the primary cilium are targeted to the ciliary base and selectively imported into the ciliary compartment at the transition zone. Connection between the Golgi and basal body is thought to facilitate this trafficking (Follit et al., 2006; Greer et al., 2014; Hurtado et al., 2011). Newly synthesized proteins are transported from the Endoplasmic Reticulum (ER) to the Golgi where they undergo post-translational modifications, sorting into carriers, and transport to the plasma membrane, ciliary membrane, and endosomal-lysosomal system. A crucial component of the IFT machinery, IFT20, localizes to the Golgi and cilia, and functions to produce transport carriers at the Golgi necessary for the formation of the primary cilium. Loss of IFT20 results in impairment of ciliogenesis (Follit et al., 2006). A similar role is proposed for the small GTPase Rab8 in direction-specific targeting of

cargo components to the ciliary membrane (Nachury et al., 2007). The Arf and Arl families of small GTPases are involved in Golgi-mediated membrane and vesicular trafficking as well. Arf4 and several Arl proteins are thought to participate in specialized membrane transport targeting the primary cilium (Deretic et al., 2005).

1.13 Hypothesis

The factors that regulate and mediate the effects of INF1 on cytoskeletal dynamics, Golgi morphology, and ciliogenesis are unknown. We hypothesize that INF1 interacts with unique targets to mediate actin and microtubule dynamics involved in the regulation of ciliogenesis. To test this hypothesis I identified and characterized INF1 binding proteins using a new proximity-dependent protein labeling technique termed BioID.

1.14 Biotin Ligase Identification (BioID) Protein Labeling Technique

The biotin ligase identification (BioID) technique utilizes a 35-kD prokaryotic mutant biotin ligase (BirA*) fused to a bait protein of interest (Roux et al., 2012). The mutant derivative BirA* (R118G) decreases site-specificity of its enzymatic biotinylation activity, permitting premature release of highly reactive bioAMP generated by the combination of biotin and ATP. Free bioAMP readily reacts with primary amines permitting promiscuous biotinylation of proteins by BirA* in a proximity-dependent manner (Choi-Rhee et al., 2004; Cronan, 2005).

Biotin (Vitamin H) treatment of cells expressing the BirA* fusion protein allows covalent biotin labeling of proximal proteins within <20nm radius, generating a history of the fusion proteins' numerous interactions (Figure 1.7) (Kim et al., 2014). Selective isolation of the biotinylated proteins exploits the strong non-covalent biological interaction between streptavidin and biotin (Kd = 10^{-14} M). Biotin-tagged proteins are affinity purified with streptavidin-conjugated agarose permitting identification of multiple events and proximity interacting proteins by quantitative mass spectrometry. Alongside identification of the bait proteins' transient, low affinity, and direct protein interactions, the strong non-covalent bond between biotin and streptavidin permits stringent cell lysis and protein solubilization conditions, as endogenous protein-protein interactions need not be maintained. The biotinylated proteins may also be stained with fluorophore-conjugated streptavidin for observation of the proximal interactions by immunofluorescence (Roux et al., 2012).

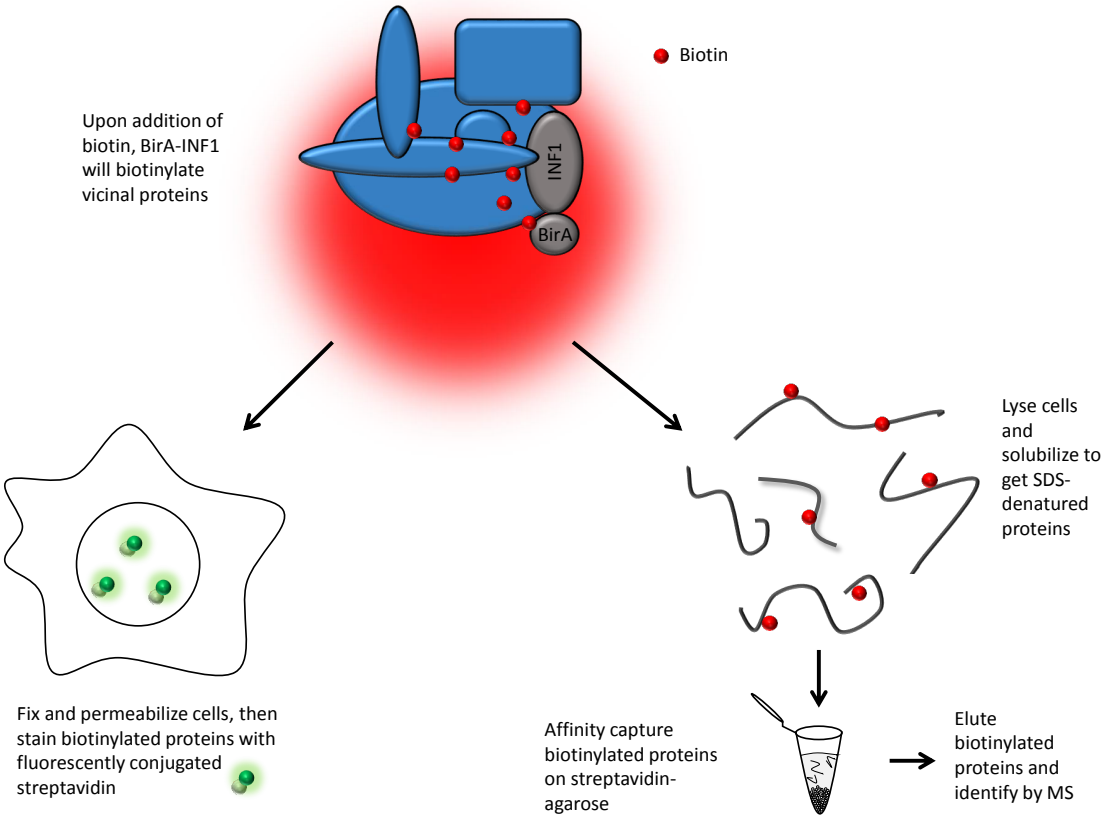

Adapted from Mehta and Trinkle-Mulcahy, F1000Prime Rep., 2013

Figure 1.7. Biotin-ligase identification (BioID) protein labeling technique.
Cells expressing the BirA*-fusion protein, BirA*-INF1, are treated with 50µM of biotin. The BirA*-INF1 fusion protein itself becomes biotinylated as well as biotinylating vicinal proteins. The biotinylated proteins are analyzed by staining with fluorophore-conjugated streptavidin, or by lysing and solubilizing the cells to affinity capture the biotinylated proteins with streptavidin-conjugated agarose beads. The biotinylated proteins are eluted and identified by quantitative mass spectrometry.

Chapter 2: Materials and Methods

2.1 RT-PCR Amplification:

Total RNA was harvested from HEK 293T/17 cells using RNeasy Mini Kit (Qiagen), followed by cDNA synthesis using iScript Reverse Transcription Supermix for RT-qPCR (BioRad). One step RT-PCR was performed with Taq DNA polymerase to detect and amplify cDNA. The amplified cDNA and primers used are listed in Table 2.1.

2.2 Plasmid Construction:

PCR products were cloned into either pEGFP-C1 (Clontech) or pEF Flag. The restriction sites for the GFP- and flag-tagged constructs prepared are listed in Table 2.1.

INF1 full length and truncation plasmids were previously generated as EF plink derivatives with myc, flag, cherry, or YFP tags. The INF1 derivatives were cloned into pcDNA3.1 myc.BirA* using BamH1/EcoR1 restriction sites. The pcDNA3.1BirA* vector was acquired from Dr. Trinkle-Mulcahy (University of Ottawa).

Table 2.1. Primers for RT-PCR amplification of putative INF1 interacting partners

Name	Primer Sequence (5'-3')	Restriction Enzyme	Tag
PFN2	GGA ATT CGA TGG CCG GTT GGC AGA GCT AC GGG ATC CGT TAC ACA TCA GAC CTC CTC AG	EcoR1 BamH1	GFP
ARL2	GGG ATC CAT GGG GCT CCT GAC CAT TCT GAA GAA GGA ATT CGT CAG TCA GCT GTG AAA ATG CGG CTG GAA AT	BamH1 EcoR1	Flag

2.3 Cell Culture:

NIH 3T3 mouse fibroblasts were cultured in Dulbecco's Modified Eagle Media (DMEM, ATCC), supplemented with L-Glutamine, and 10% donor bovine serum (DBS, ATCC). HEK 293T/17 cells were cultured in DMEM (ATCC) supplemented with L-Glutamine, and 10% fetal bovine serum (FBS, ATCC). HeLa cells were cultured in Eagle's Minimum Essential Medium (ATCC), supplemented with 10% FBS (ATCC). U-2 OS cells were cultured in McCoy's 5a Medium Modified (ATCC) supplemented with 10% FBS. The aforementioned cell lines were grown in 5% CO_2 at 37°C. Trypsinization was accomplished with 0.05% trypsin (ATCC) for NIH 3T3 cells, 0.25% trypsin, 0.53mM EDTA (ATCC) for HEK 293T/17 and HeLa cells, and 0.25% trypsin, 0.03% EDTA (ATCC) for U-2 OS cells.

2.4 PEI Transient Transfection of NIH 3T3 Cells:

One day prior to transfection NIH 3T3 cells were seeded at a density of 125,000 cells/well (Golgi dispersion assays) or 175,000 cell/well (acetylated tubulin assays) of a 6-well plate on acid-treated coverslips. Cells were approximately 80% confluent upon transfection. 50µl OptiMEM media (Gibco) and 6µl of polyethlyenimine (PEI) transfection reagent (1:4, DNA:PEI) (Polyscience) were mixed with a total of 1.5µg of DNA. Cells were washed with 2ml OptiMEM while the DNA-PEI complex incubated at room temperature for 20 minutes. The DNA-PEI complex was added to cells with 1ml OptiMEM in a dropwise manner. After 5hrs of incubation the cell culture media was

changed to 2ml DMEM + 10% DBS (MT affinity and Golgi dispersion assays), or DMEM + 0.5% DBS (acetylated tubulin assays).

2.5 PEI Transient Transfection of HEK 293T/17 Cells:

One day prior to transfection HEK 293T/17 cells were seeded at a density of $1.25x10^6$ cells/6cm dish, $3.125x10^6$ cells/10cm dish, or $8.2x10^6$ cells/15cm dish. Cells were approximately 80% confluent upon transfection. OptiMEM media (Gibco) and PEI reagent (1:5, DNA:PEI) were mixed with DNA. The DNA-PEI complex was incubated and added to pre-washed cells as described above. After 5hrs of incubation the cell culture media was changed to DMEM + 10% FBS.

2.6 Calcium Phosphate Transfection of HEK 293T/17 Cells:

HEK 293T/17 cells were seeded at $1.25x10^6$ cells/6cm dish 2hrs prior to transfection. In separate microfuge tubes, 0.18ml of 2X HBS (8g NaCl, 0.2g Na_2HPO_4-$7H_2O$, 6.5g HEPES, pH 7.0) and 5µg DNA with 22µl of 2M $CaCl_2$ (87.6g $CaCl_2$-$6H_2O$, filter sterilized) brought to a final volume of 0.36ml, were aliquoted. The $CaCl_2$/DNA mix was added to the HBS and directly added to the cells dropwise. Cells were incubated for 16-24hrs, washed and 4ml of fresh cell culture media was replaced.

2.7 Immunofluorescence:

Cells were fixed 24hrs (Golgi dispersion assays) or 48hrs (acetylated tubulin assays) after transfection in ice-cold methanol at -20°C for 5 minutes or 4%

paraformaldehyde in PHEM buffer (60mM PIPES, 25mM HEPES, 10mM EGTA, 2mM $MgSO_4$, pH 7.0) for 10 minutes. Cells were permeablized for 5-10 minutes with 0.3% Triton X-100 and 10% donkey serum in PBS. Cells were incubated with primary antibodies (Table 2.2) in 0.03% Triton X-100 and 5% donkey serum in PBS at room temperature for 1hr. Cells were washed thrice with PBS and incubated with secondary antibodies (Table 2.2) in 0.03% Triton X-100 and 5% donkey serum in PBS at room temperature for 1 hr. Cells were washed 3X in PBS and mounted with Vectashield mounting media (Vector Labs) with or without DAPI. Visualization of stained cells used a Zeiss Axio Imager Z1 fluorescent microscope with AxioCam HRm camera. A 63X Plan Apochromat objective lens was used to acquire images that were processed using Axiovision software.

2.8 Immunoblotting

Cells grown in a 6cm dish were lysed in 240µl 1x Laemmli SDS-sample buffer, separated by SDS-PAGE and transferred to PVDF membrane. Immunoblotting was performed with antibodies (Table 2.2) in 0.2% Tween-20, 5% non-fat dried milk in PBS. Membranes analyzed for biotinylated proteins were blocked with 0.2% Triton X-100, 1% bovine serum albumin in PBS and detected with HRP-conjugated streptavidin in the same buffer (1:25,000; Invitrogen).

Table 2.2: Antibodies

Primary:

Antibody	Dilution	Company
Mouse anti-acetylated tubulin	1:500	Sigma
Rabbit anti-acetylated tubulin	1:200	Cell Signaling
Rabbit anti-Flag	IF 1:500 Wb 1:1000	Sigma
Rabbit anti-Myc	IF 1:500 Wb 1:1000	Santa Cruz
Mouse anti-c-Myc (9E10)	1:500	Santa Cruz
Mouse anti-alpha tubulin	IF 1:500 Wb 1:1000	Sigma
Mouse anti-GM130	1:500	BD Biosciences
Mouse anti-gamma tubulin	1:500	Sigma
Rabbit anti-Cep170	Wb 1:500/ 1:1000	Biorbyt
Rabbit anti-GFP	Wb 1:1000	Santa Cruz
Mouse anti-EB1	1:500	Santa Cruz
Streptavidin-568	1:600	ThermoFisher

Secondary:

Antibody	Dilution	Company
Donkey anti-Mouse 488	7.5ug/ml -1:200	Jackson Immunoresearch
Donkey anti-rabbit 488	15ug/ml – 1:200	Jackson Immunoresearch
Donkey anti-mouse 594	15ug/ml – 1:200	Jackson Immunoresearch
Donkey anti-rabbit 594	15ug/ml -1:200	Jackson Immunoresearch
Donkey anti-chicken 594	15ug/ml -1:200	Jackson Immunoresearch
Donkey anti-mouse Cy5	15ug/ml – 1:100	Jackson Immunoresearch
Donkey anti-rabbit Cy5	15ug/ml – 1:100	Jackson Immunoresearch
Donkey anti-rabbit HRP	0.8ug/ml – 1:30,000	Jackson Immunoresearch
Donkey anti-mouse HRP	0.8ug/ml - 1:50,000	Jackson Immunoresearch

2.9 Stable Isotopic Labeling by Amino Acids in Cell Culture:

HEK 293T/17 cell were seeded at 1:5 in either R0K0 “light” DMEM for the control, and R10K8 (L-Arginine:HCL (U-13C6, 98%;15N4, 98%), L-Lysine-2HCl (U13C6, 98%; 15N2, 98%) (Invitrogen) “heavy” DMEM supplemented with 10% Dialyzed Fetal Calf Serum (Invitrogen). The cells were washed with D-PBS (ATCC), trypsinized with 0.25% Trypsin, and neutralized with the corresponding R0K0 or R10K8 DMEM. The cells were serially passaged and expanded in the appropriate media for a total of 7 days. The

cells were seeded at $8.2x10^6$ in 15cm dishes containing a single acid-washed coverslip with the corresponding media one day prior to transfection when 90% confluence was reached.

2.10 BioID Affinity Purification and Mass Spectrometry:

The labeled cells were transiently transfected as previously described with myc-FL INF1 in the R0K0 DMEM and BirA*-FL INF1 in the R10K8 DMEM. The DNA-PEI complex was incubated in serum free SILAC media and added drop-wise to SILAC media supplemented with 10% FBS. The cells were incubated for 24hrs with 50µM biotin (Sigma). The coverslips were fixed in -20°C methanol and stained with fluorophore conjugated streptavidin to determine transfection efficiency. The remaining cells were lysed in high salt RIPA buffer, incubated on ice for 15min, sonicated for 1min (10sec on/off), and centrifuged at 4°C for 10min at 4000rpm. The lysates were incubated separately with 100µl of equilibrated Streptavidin Ultra Performance agarose beads for 3.25hrs at 4°C on a rotator. The beads were washed separately twice with high salt RIPA buffer followed by 2min of centrifugation. Myc-FL INF1 and BirA*-FL INF1 beads were combined and washed X5 followed by centrifugation. The biotinylated proteins were eluted with 200µl elution buffer (30mM biotin and 2% SDS supplemented PBS) at 98°C. The eluate was diluted with 800µl sterile water, vortexed, and spun at 1000rpm for 2min. The diluted eluate was concentrated to 100µl using a speed vacuum. The eluate was mixed with 1.0µl 1M DTT and boiled, followed by the addition of 5µl 1M Iodoacetamide (IAA) and a 30min incubation in the dark.

The eluate was diluted with 1x Laemmli buffer and separated using SDS-PAGE followed by coomassie staining or immunoblot analysis probing with streptavidin-*hrp*. Sections of the coomassie stained gel were excised and subjected to in-gel digestion with the resulting tryptic peptides being eluted and analyzed by LC MS/MS.

2.11 BioID GFP Trap

HEK 293T/17 cells were seeded in 10cm dishes at $3.125x10^6$ one day prior to transfection. Upon transfection cells were roughly 70% confluent. A total of 8µg of DNA mixed with OptiMEM media and PEI followed the previously described protocol of transient transfection. Approximately 24hrs after transfection, the cells were incubated for 24hrs in fresh complete media supplemented with 50µM biotin. After two PBS washes, cells were lysed in 600µl high salt RIPA buffer (50mM Tris, pH 7.4, 500mM NaCl, 0.4% SDS, 5mM EDTA, 1mM DTT, 100µM antipain, and 1x Complete protease inhibitor [Roche]), sonicated for 1min (10sec on/off), and centrifuged for 15min at 13K rpm. Supernatants were incubated with 20µl GFP-Trap_A gta-20 (Chromotek) slurry for 1hr at 4°C. Beads were collected, washed thrice, and centrifuged for 2min at 4°C. Bound proteins were removed with 70µl 1x Laemmli SDS-sample buffer at 98°C.

2.12 BioID Flag Immunoprecipitation

HEK 293T/17 cells were seeded in 6cm dishes at $1.25x10^6$ one day prior to transfection. Transient transfection and biotin treatment followed the previously described protocol. After two PBS washes, cells were lysed in 300µl lysis buffer (50mM

Tris, pH 7.0, 150mM NaCl, 1mM EDTA, 1mM DTT, 100µM antipain, and 1x Complete protease inhibitor [Roche]) or cytoskeletal specific buffer (50mM Tris, pH 7.5, 75mM KCl, 0.2mM EGTA, 1mM NaF, 0.5% Triton-X 100, 5% Glycerol, 1mM PMSF), incubated on ice for 10min, sonicated for 1min (10s on/off), and centrifuged for 15min at 13K rpm. Supernatants were incubated with 20µl EZview Red ANTI-FLAG M2 affinity gel slurry (Sigma) for 1hr at 4°C. Beads were collected, washed thrice, and centrifuged for 2min at 4°C. Bound proteins were removed with 50ul 1x Laemmli SDS-sample buffer at 98°C.

Chapter 3: Results

3.1 Characterization of BirA*-INF1 Derivatives

The BioID vector encodes an N-terminal myc epitope followed by the promiscuous biotin ligase (BirA*) and was used to generate an N-terminal BirA*-INF1 derivative. BirA*-FL INF1 was used as the bait protein for BioID AP/MS to identify INF1 interacting proteins. A series of BirA*-INF1 fusion proteins were generated for INF1 interaction domain mapping and potential future fragmentome work. The BioID vector was used to generate the following INF1 mutation and deletion derivatives: BirA*-FL INF1, BirA*-INF1 ΔFH1, BirA*-FL INF1 I180A, BirA*-INF1 1004N, BirA*-INF1 958N, BirA*-INF1 485N, BirA*-INF1 485N I180A, BirA*-INF1 486C, BirA*-INF1 FH2, and BirA*-INF1 958C.

To determine if the BirA* tag interfered with the known effects of INF1, the BirA*-INF1 fusions were compared to the corresponding myc-tagged INF1 derivative, and the effects on Golgi morphology and ciliogenesis were analyzed by immunofluorescence microscopy (IFM). The Golgi morphology of transfected cells was classified as either perinuclear ribbon, intermediate (compact circular ribbon or loss of polarity), or dispersed Golgi (Figure 3.1, A-C). The myc- and BirA*-INF1 derivatives had comparable effects on Golgi morphology; the majority of myc- and BirA*-FL INF1 expressing cells had dispersed Golgi ribbons, as expected. This was also true of the INF1 derivative 1004N that lacks a portion of the MTBD. In contrast, the majority of cells expressing myc- or BirA*-INF1 derivatives that lacked or deactivated the MTBD or FH2 domain had perinuclear Golgi ribbons.

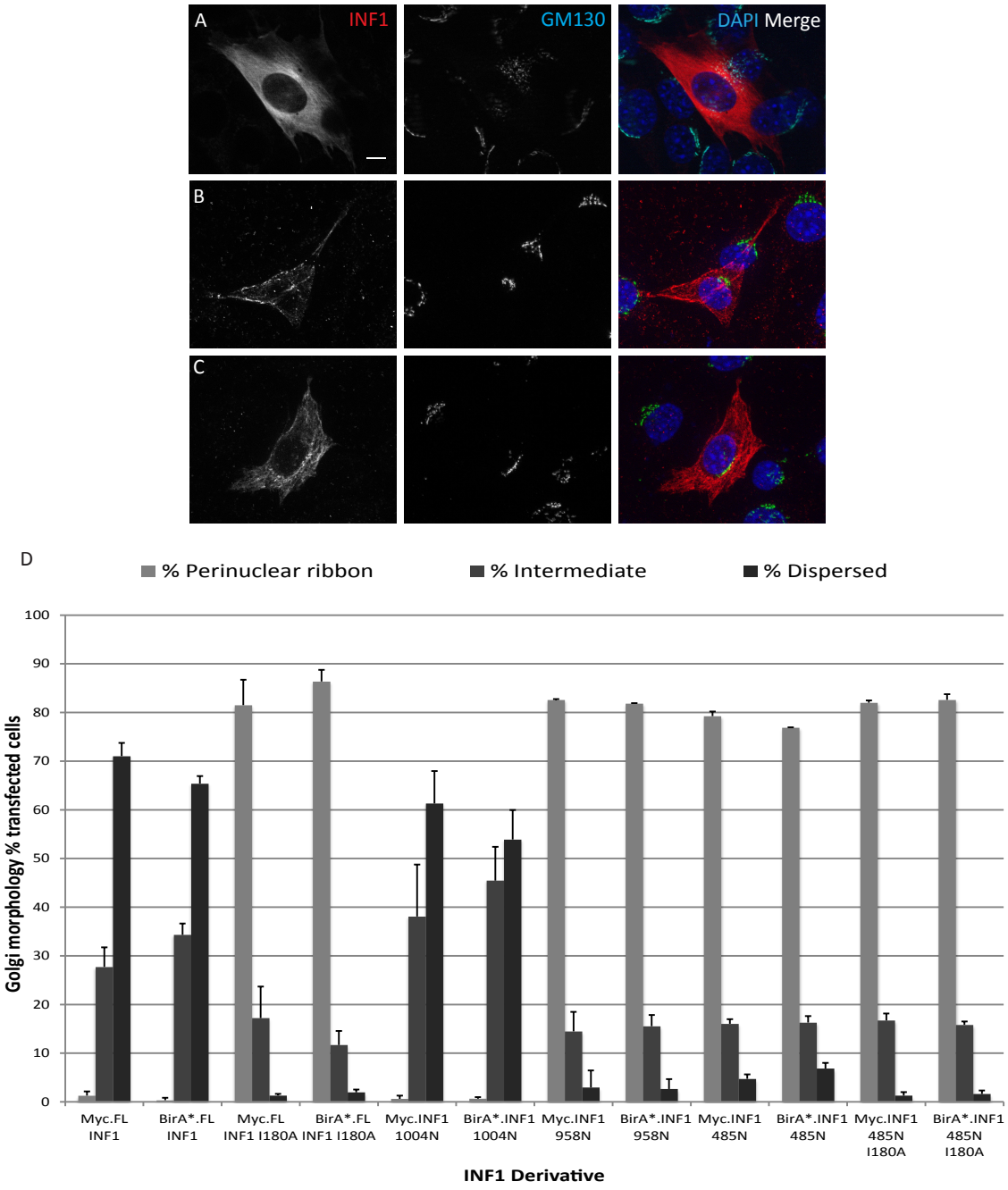

Figure 3.1. INF1-induced Golgi dispersion is not affected by BirA* tag.
NIH 3T3 cells were transfected with myc- or BirA*-FL INF1, FL INF1 I180A, INF1 1004N, INF1 958N, INF1 485N, and INF1 485N I180A. Cells were fixed after 24hrs in complete media. The myc-epitope tag of both myc- and BirA*-INF1 derivatives was stained with rabbit anti-myc (red). The cis-Golgi marker GM130 was stained for using mouse anti-GM130 (green), and the nucleus using DAPI. The INF1 over-expressing cells were classified by Golgi phenotypes: perinuclear (A), intermediate (B), and dispersed (C). Results shown in (A-C) were quantified for each myc- and BirA*-INF1 derivative. (N=3, 100 cells/experiment, error bars = SEM) (Scale bar= 10µM)

Similar results were obtained when comparing the effects of INF1 over-expression on ciliogenesis. The percentage of INF1 over-expressing serum-starved cells forming cilia were quantified and, when present, cilia length was measured. The myc- and BirA*-INF1 derivatives had comparable effects on cilia number and length (Figure 3.2). In the majority of myc- and BirA*-FL INF1 expressing cells, cilia were not present. The cilia formed in myc- and BirA*-FL INF1 expressing cells were elongated with a wide range in length. In contrast, the cells expressing myc- and BirA*-INF1 derivatives that lacked MTBD or FH2 domain function had only minor effects on the number of cells with cilia. The mean values of cilia length were also comparable for all the corresponding myc- and BirA*-INF1 derivatives. The cells expressing myc- and BirA*-INF1 constructs with a deactivated FH2 domain or lacking a small portion of the MTBD had increased average cilium lengths compared to control mCherry expressing cells. The myc- and BirA*-INF1 derivatives that completely lacked the MTBD had compact length distributions, and comparable average lengths to control cells.

To ensure proper sub-cellular localization of the small INF1 derivative 958C, myc- and BirA*-INF1 958C were compared by immunofluorescence detecting the myc-epitope of INF1 958C with anti-myc. Differential sub-cellular localization was observed when INF1 958C was over-expressed in NIH 3T3 fibroblasts. The percent of transfected cells with cytoplasmic or nuclear localization were quantified. The majority of myc- and BirA*-INF1 958C expressing cells had cytoplasmic localization with a small percentage (~30%) of the cells having nuclear localization (Figure 3.3).

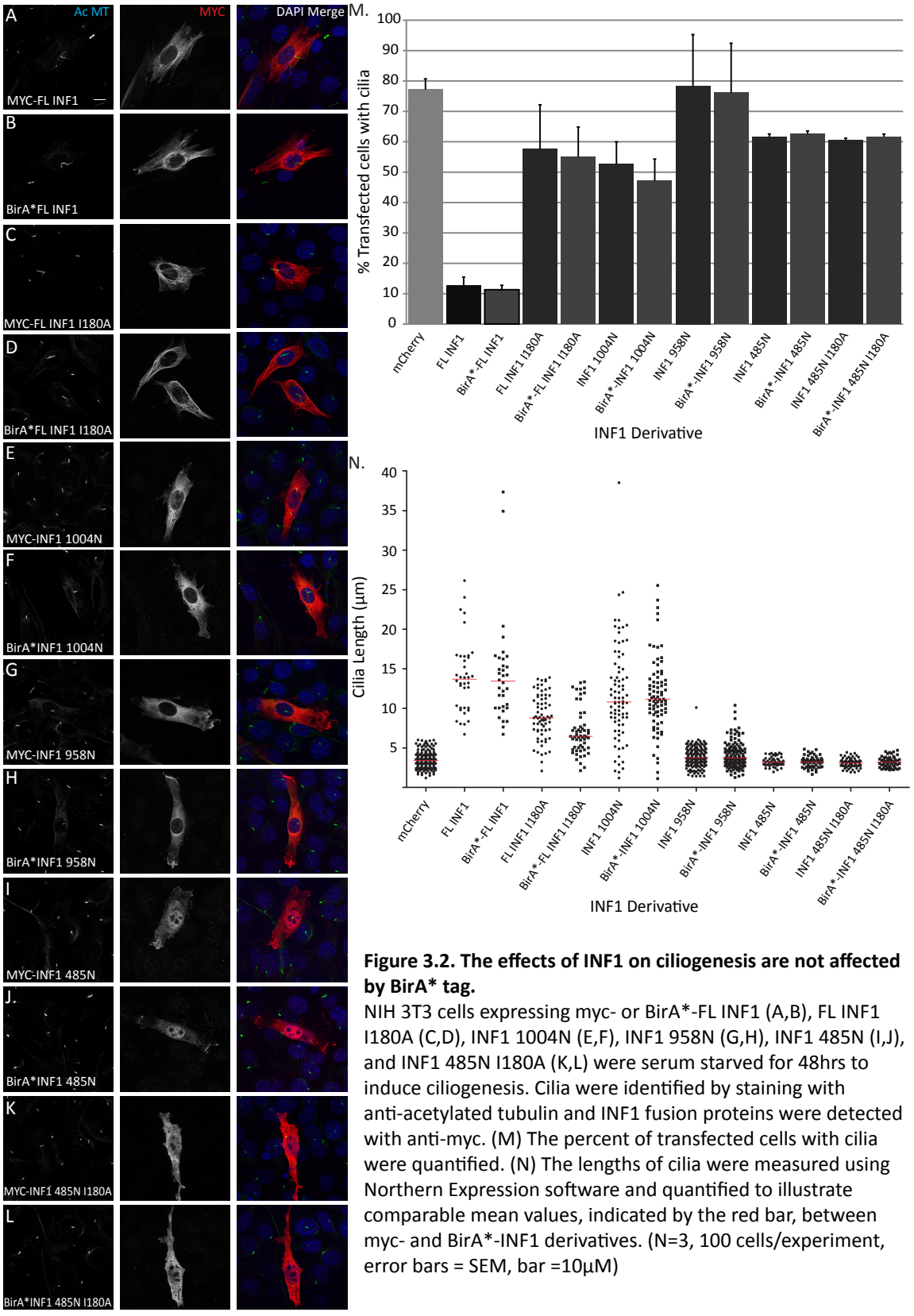

Figure 3.2. The effects of INF1 on ciliogenesis are not affected by BirA* tag.

NIH 3T3 cells expressing myc- or BirA*-FL INF1 (A,B), FL INF1 I180A (C,D), INF1 1004N (E,F), INF1 958N (G,H), INF1 485N (I,J), and INF1 485N I180A (K,L) were serum starved for 48hrs to induce ciliogenesis. Cilia were identified by staining with anti-acetylated tubulin and INF1 fusion proteins were detected with anti-myc. (M) The percent of transfected cells with cilia were quantified. (N) The lengths of cilia were measured using Northern Expression software and quantified to illustrate comparable mean values, indicated by the red bar, between myc- and BirA*-INF1 derivatives. (N=3, 100 cells/experiment, error bars = SEM, bar =10µM)

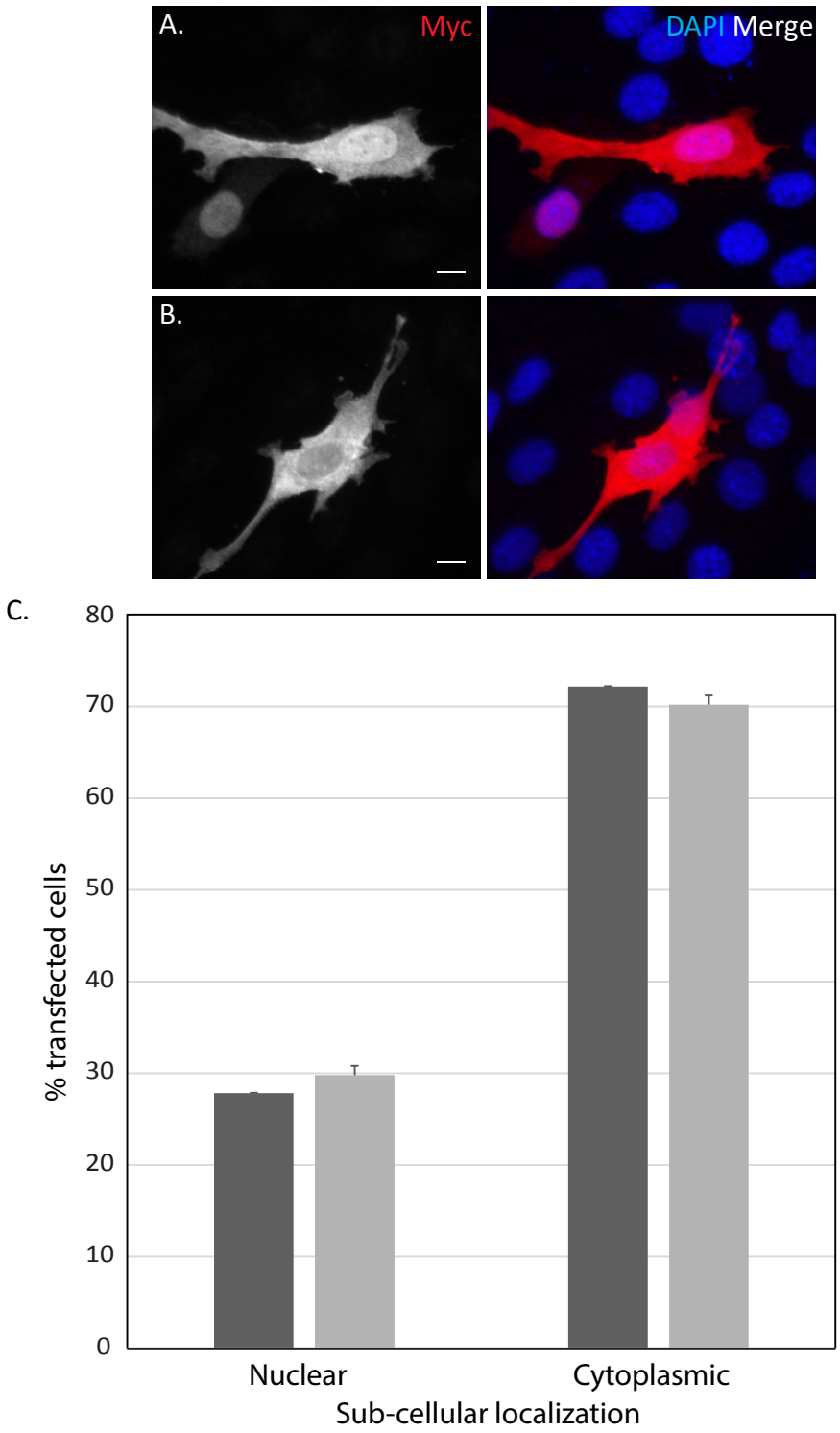

Figure 3.3. INF1 958C has cytoplasmic and nuclear sub-cellular localization.
NIH 3T3 cells transiently transfected with myc-INF1 958C or BirA*-INF1 958C were fixed and stained with anti-myc to detect INF1 958C. (A,B) INF1 958C has both nuclear and cytoplasmic localization. (C) The percent of transfected cells with either nuclear or cytoplasmic sub-cellular localization were quantified. The majority of myc- and BirA*-INF1 958C expressing cells had cytoplasmic sub-cellular localization (N=3, 100 cells/experiment, error bars =SEM, scale bar =10µm

3.2 Establishing BioID SILAC AP/MS Conditions

BirA* alone is not an appropriate control for BioID screening as it is distributed throughout the entire cell and non-specifically biotinylates all vicinal proteins (Lambert et al., 2015). In contrast, most BirA*-fusion proteins are targeted to the normal subcellular domain of the protein of interest and selectively biotinylate vicinal proteins. The series of BirA*-INF1 derivatives, as well as myc-epitope tagged FL INF1, were evaluated as specificity controls for the BioID AP/MS using two methods: IFM and BioID affinity purification (AP) of the BirA*-INF1 derivatives followed by western blot analysis (Table 3.1). IFM and western blot probing of the biotinylated proteins highlighted subcellular localization and induction of biotinylated bands similar to those produced by FL INF1. This suggested that none of the BirA* tagged INF1 derivatives would be suitable negative controls as many potential INF1 interacting proteins would likely be targeted by these proteins as well. Myc-FL INF1 was then tested as a BioID AP specificity control. IFM showed that myc-FL INF1 had corresponding sub-cellular localization and function with BirA*-FL INF1, however, immunoblot analysis showed that myc-FL INF1 did not biotinylate vicinal proteins. Myc-FL INF1 was used as a negative control because it identified non-specific biotinylation and binding to the affinity matrix necessary to identify background contaminants of the BioID SILAC AP/MS screen.

BioID AP conditions for BirA*-FL INF1 had to be established to ensure optimal protein expression, biotinylation, cell lysis, prevention of INF1 degradation, binding to the affinity matrix, and elution (Table 3.1). The transfection efficiency of BirA*-FL INF1 was compared across various cell lines by IFM. HEK 293T/17 cells had 25% transfection

Table 3.1: Experimental conditions to optimize BioID affinity capture of BirA*-FL INF1.

Method	Attempted Conditions	Optimized Condition
Negative Control	BirA*-FL INF1 I180A, BirA*-INF1 958N, BirA*-INF1 485N, myc-FL INF1	Myc-FL INF1
Cell type transfection efficiency	HeLa, HEK293T/17, NIH 3T3, U-2 OS	HEK293T/17
Cell density for 15cm dish	$9x10^6$ vs $8x10^6$	$8.2x10^6$
Total DNA for 15cm dish	10µg, 15µg, 20µg	21.6µg
Transfection reagent	PEI vs $CaP0_3$	PEI
Biotin treatment	0, 2, 4, 6, 8, 12, 24, 32, 48hrs of 50µM biotin treatment	24hrs of 50µM biotin treatment
Lysis buffer	*Low salt RIPA:* 50mM Tris, pH 7.4, 150mM NaCl, 0.4% SDS, 5mM EDTA, 1mM DTT *High salt RIPA*: 50mM Tris, pH 7.4, 500mM NaCl, 0.4% SDS, 5mM EDTA, 1mM DTT *NP-40:* 50mM Tris, pH 8.1, 150mM NaCl, 0.5% NP-40, 5mM EDTA, 1mM DTT *Roux buffer:* 50mM Tris, pH 7.4, 150mM NaCl, 1% Triton-X 100, 0.5% sodium deoxycholate, 0.1% SDS, 5mM EDTA, 1mM DTT	High salt RIPA
Protease inhibitors	Sigma and Roche protease inhibitor cocktails alone, and supplemented with antipain	Roche PIC + 100µM antipain
Sonication	1min (10s on/5s off at 25%), add Triton-X 100 to 2% final concentration, sonicate 1min, add equal vol. 50mM Tris (pH 7.4), sonicate 1min vs 1min (10s on/off)	1min (10 sec on/off)
Bead type	Streptavidin Ultra Performance agarose bead (Solulink) vs Dynabeads MyOne Streptavidin C1 magnetic bead (Invitrogen)	Ultra Performance Agarose
Bead volume	4µl, 8µl, 10µl, 20µl, 40µl, 60µl beads/6cm dish	14µl/6cm
Bead incubation	1, 2, 3, 4, 6hr incubation on 4°C rotator	3.25hrs
Wash buffer	Corresponding lysis buffer lacking protease inhibitors vs Wash Buffer 1 (2% SDS in dH_20), Wash Buffer 2 (0.1% deoxycholate, 1% Triton-X 100, 500mM NaCl, 1mM EDTA, 50mM HEPES, pH 7.5), Wash Buffer 3 (250mM LiCl, 0.5% NP-40, 0.5% deoxycholate, 1mM EDTA, 10mM Tris, pH 8.1), Wash Buffer 4 (50mM Tris, pH 7.4, 50mM NaCl)	High salt RIPA lacking protease inhibitors
Elution buffer	1X Laemmli buffer vs 30mM biotin, 2% SDS in PBS	30mM biotin, 2% SDS in PBS

efficiency while the HeLa, U-2 OS, and NIH 3T3 cells ranged from 8-20% efficiency. Optimal cell density, total DNA transfected and transfection reagent were investigated by IFM and a density of $8.2x10^6$ HEK293T/17 cells in a 15cm dish, transfected with a total of 21.6µg of DNA using PEI were chosen for affinity purification of BirA*-FL INF1.

The BioID system requires addition of excess biotin to the media of cultured cells to provide substrate for the over-expressed BirA*-fusion protein (Roux *et al*, 2012). The biotinylation of BirA*-FL INF1 and proximal proteins were compared by immunoblot analysis and IFM for a series of biotin treatment times (Table 3.1). The relative levels of protein expression and staining were also compared for these times. Not surprisingly, an increase in biotin incubation time resulted in an increase in accumulation of biotinylated proteins that plateaued after 24hrs.

The optimal lysis conditions necessary to solubilize the large cytoskeletal protein, INF1 were evaluated (Table 3.1). A mild NP-40 buffer, high salt and detergent Roux buffer (500mM NaCl, 2%SDS), as well as a high and low salt RIPA buffer were compared by BirA*-FL INF1 affinity capture and immunoblot analysis. Sigma (P8340) and Roche cOmplete Tablet (EDTA-free) protease inhibitor cocktails (PIC) alone or supplemented with antipain (Sigma) were also compared by affinity capture of BirA*-FL INF1 and immunoblotting. The Sigma PIC inhibits serine, cysteine, acid proteases, and aminopeptidases, while the Roche PIC inhibits serine, and cysteine, but not metalloproteases. The high salt (500mM) RIPA buffer ensured optimal cell lysis and Roche cOmplete PIC and antipain ensured preservation of the proteins during extraction and purification. High salt RIPA buffer was sufficient to induce cell lysis, but sonication

was required to ensure near complete recovery of biotinylated proteins. Immunoblot analysis was used to compare lysate that was sequentially sonicated with additional detergents or sonicated for 1min to ensure complete cell lysis. Sonication for 1min (10sec on/off) produced optimal lysis.

To optimize capture of the biotinylated proteins, magnetic and agarose beads were compared by immunoblot analysis of affinity captured BirA*-FL INF1 (Table 3.1). Additional parameters tested include bead volumes ranging from 4-60µl/6cm dish, incubation times ranging from 1-6hrs, bead wash buffers, and elution buffers. Immunoblots of biotinylated proteins captured by the streptavidin agarose beads indicated a higher biotin binding capacity compared to the magnetic beads. A bead volume of 14µl/6cm dish incubated for 3.25hrs ensured optimal affinity capturing of biotinylated proteins. Wash and elution buffers were compared by immunoblotting to ensure non-specific proteins were washed from the affinity matrix while maintaining captured biotinylated proteins and efficiently eluting proteins from the matrix (Table 3.1). The high salt RIPA buffer and biotin-supplemented SDS elution buffer ensured proper washing of the beads and elution of the biotinylated proteins.

To increase specificity of the screen, label-based quantitative mass spectrometry using stable isotopic labeling of amino acids in cell culture (SILAC) was used (Figure 3.4). SILAC labels proteins with isotopic tags at the cellular level by feeding isotopic variants of essential amino acids to the cells over time. SILAC was used to metabolically label two cell populations, one grown in heavy (Arg10Lys8) media, and the other in light (Arg0Lys0) media. The labeled cell populations were used in parallel control (light, myc-

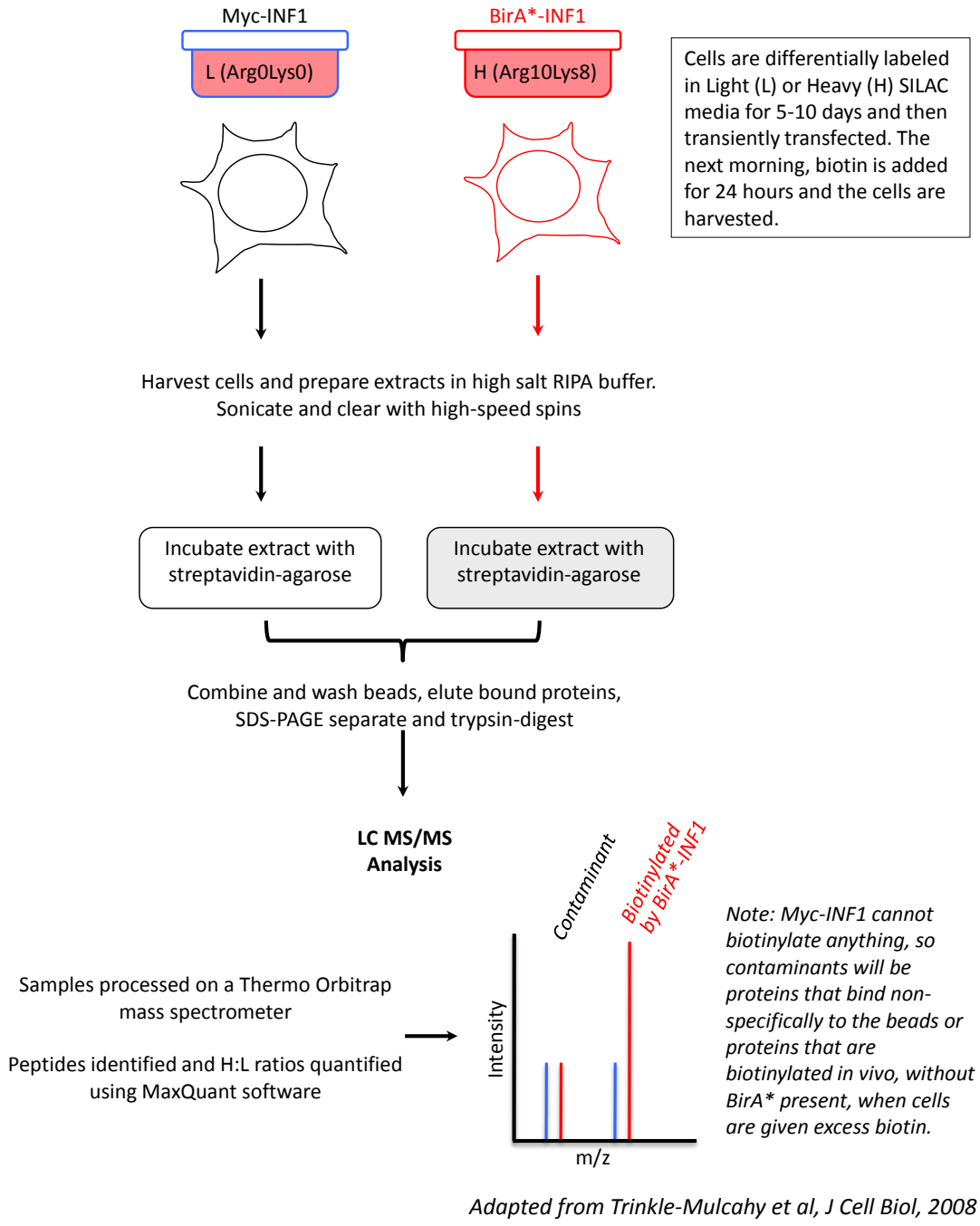

Adapted from Trinkle-Mulcahy et al, J Cell Biol, 2008

Figure 3.4. BioID and SILAC AP/MS identification of INF1 interacting protens.
HEK 293T/17 cells were labeled with SILAC followed by BioID affinity purification/mass spectrometry (AP/MS) to generate a list of potential INF1 interacting proteins. The control cells labeled with light SILAC media were transfected with myc-INF1 while the heavy SILAC media labeled cells were transfected with BirA*-INF1. MaxQuant software quantified the number of peptides and heavy-to-light ratios of purified proteins to identify contaminants and highlight proteins specifically biotinylated by BirA*-INF1.

FL INF1 transfected), and experimental (heavy, BirA*-FL INF1 transfected) pull-downs were performed by Sarah Copeland and the two affinity captured samples were combined for mass spectrometry analysis.

3.3. Bioinformatic Analysis of BioID SILAC AP/MS

Over 700 putative INF1-interacting proteins were identified by the BioID SILAC AP/MS analysis that was performed in collaboration with Dr. Laura Trinkle-Mulcahy (University of Ottawa). These proteins were ranked based on signal intensity and SILAC ratio. Non-specifically bound proteins equally represented in both heavy and light populations should have a 1:1 heavy-to-light ratio, whereas specifically bound proteins should be more abundant in the experimental heavy sample and have a ratio greater than 1. Proteins specifically biotinylated by BirA*-FL INF1 were identified by a cutoff with a heavy-to-light ratio larger than two. Proteins identified as common background contaminants that bind to affinity matrices were filtered out of the putative hit list by cross-reference with an established agarose bead proteome (Trinkle-Mulcahy et al., 2008). The list was further reduced by cross-reference with a catalogue of background biotin hits (Lambert et al., 2015). Priorities were assigned based on gene function corresponding to known INF1 function generating a short-list of potential INF1-interacting proteins from the INF1 BioID interactome (Table 3.2). Expected proteins such as the formin binding proteins, profilin2, and VASP, were identified on the short list of hits. The basal body associated proteins Cep170, and Snap29 were of primary interest based on data suggesting a role for INF1 in ciliogenesis (Copeland et al., manuscript in

Table 3.2. Prioritized list of INF1 interacting proteins identified by BioID AP/MS

Average Ratio H/L: 2.76
Average Normalized Intensity: 3.43
NaN: Not-a-Number

Actin Associated Proteins

Protein Name	Gene Name	Peptides	Ratio H/L
Profilin-2	PFN2	5	15.327
Protein enabled homolog	VASP	2	5.0438

MT Associated Proteins

Protein Name	Gene Name	Peptides	Ratio H/L
MT associated protein RP/EB family member1	MAPRE1 (EB1)	5	12.601

Cilia/Centrosome Associated Proteins

Protein Name	Gene Name	Peptides	Ratio H/L
Centrosomal protein of 170kDa	CEP170	8	7.2057
Synaptosomal-associated protein 29kDa	SNAP29	2	7.7755
Centrosomal protein of 164kDa	Cep164	1	NaN

Golgi/Trafficking Associated Proteins

Protein Name	Gene Name	Peptides	Ratio H/L
Ras-related protein RAB-1A	RAB1A	4	4.1166
Ras-related protein RAB-5A	RAB5A	2	6.1283
Ras-related protein RAB-14	RAB14	5	23.897
Ras-related protein RAB-2B	RAP2B	2	5.3376
Ras-related protein RAB-21	RAB21	2	4.907
ADP-ribosylation factor-like protein2	ARL2	2	2.062
ADP-ribosylation factor-like protein 8A	ARL8A	3	4.491
ADP-ribosylation factor-like protein 8B/10C	ARL8B/10C	3	4.491
ADP-ribosylation factor 1	ARF1	7	8.7018
ADP-ribosylation factor 3	ARF3	7	8.7018
ADP-ribosylation factor 4	ARF4	6	9.6744
ADP-ribosylation factor 5	ARF5	6	11.93
ADP-Ribosylation factor 6	ARF6	2	5.998

prep). Arl2 and EB1 were intriguing as well given their association with the early stages of cilia formation (Davidson et al., 2013; Louie et al., 2004). The identification of numerous small GTPases involved in trafficking as well as MT associated proteins (MAPs) were also of interest based on the role of INF1 in Golgi assembly and as a MAP (Copeland et al., 2015; Young et al., 2008).

3.4 Direct Validation of Putative INF1 Interacting Proteins

To directly confirm the putative INF1 interacting proteins of the mass spectrometry analysis the list of 19 prioritized INF1 interacting partners (Table 3.2) were validated using BioID labeling combined with GFP trap or flag immunoprecipitation of the protein of interest (POI). Prior to validation tests the optimal co-expression of the epitope tagged POI and BirA*-FL INF1 were investigated by immunoblotting. A titration of total plasmid encoding the POI was transfected with BirA*-FL INF1 in HEK 293T/17 cells followed by biotin treatment, cell lysis, and immunoblot analysis probing for the epitope tag of the POI and anti-myc to detect BirA*-FL INF1. The appropriate total plasmid encoding the POI was identified by strong expression of both BirA*-FL INF1 and the POI (data not shown).

The direct validation of the mass spectrometry results tested the ability of BirA*-FL INF1 to biotinylate a co-expressed GFP or flag-tagged derivative of the POI. The epitope tagged POI or BirA*-FL INF1 were expressed individually for specificity controls. The transfected cells were incubated with biotin for 24hrs, lysed, and the solubilized proteins were pulled down via the tag on the POI. The lysate was run in duplicate and

probed for biotinylated proteins using streptavidin-*hrp*, or the corresponding POI tag, either anti-GFP or anti-flag, to confirm pull-down efficiency. A band in the pull-down eluate lane on the streptavidin-*hrp* blot that corresponds to the molecular weight of the POI was taken as a positive validation. It should be noted that a positive validation indicates a proximal, and not a direct interaction between the over-expressed POI and BirA*-FL INF1. The pull-down validation was complemented by immunofluorescence on NIH 3T3 cells expressing the epitope-tagged POI alone, and co-expressed with BirA*-FL INF1. Biotinylated proteins were stained with fluorophore-conjugated streptavidin.

The proximal interactions between INF1 and the known formin binding proteins, profilin2 (PFN2) and vasodilator-stimulated phosphoprotein (VASP), were tested as described (Grosse et al., 2003; Kovar, 2006; Pring et al., 2003; Schirenbeck et al., 2006). Endogenous PFN2 has cytoskeletal and cytoplasmic localization, while VASP localizes to stress fibers and the tips of actin bundles (Figure 3.5) (Gambaryan et al., 2001; Kwiatkowski et al., 1990). IFM analysis showed GFP-PFN2 localization throughout the cytoplasm and filamentous localization was observed for flag-VASP. Although a bleed through control is lacking, when BirA*-INF1 was co-expressed with the aforementioned proteins, BirA*-INF1 appears to localize with GFP-PFN2 and flag-VASP. Immunoblotting analysis of the BioID pull-downs showed strong biotinylated bands corresponding to PFN2 and VASP in the eluate lanes validating their proximal interaction with INF1.

The INF1 proximal interaction with centrosome associated proteins EB1, Cep170, SNAP29, and Arl2 were tested as described above. The centrosomal protein of 160kDa (Cep164) was also tested for INF1 proximity interaction. Endogenous EB1 localizes along

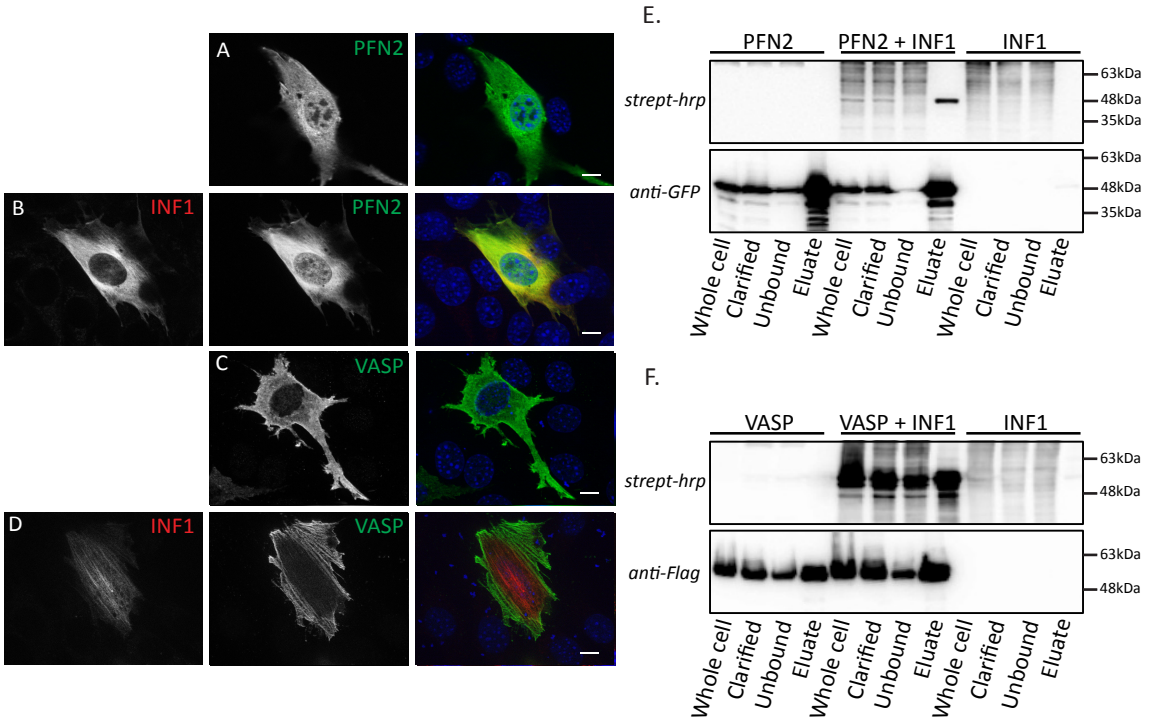

Figure 3.5. INF1 proximally interacts with formin-associated proteins Profilin2 & VASP. (A-D) Putative INF1 interacting proteins PFN2 and VASP were expressed as GFP- or flag-tagged proteins in NIH 3T3 cells with or without BirA*-INF1. The transfected cells were incubated with biotin for 24hrs, fixed and stained with fluorophore-tagged streptavidin (red). (E,F) The indicated proteins were expressed in HEK 293T/17 cells with or without BirA*-INF1 co-expression. BirA*-INF1 was expressed alone as an additional negative control. Following biotin treatment the cells were lysed and the GFP/Flag-tagged proteins were affinity purified with GFP Trap beads or anti-flag affinity gel. Samples of the whole cell lysate, clarified lysate, unbound fraction, and bead eluate were subjected to SDS-PAGE and duplicate blots were probed with streptavidin-HRP (top box) or, anti-GFP or -flag (bottom box). Specific biotinylation of the GFP- or flag-tagged protein by co-expression with BirA*-INF1 confirmed the interaction between INF1 and the protein of interest. (E) Biotinylated GFP-PFN2 was detected in the eluate from GFP-PFN2/BirA*-INF1 expressing cells but not in eluates from cells expressing GFP-PFN2 or BirA*-INF1 alone. The bands below the expected 48kDa molecular weight (MW) of GFP-PFN2 were likely degradation products. (F) Flag-VASP also proximally interacted with BirA*-INF1 in this assay with an anticipated MW of 55kDa. (Bar= 10µM)

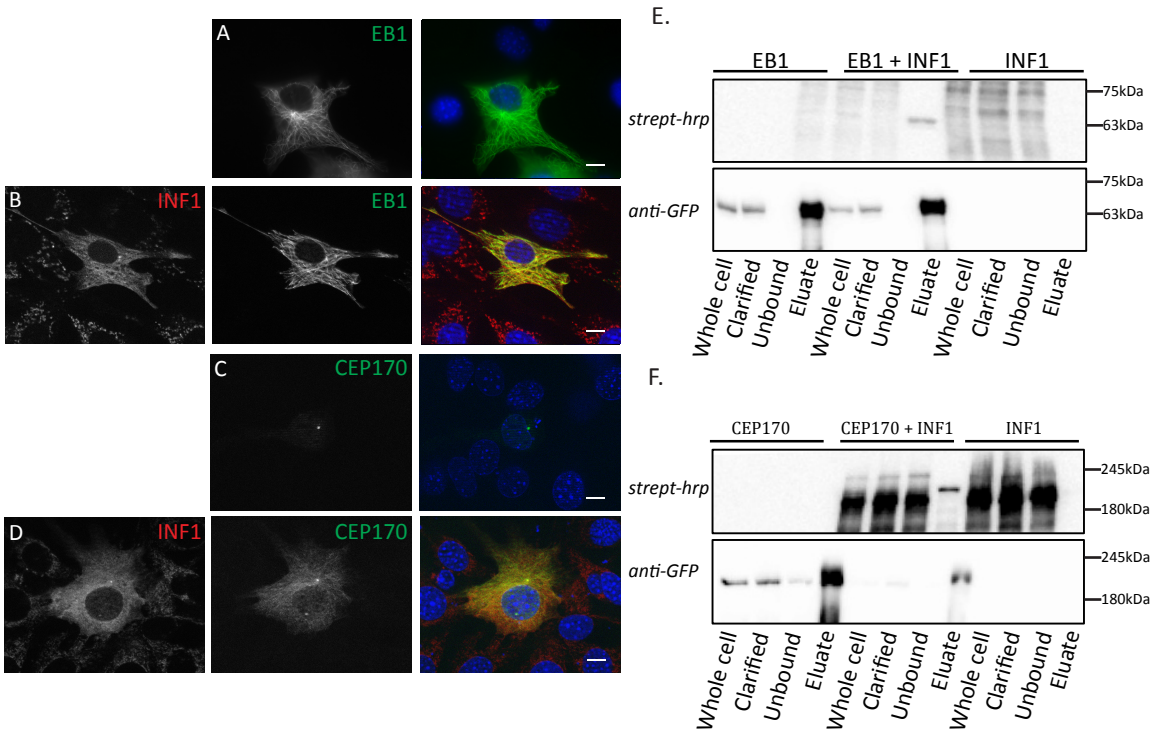

Figure 3.6. INF1 proximally interacts with basal body-associated proteins EB1 and Cep170.

(A-D) Putative INF1 interacting proteins EB1 and Cep170 were expressed as GFP-tagged proteins in NIH 3T3 cells with or without BirA*-INF1. The transfected cells were incubated with biotin for 24hrs, fixed and stained with fluorophore-tagged streptavidin (red). (E,F) The indicated proteins were expressed in HEK 293T/17 cells with or without BirA*-INF1 co-expression. BirA*-INF1 was expressed alone as an additional negative control. Following biotin treatment the cells were lysed and the GFP-tagged proteins were affinity purified with GFP Trap beads. Samples of the whole cell lysate, clarified lysate, unbound fraction, and bead eluate were subjected to SDS-PAGE and duplicate blots were probed with streptavidin-HRP (top box) or anti-GFP (bottom box). Specific biotinylation of the GFP-tagged protein by co-expression with BirA*-INF1 confirmed the interaction between INF1 and the protein of interest. (E) GFP-EB1 had an expected MW of 63kDa and biotinylated GFP-EB1 was detected in the eluate from GFP-EB1/BirA*-INF1 expresing cells but not in eluates from cells expressing GFP-EB1 or BirA*-INF1 alone. (F) GFP-Cep170 also proximally interacted with BirA*-INF1 in this assay with an expected MW of 200kDa. (Bar =10µM)

cytoplasmic MTs as well as at the centrosome, and similar sub-cellular localization was observed by IFM for GFP-EB1 (Figure 3.6) (Louie et al., 2004; Wen et al., 2004). Co-expression of BirA*-FL INF1 and GFP-EB1 highlighted similar subcellular localization, though a bleed through control is lacking. GFP-Cep170 localized to the mother centriole similar to reported endogenous sub-cellular localization (Guarguaglini et al., 2005). Immunoblotting analysis of the BioID pull-downs showed strong biotinylated bands corresponding to EB1 and Cep170 in the eluate lanes validating their proximal interaction with INF1.

IFM analysis of flag-SNAP29 and flag-Arl2 were similar to the reported endogenous cytoplasmic localization, as was GFP-Cep164 with endogenous localization to the mature centriole (Figure 3.7) (Davidson et al., 2013; Graser et al., 2007; Lu et al., 2015). When BirA*-FL INF1 was co-expressed with flag-SNAP29, flag-Arl2, and GFP-Cep164, similar localization of the epitope tagged proteins and BirA*-FL INF1 was observed, though a bleed through control is lacking. The BioID pull-downs and immunoblot analysis showed strong biotinylated bands corresponding to SNAP29 and Arl2 in the eluate lanes, while a weak band corresponding to Cep164 was present. The weak INF1 proximal interaction with Cep164 was expected given the below average SILAC H/L ratio and only one peptide present in the mass spectrometry analysis (Table 3.2)

Numerous small GTPases involved in recruitment of structural effector proteins to the Golgi were identified in the short list of INF1 interacting partners (Copeland et al., 2015; Donaldson and Jackson, 2011). Caveats of validating these small GTPases included

the bioinformatics analysis of the MS results that identified seven peptides corresponding to either Arf1 or Arf3 (Table 3.2), as well as many of the small GTPases being known agarose proteome contaminants (Copeland et al., 2015; D'Souza-Schorey and Chavrier, 2006; Gillingham and Munro, 2007; Trinkle-Mulcahy et al., 2008). Nevertheless, their function prompted direct testing of the Arfs for INF1 proximity interaction. Endogenous Arf1 &4 localize to the cis-Golgi while Arf3 & 5 localize to the *trans*-Golgi network (TGN) (Donaldson and Jackson, 2011). IFM analysis of GFP-Arf1, -Arf3, -Arf4, and –Arf5 showed perinuclear ribbon-like localization likely corresponding to the cis- and trans-Golgi (Figure 3.8 & 3.9) (Donaldson and Jackson, 2011; Manolea et al., 2010). When GFP-Arf1, -Arf4, and –Arf5 were co-expressed with BirA*-FL INF1 similar localization was observed, though a bleed through control is missing. Immunoblotting of the BioID pull-downs highlighted a strong biotinylated band corresponding to Arf1 in the eluate lane confirming the proximal INF1 interaction with GFP-Arf1. GFP-Arf3, 4, and 5 were not positively validated using the BioID pull-down technique.

The function of Rab5A as a trafficking protein prompted direct testing for INF1 proximity interaction. IFM analysis showed GFP-Rab5A towards the cell periphery of the cytoplasm corresponding to reported endogenous localization (Figure 3.10) (Chavrier et al., 1990). A strong biotinylated band corresponding to Rab5A was present in the eluate lane of the BioID pull-down immunoblot confirming Rab5A as an INF1 proximity interacting partner (Figure 3.10).

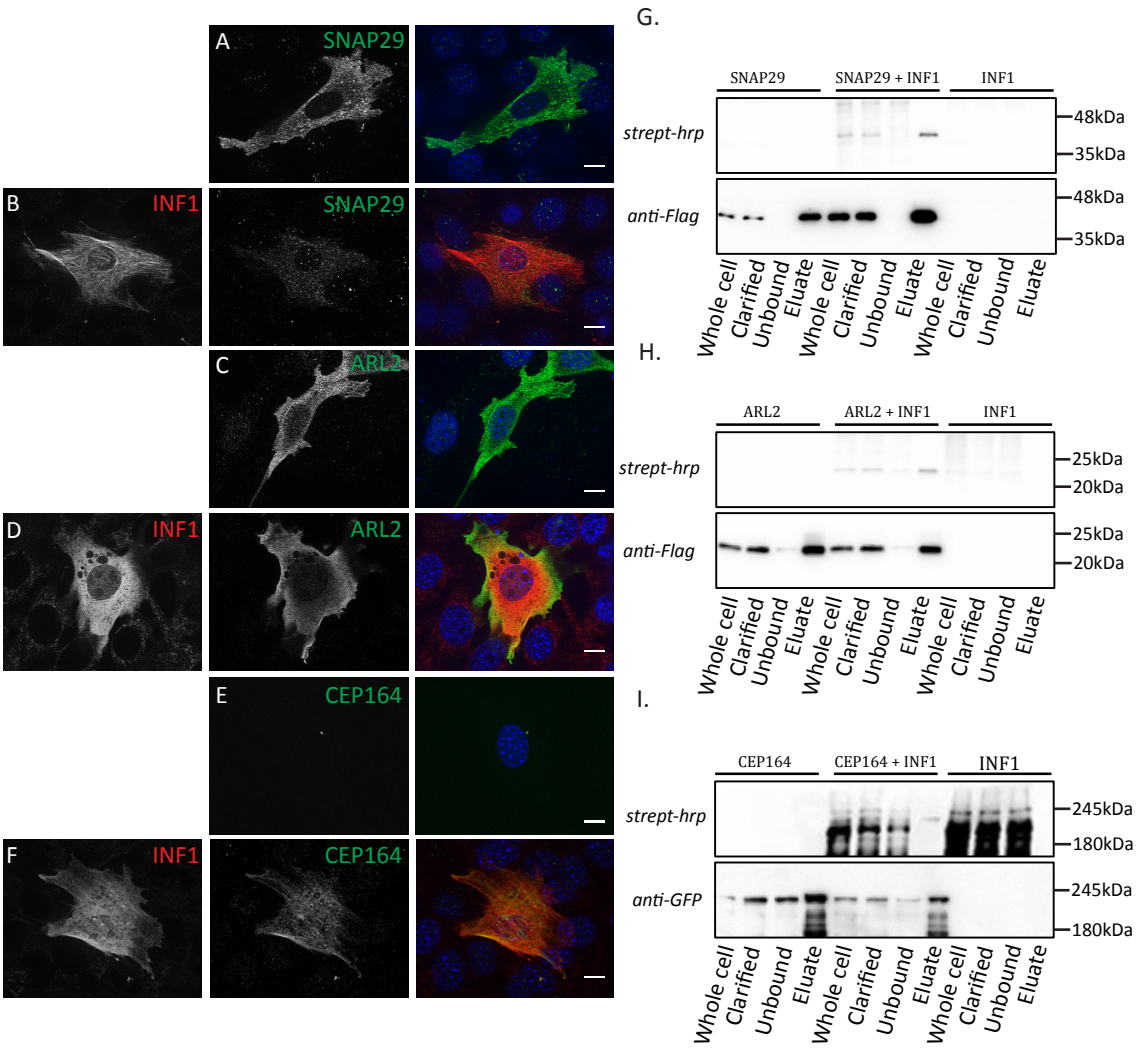

Figure 3.7 SNAP29, Arl2, and Cep164 proximally interact with INF1.
(A-I) The interaction between BirA*-INF1 and the indicated proteins was tested as in figure 3.5. (G) Biotinylated flag-SNAP29, with an expected MW of 44kDa, was detected in the eluate from flag-SNAP29/BirA*-INF1 expressing cells but not in eluates from cells expressing flag-SNAP29 or BirA*-INF1 alone. (H,I) Flag-Arl2, with an expected MW of 21kDa, proximally interacted with INF1 in this assay. A weak band corresponding to GFP-Cep164 with with an anticipated MW of 200kDa was detected in the eluate from GFP-Cep164/BirA*-INF1 expressing cells. (Bar=10µM)

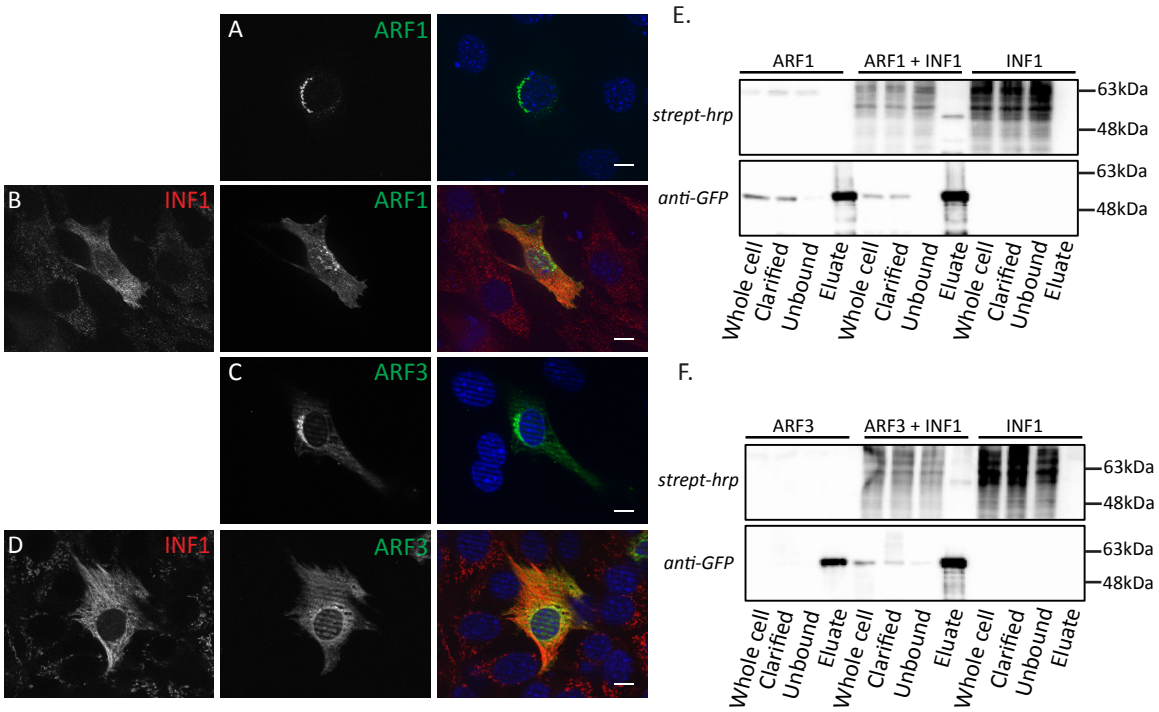

Figure 3.8. The small GTPase, Arf1, is an INF1 proximal interacting protein.
(A-F) The interaction between BirA*-INF1 and the indicated proteins was tested as in figure 3.5. (E) Biotinylated GFP-Arf1 had an expected MW of 54kDa and was detected in the eluate from GFP-Arf1/BirA*-INF1 expressing cells but not in eluates from cells expressing GFP-Arf1 or BirA*-INF1 alone. (F) A faint biotinylated band was present for GFP-Arf3 with an expected MW of 54kDa. (Bar= 10µM)

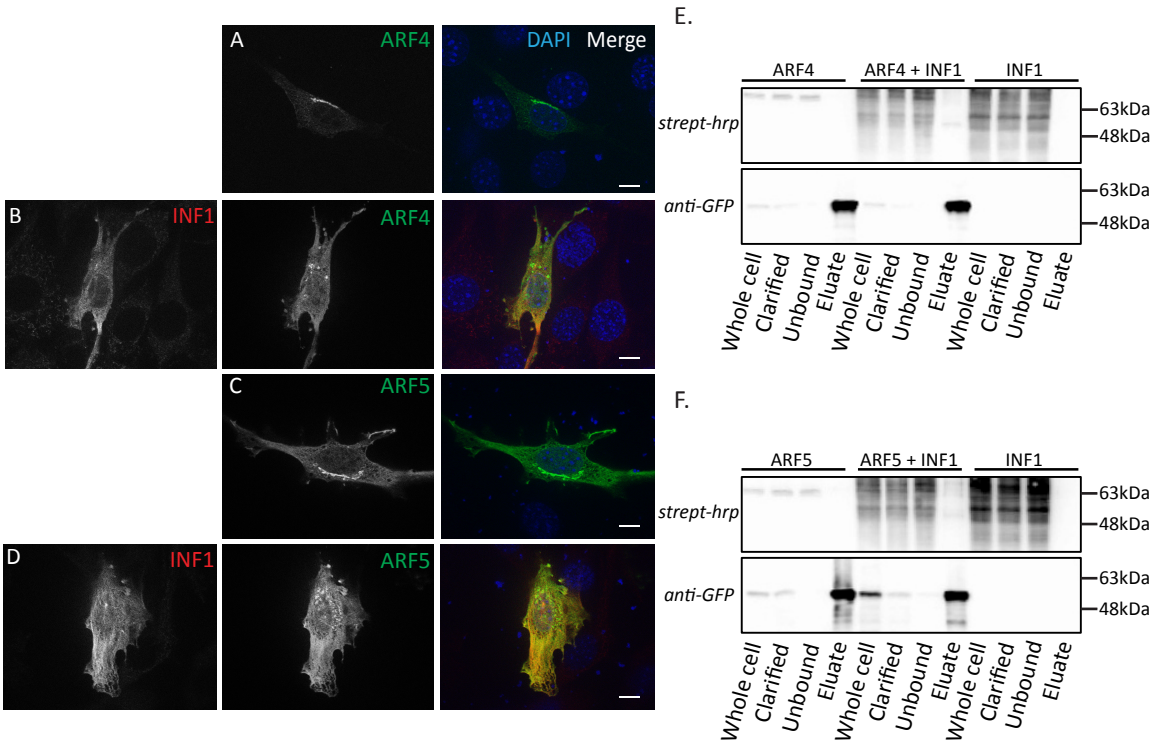

Figure 3.9. The small GTPases Arf4 and Arf5 do not proximally interact with INF1. (A-F) The interaction between BirA*-INF1 and the indicated proteins was tested as in figure 3.5. (E) Weak biotinylated GFP-Arf4 was faintly detected in the eluate at the expected MW of 51kDa from GFP-Arf4/BirA*-INF1 expressing cells but not in eluates from cells expressing GFP-Arf4 or BirA*-INF1 alone. (F) A faint biotinylated band was also present for GFP-Arf5 at the anticipated MW of 51kDa in the eluate lane from GFP-Arf5/BirA*-INF1 expressing cells. (Bar= 10µM)

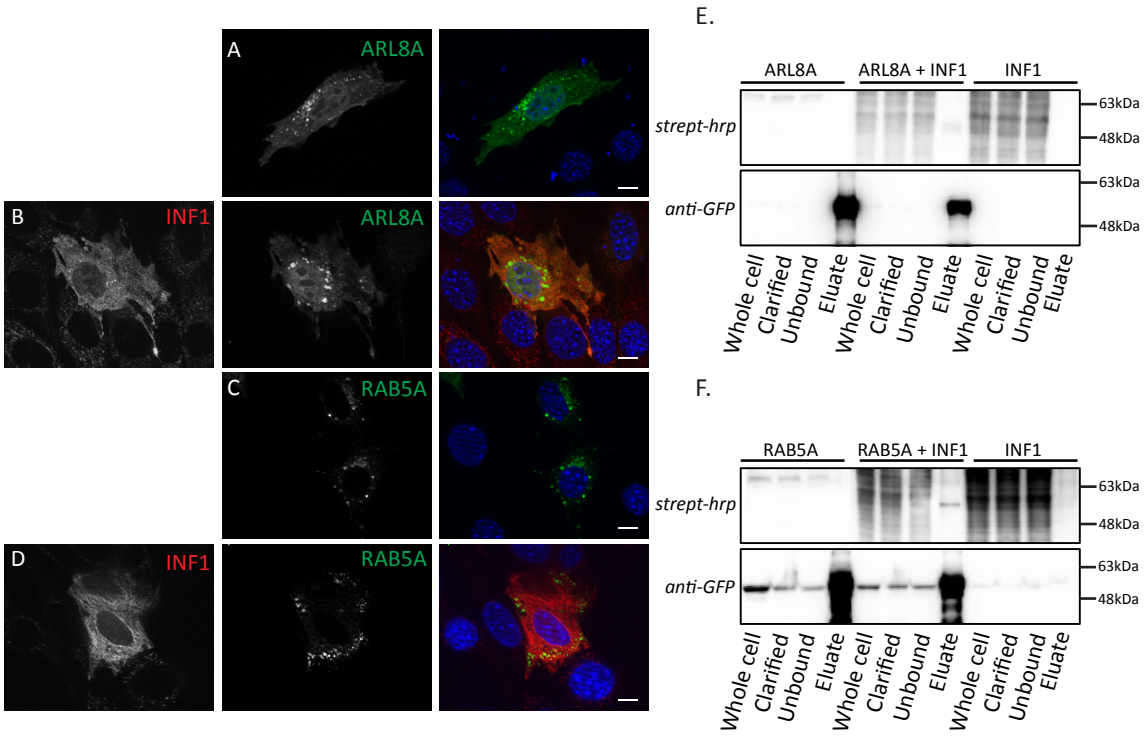

Figure 3.10. Rab5A is an INF1 proximity interacting protein.
(A-F) The interaction between BirA*-INF1 and the indicated proteins was tested as in figure 3.5. (E,F) Strong positive results were obtained for GFP-Rab5A with an anticipated MW of 57kDa, while a weak band was present for GFP-Arl8A with an expected MW of 51kDa. (Bar= 10µM)

The small GTPases Arl8A, Arl8B/10C, Rab1A, Rab14, Rap2B, Rab21, and Arf6 were also tested as described and did not positively validate using the BioID pull-down technique.

3.5 INF1 Interaction Domain Mapping with Validated Proteins

The INF1 domains required for the proximity interaction with profilin2, VASP, EB1, SNAP29, and Cep170 were mapped with the same strategy described in section 3.4 using a series of BirA*-INF1 deletion and point mutation derivatives.

To verify the reported profilin2 interaction with the FH1 domain of formins, the INF1 proximity interaction domain with profilin2 was mapped (Kovar et al., 2006). GFP-PFN2 was co-expressed with BirA*-FL INF1, -FL INF1 I180A, -INF1 ΔFH1, -INF1 485N, and -INF1 485N I180A (Figure 3.11 & 3.12). As expected, the immunoblot of the BioID pull-downs highlighted proximal interactions between GFP-PFN2 and the BirA*-INF1 derivatives that contained the FH1 domain (FL INF1, INF1 I180A, 485N, and 485N I180A). In contrast, GFP-PFN2 did not interact with BirA*-INF1 ΔFH1 (Figure 3.11). Sub-cellular localization of the GFP and streptavidin signals corresponding to the various BirA*-INF1 derivatives complemented the pull-down results.

Similarly, the INF1 proximity interaction domain with VASP was mapped based on the known overlapping interaction with the FH1/FH2 domains of formins (Barzik et al., 2014; Grosse et al., 2003). Flag-VASP was co-expressed with BirA*-FL INF1, -FL INF1 I180A, -INF1 ΔFH1, -INF1 485N, -INF1 485N I180A, and -INF1 FH2 (Figure 3.13 & 3.14). The BioID pull-down and immunoblot analysis showed strong proximity interactions

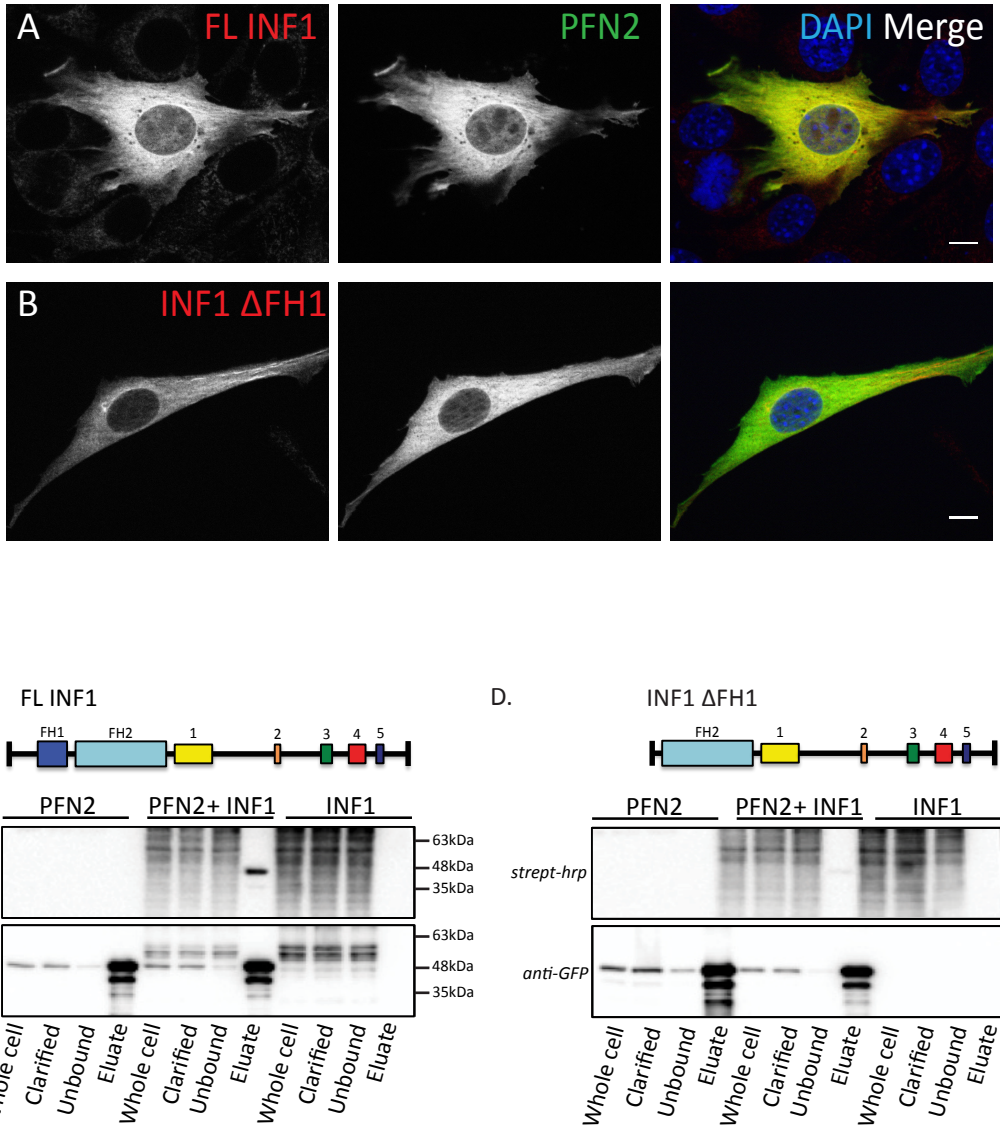

Figure 3.11. The FH1 domain of INF1 is required for its proximal interaction with profilin2.

The INF1 interaction domain was mapped as in the initial validation in figure 3.5 using GFP-tagged PFN2 and various INF1 deletion and point mutation derivatives. (A,B) BirA*-FL INF1 or -INF1 ΔFH1 were co-expressed with GFP-PFN2 by transient transfection in NIH 3T3 cells. Following biotin incubation cells were fixed and stained with fluorophore-tagged streptavidin (red). (C) Biotinylated GFP-PFN2 was detected in the eluate from GFP-PFN2/BirA*-FL INF1 expressing HEK 293T/17 cells but not in eluates from cells expressing GFP-PFN2 or BirA*-FL INF1 alone. The expected MW of GFP-PFN2 was 48kDa, the bands higher than GFP-PFN2 were likely oligmers while the lower bands were likely degradation product or background. (D) Biotinylated GFP-PFN2 was not detected in the eluate from GFP-PFN2/BirA*-INF1 ΔFH1. (Bar =10μM))

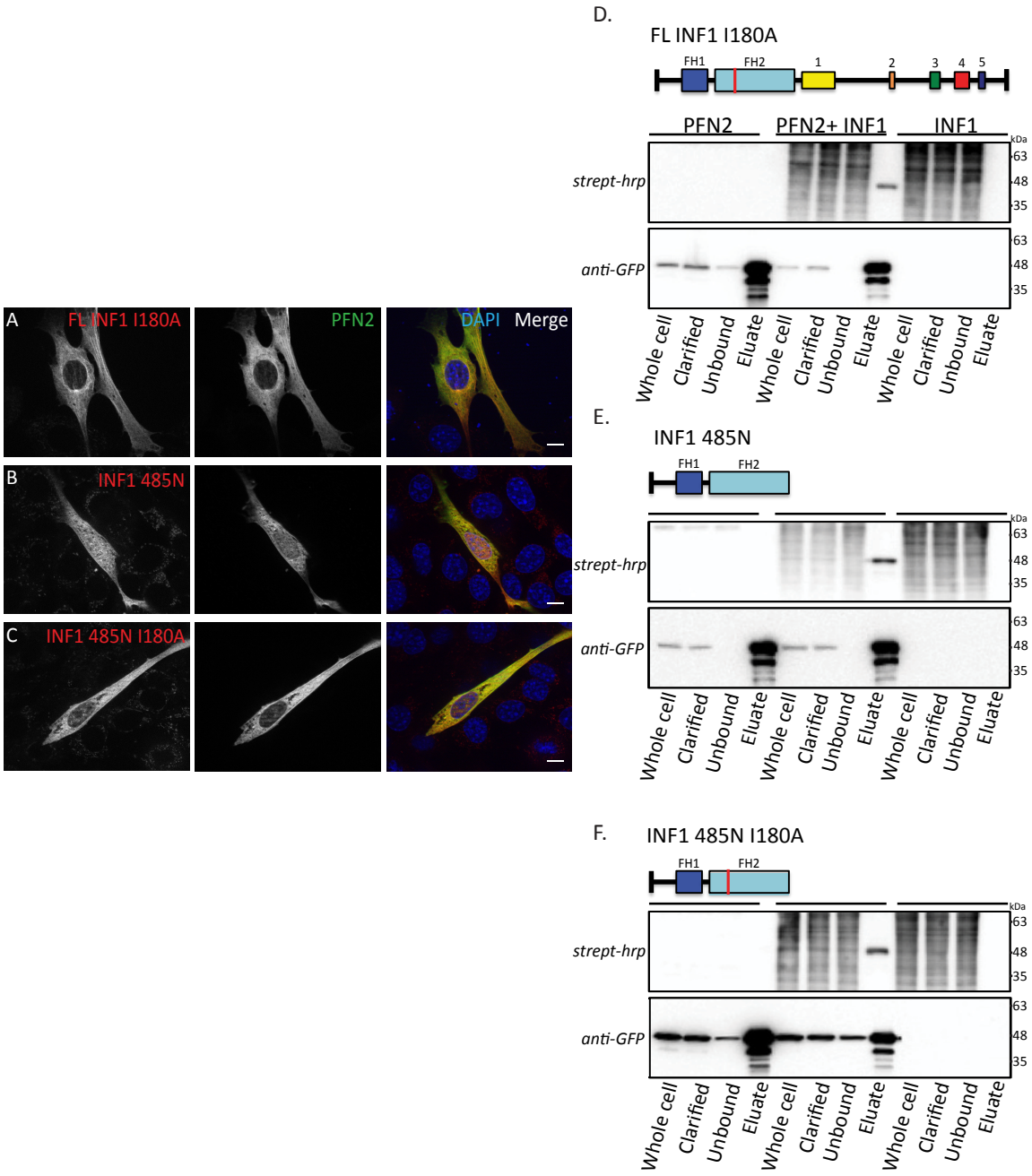

Figure 3.12. The FH1 domain of INF1 is required for its proximal interaction with profilin2.

The interaction domain of INF1 was mapped as in figure 3.5 using GFP-tagged PFN2 and various BirA*-INF1 deletion and point mutation derivatives. (A-C) BirA*-FL INF1 I180A, -INF1 485N, and -INF1 485N I180A were co-expressed with GFP-PFN2 by transient transfection in NIH 3T3 cells. Following biotin incubation cells were fixed and stained with fluorophore-tagged streptavidin (red). Biotinylated GFP-PFN2 was detected in the eluate from GFP-PFN2/BirA*-FL INF1 I180A (D), -INF1 485N (E), and -INF1 485N I180A (F). (Bar = 10µM)

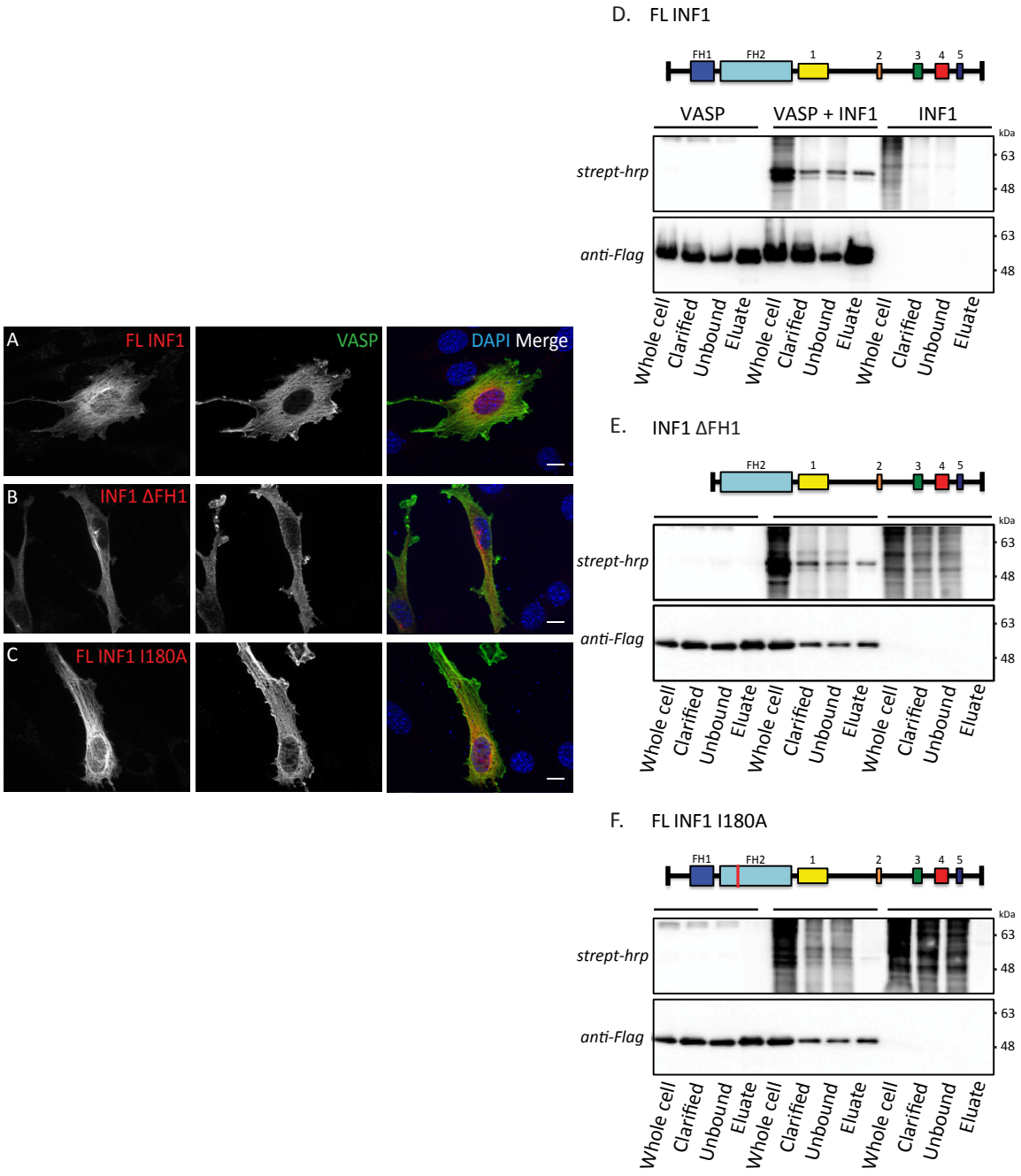

Figure 3.13. Mapping the INF1 proximal interaction domain with VASP.
The interaction domain of BirA*-INF1 was mapped as in figure 3.5 using flag-tagged VASP and various BirA*-INF1 deletion and point mutation derivatives. (A-C) BirA*-FL INF1, -INF1 ΔFH1, and -FL INF1 I180A were co-expressed with flag-VASP in NIH 3T3 cells. Post-biotin treatment cells were fixed and stained with fluorophore-tagged streptavidin (red), and anti-flag (green). (D-F) Biotinylated flag-VASP was detected in the eluate from flag-VASP/BirA*-FL INF1 (D) and -INF1 ΔFH1 (E), but was not present in the eluate from flag-VASP/BirA*-FL INF1 I180A (F). (Bar = 10µM)

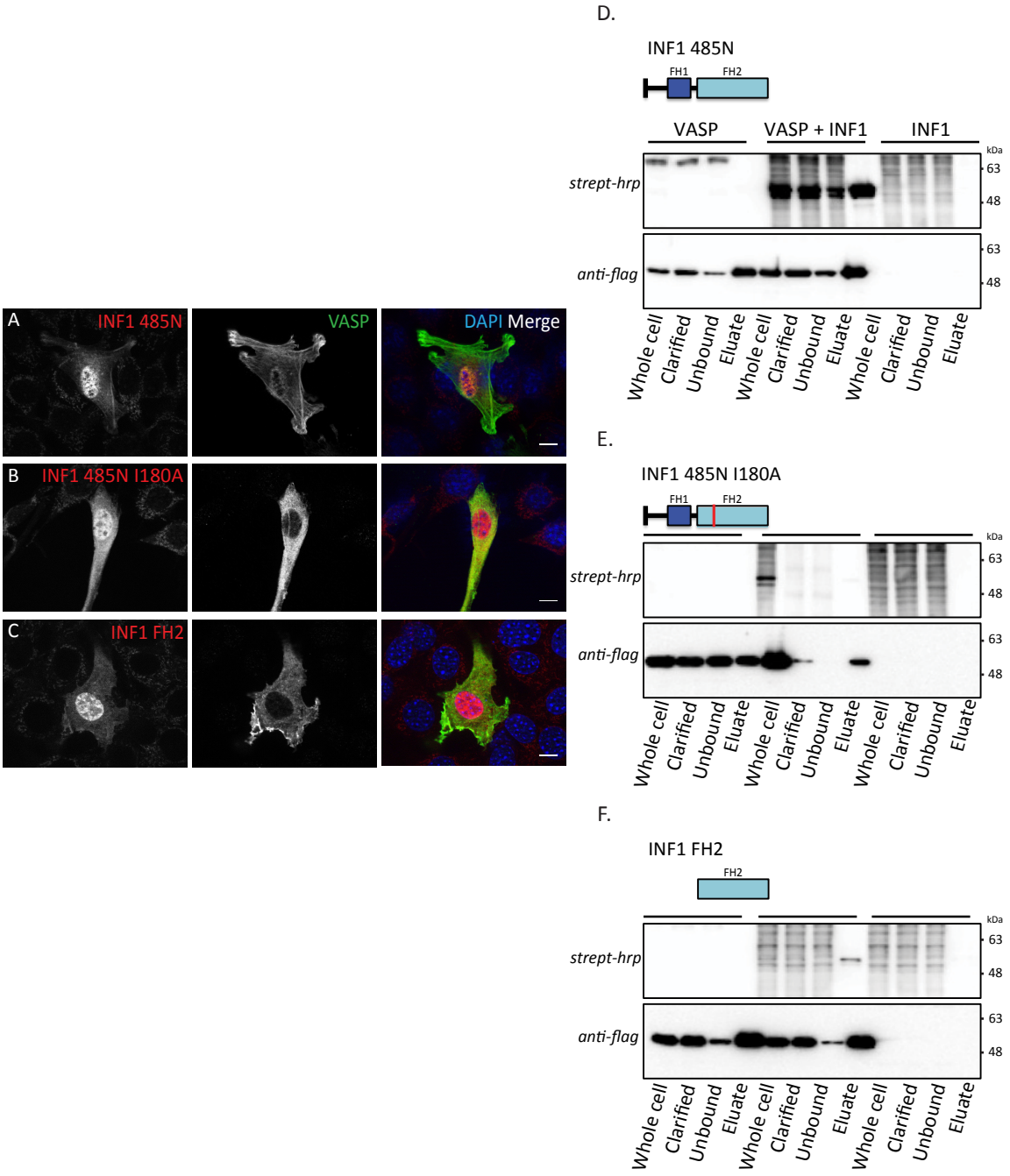

Figure 3.14. The FH2 domain of INF1 is required for its proximal interaction with VASP. The interaction domain of BirA*-INF1 was mapped as in figure 3.5 using flag-tagged VASP and various BirA*-INF1 deletion and point mutation derivatives. (A-C) BirA*-INF1 485N, -INF1 485N I180A, and -INF1 FH2 were co-expressed with flag-VASP in NIH 3T3 cells. Post-biotin treatment cells were fixed and stained with fluorophore-tagged streptavidin (red) and anti-flag (green). (D-F) Biotinylated flag-VASP was detected in the eluate from flag-VASP/BirA*-INF1 485N (D) and -INF1 FH2 (F), however it was not present in the eluate of flag-VASP/BirA*-INF1 485N I180A (E). (Bar=10µM)

between flag-VASP and the BirA*-INF1 derivatives containing the FH2 domain (FL INF1, ΔFH1, 485N, and FH2). In contrast, proximity interactions between flag-VASP and BirA*-FL INF1 I180A, and –INF1 485N I180A were not present (Figure 3.13-14). Localization of the flag and streptavidin signals complemented the pull-down results.

EB1 is shown in the literature to interact with the FH2 domain of formins (Wen et al., 2004). To confirm this the INF1 proximity interaction domain was mapped. GFP-EB1 was co-expressed with BirA*-FL INF1, -FL INF1 I180A, -INF1 ΔFH1, -INF1 958N, -INF1 485N, -INF1 485N I180A, -INF1 486C, -INF1 958C, and -INF1 FH2 (Figure 3.15-17). Immunoblot analysis of the BioID pull-downs indicated GFP-EB1 proximity interaction with the BirA*-INF1 derivatives containing the FH2 domain (FL INF1, ΔFH1, 958N, 485N, FH2), FH1 domain (485N I180A), and MTBD (INF1 I180A, 486C, 958C). Localization of GFP and streptavidin signals complemented the pull-down results.

The INF1 proximity interaction domains required for SNAP29 and Cep170 association were investigated as described. Immunoblot analysis of the BioID pull-downs showed that the proximal interaction between flag-Snap29 and BirA*-INF1 was dependent upon the MTBD (Figure 3.18-20), while the FH2 and MTBD were necessary for proximal interaction between GFP-Cep170 and BirA*-INF1 (Figure 3.21-23).

3.6 INF1 Over-expression Disrupts Centriole Protein Sub-Cellular Localization

The INF1 biotin interactome highlighted numerous SDA (EB1, Cep170) and DA (Cep164, Snap29) proteins. Given the known effects of over-expressed INF1 on ciliogenesis the effects of INF1 on SDA sub-cellular localization was investigated by IFM.

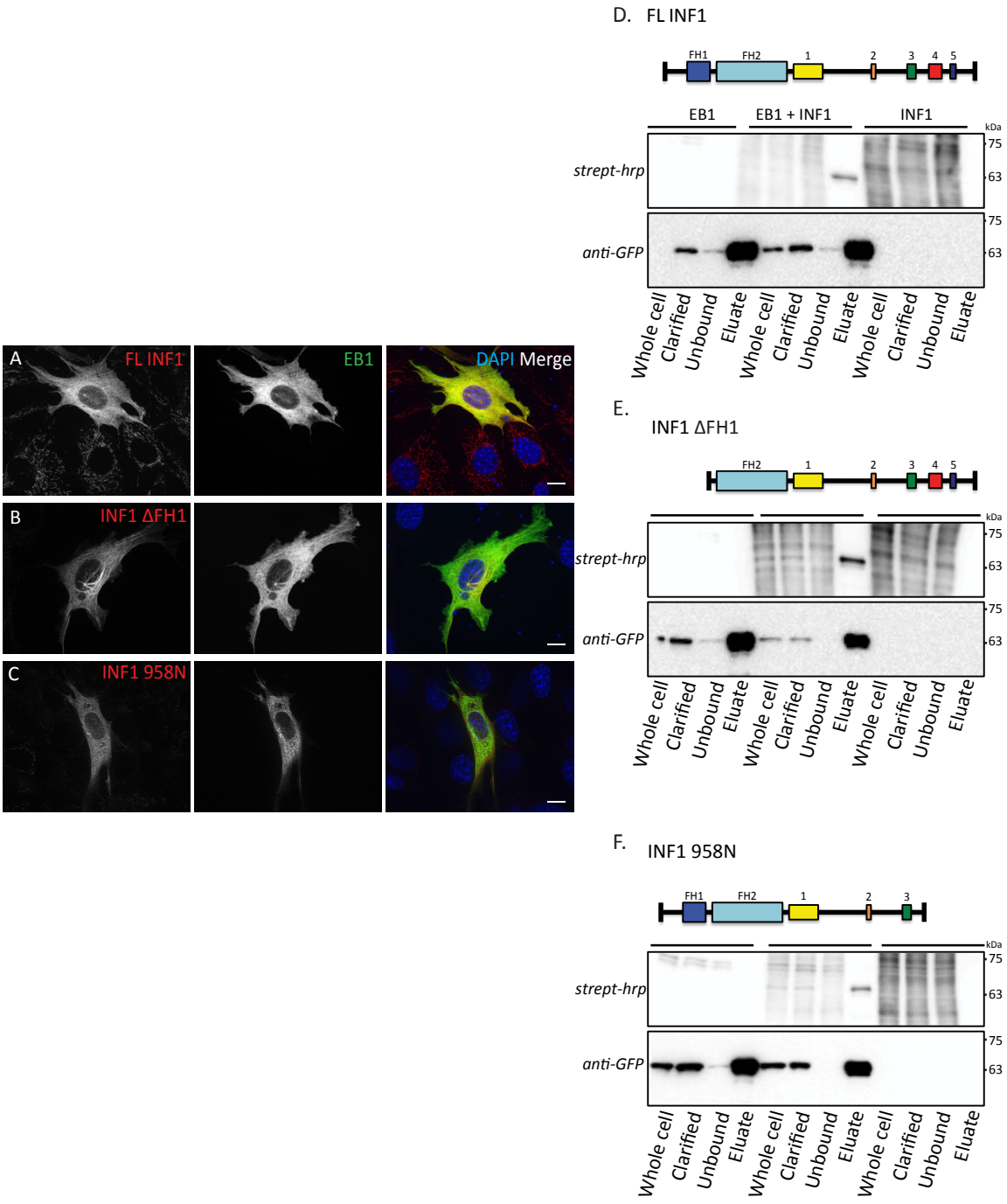

Figure 3.15. Mapping the INF1 promixity interaction domain with EB1.
The interaction domain of BirA*-INF1 was mapped as in figure 3.5 using GFP-tagged EB1 and various BirA*-INF1 deletion and point mutation derivatives. (A-C) BirA*-FL INF1, -INF1 ΔFH1, and -INF1 958N were co-expressed with GFP-EB1 in NIH 3T3 cells. Following biotin treatment cells were fixed and stained with fluorophore-tagged streptavidin (red). (D-F) Biotinylated GFP-EB1 was detected in the eluate from GFP-EB1/BirA*-FL INF1 (D), -INF1 ΔFH1 (E), and -INF1 958N (F). (Bar=10µM)

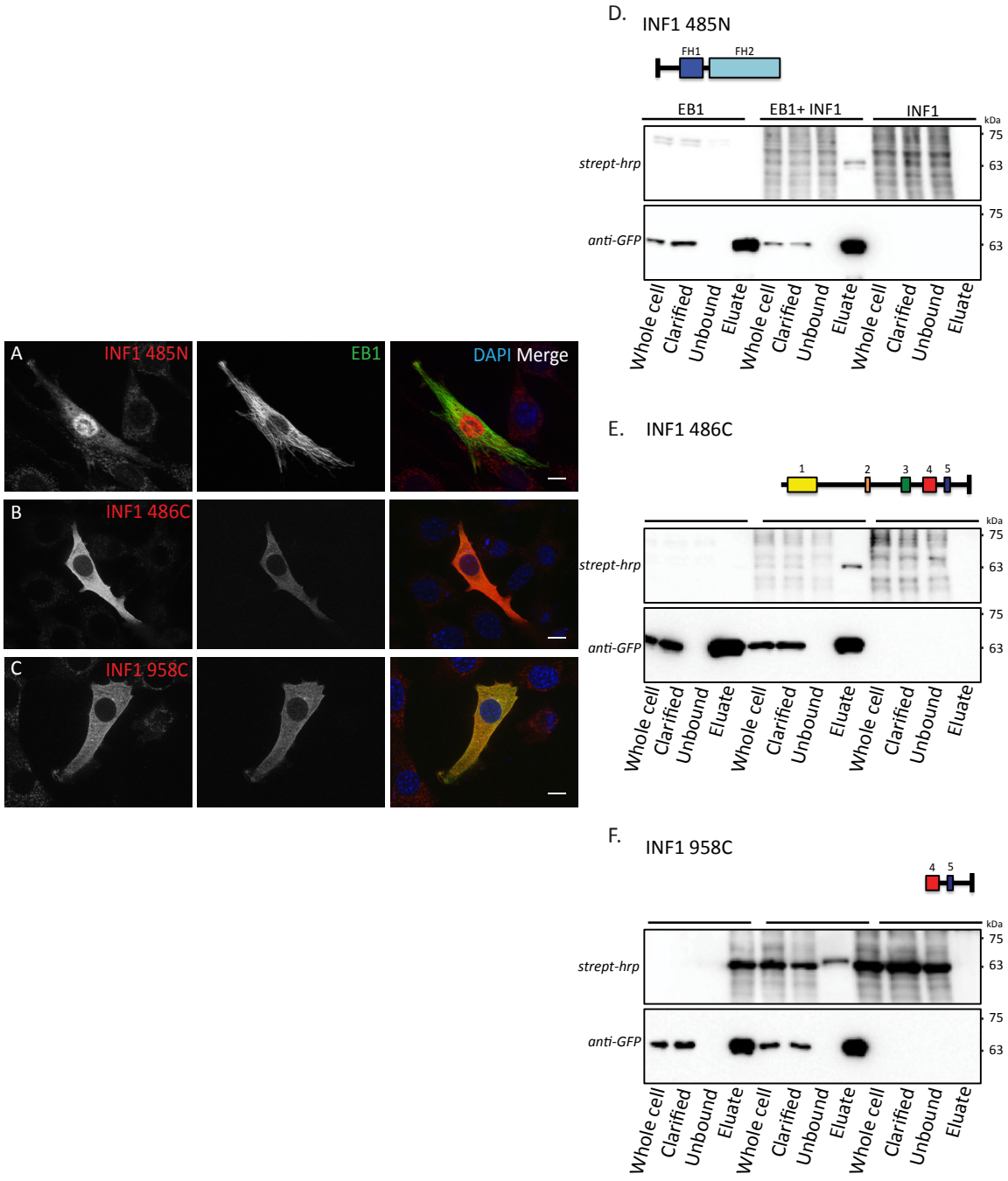

Figure 3.16. The MTBD and FH2 domain of INF1 are required for its proximal interaction with EB1.

The interaction domain of BirA*-INF1 was mapped as in figure 3.5. (A-C) BirA*-INF1 485N, -INF1 486C, and -INF1 958C were co-expressed with GFP-EB1 in NIH 3T3 cells. Biotinylated proteins were detected with fluorophore-conjugated streptavidin (red). (D-F) Biotinylated GFP-EB1 was detected in the eluate from GFP-EB1/BirA*-INF1 485N (D), -INF1 486C (E), and -INF1 958C (F). (Bar=10µM)

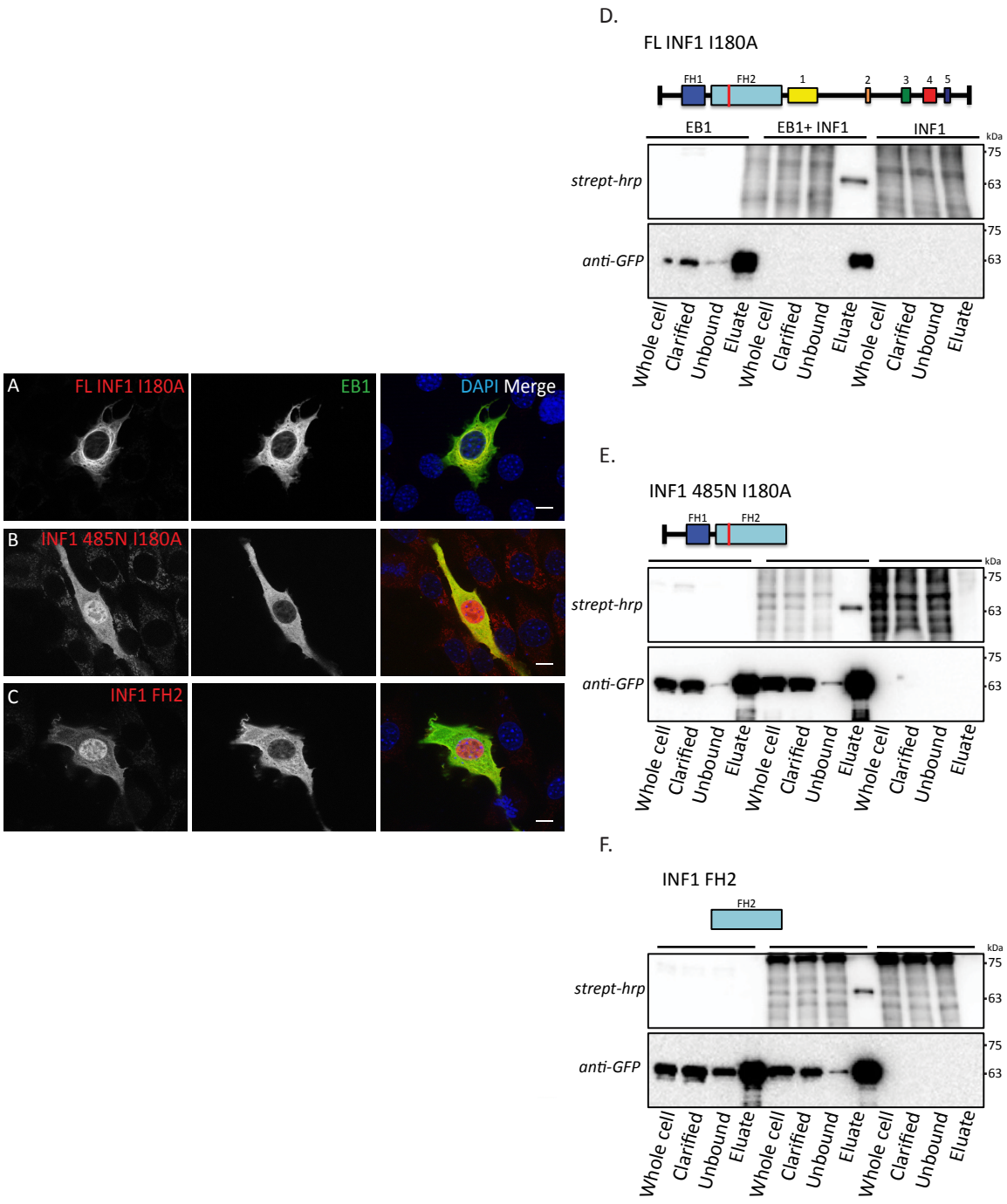

Figure 3.17. The MTBD and FH2 domain of INF1 are required for its proximal interaction with EB1.

The interaction domain of BirA*-INF1 was mapped as in figure 3.11 (A-C) BirA*-FL INF1 I180A, -INF1 485N I180A, -INF1 FH2 were co-expressed with GFP-EB1 in NIH 3T3 cells. Biotinylated proteins were detected with fluorophore-tagged streptavidin (red). (E-F) Biotinylated GFP-EB1 was detected in the eluate from GFP-EB1/BirA*-FL INF1 I180A (D), -INF1 485N I180A (E), and -INF1 FH2 (F). (Bar=10µM)

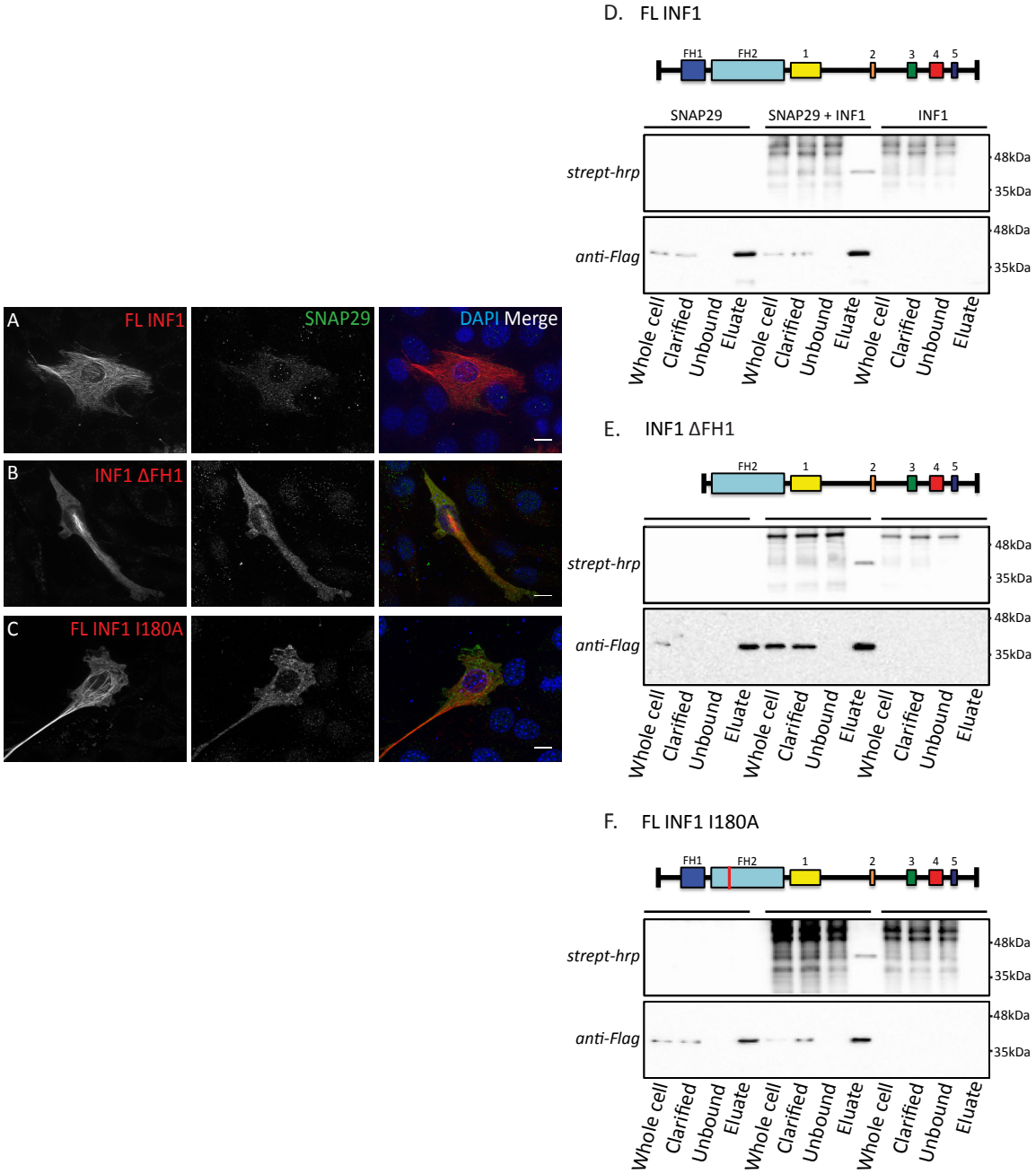

Figure 3.18. The FH1/FH2 domains of INF1 are not required for its proximal interaction with SNAP29.

The interaction domain of BirA*-INF1 was mapped as in figure 3.5 using flag-tagged SNAP29 and various BirA*-INF1 point mutation and deletion derivatives. (A-C) BirA*-FL INF1, -INF1 ΔFH1, and -FL INF1 I180A were co-expressed with flag-SNAP29 in NIH 3T3 cells. Following biotin treatment cells were fixed and stained with fluorophore-tagged streptavidin (red) and anti-flag (green). (D-F) Biotinylated flag-SNAP29 was detected in the eluate from flag-SNAP29/BirA*-FL INF1 (D), -INF1 ΔFH1 (E), and -FL INF1 I180A (F). (Bar=10μM)

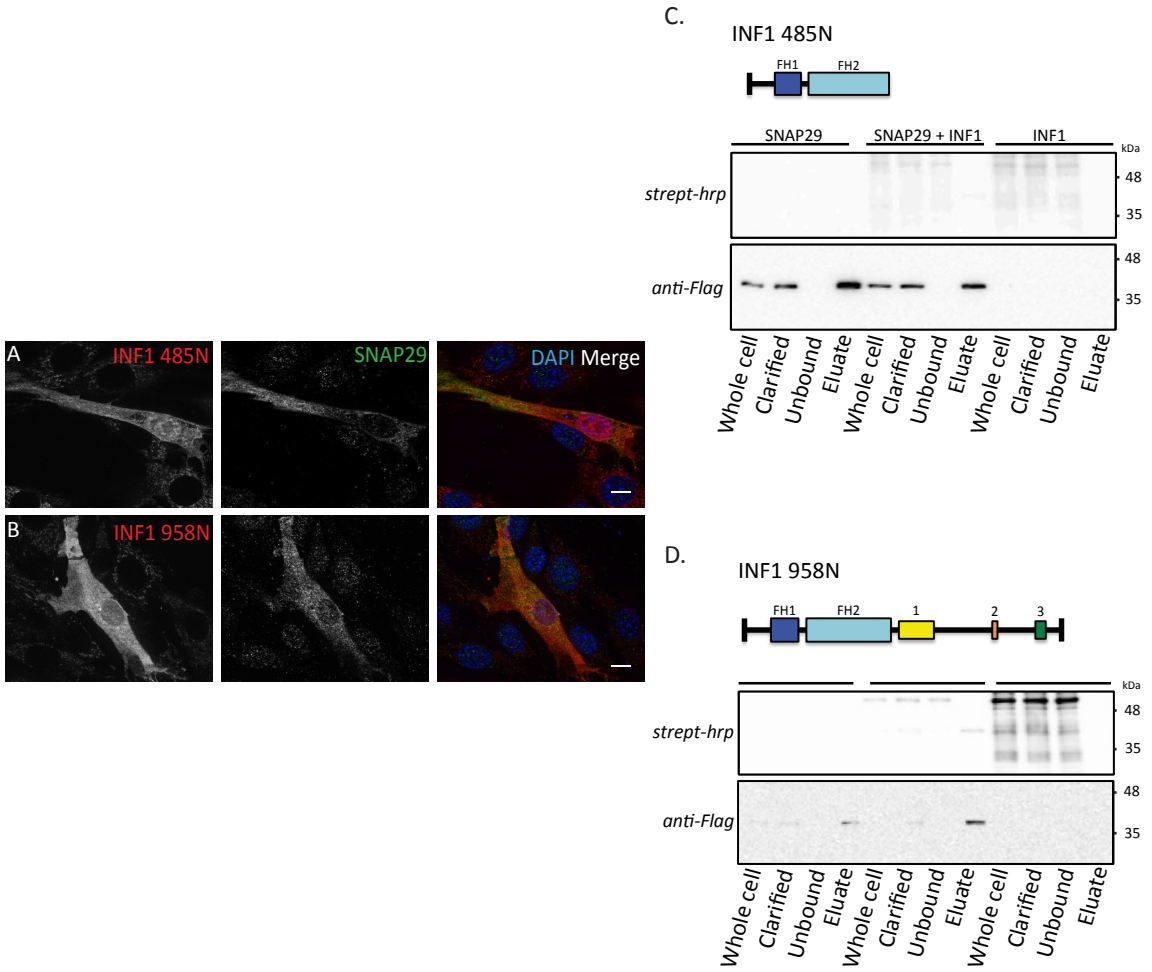

Figure 3.19. The C-terminal of INF1 is required for its proximal interaction with SNAP29.

The interaction domain of BirA*-INF1 was mapped as in figure 3.5 using flag-tagged SNAP29 and various BirA*-INF1 point mutation and deletion derivatives. (A,B) BirA*-INF1 485N and -INF1 958N were co-expressed with flag-SNAP29 in NIH 3T3 cells. Following biotin treatment cells were fixed and stained with fluorophore-tagged streptavidin (red) and anti-flag (green). (C,D) Weak biotinylated flag-SNAP29 was detected in the eluate from flag-SNAP29/BirA*-INF1 958N (D), however it was not present in the eluate from flag-SNAP29/BirA*-INF1 485N (C). (Bar=10µM

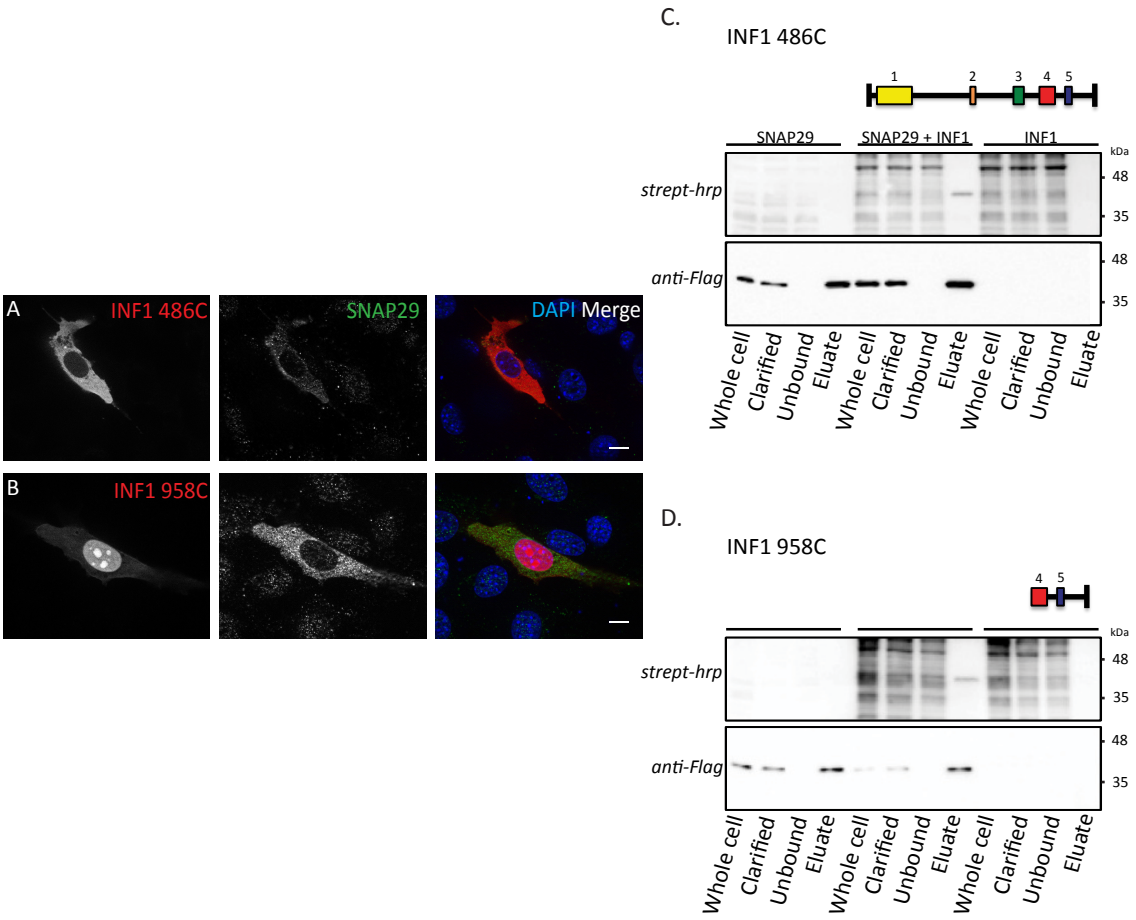

Figure 3.20. The MTBD of INF1 is required for its proximal interaction with SNAP29. The interaction domain of BirA*-INF1 was mapped as in figure 3.5 using flag-tagged SNAP29 and various BirA*-INF1 point mutation and deletion derivatives. (A,B) BirA*-INF1 486C, and -INF1 958C were co-expressed with flag-SNAP29 in NIH 3T3 cells. Post-biotin treatment cells were fixed and stained with fluorophore-tagged streptavidin (red) and anti-flag (green). (C,D) Biotinylated flag-SNAP29 was detected in the eluate from flag-SNAP29/BirA*-INF1 486C (C), and -INF1 958C (E). (Bar=10µM)

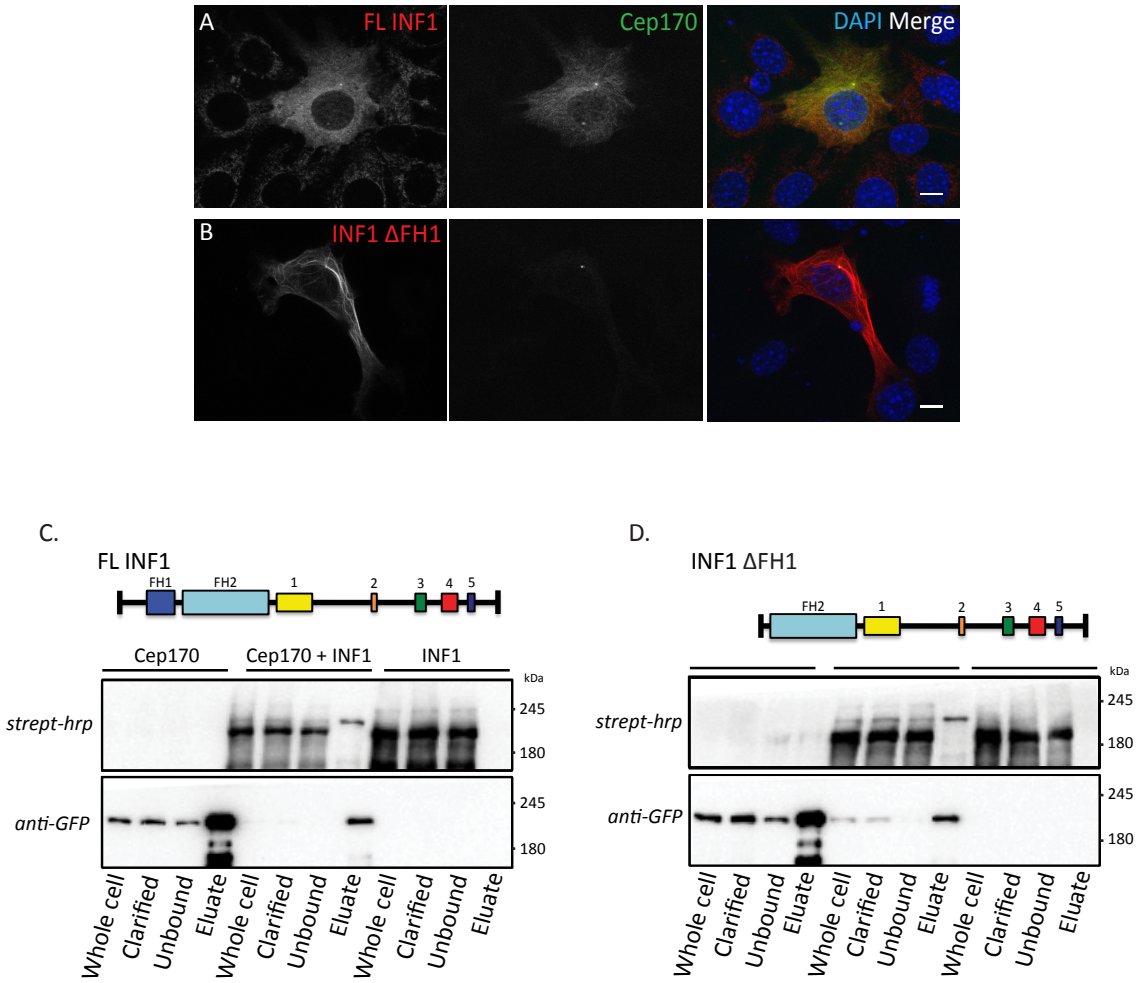

Figure 3.21. The FH1 domain of INF1 is not required for its proximal interaction with Cep170.

The interaction domain of BirA*-INF1 was mapped as in figure 3.5 using GFP-tagged Cep170 and various BirA*-INF1 point mutation and deletion derivatives. (A,B) BirA*-FL INF1, and -INF1 ΔFH1 were co-expressed with GFP-Cep170 in NIH 3T3 cells. Post-biotin treatment cells were fixed and stained with fluorophore-tagged streptavidin (red). (C,D) Biotinylated GFP-Cep170 was present in the eluate from GFP-Cep170/BirA*-FL INF1 (C), and -INF1 ΔFH1 (D). (Bar=10µM)

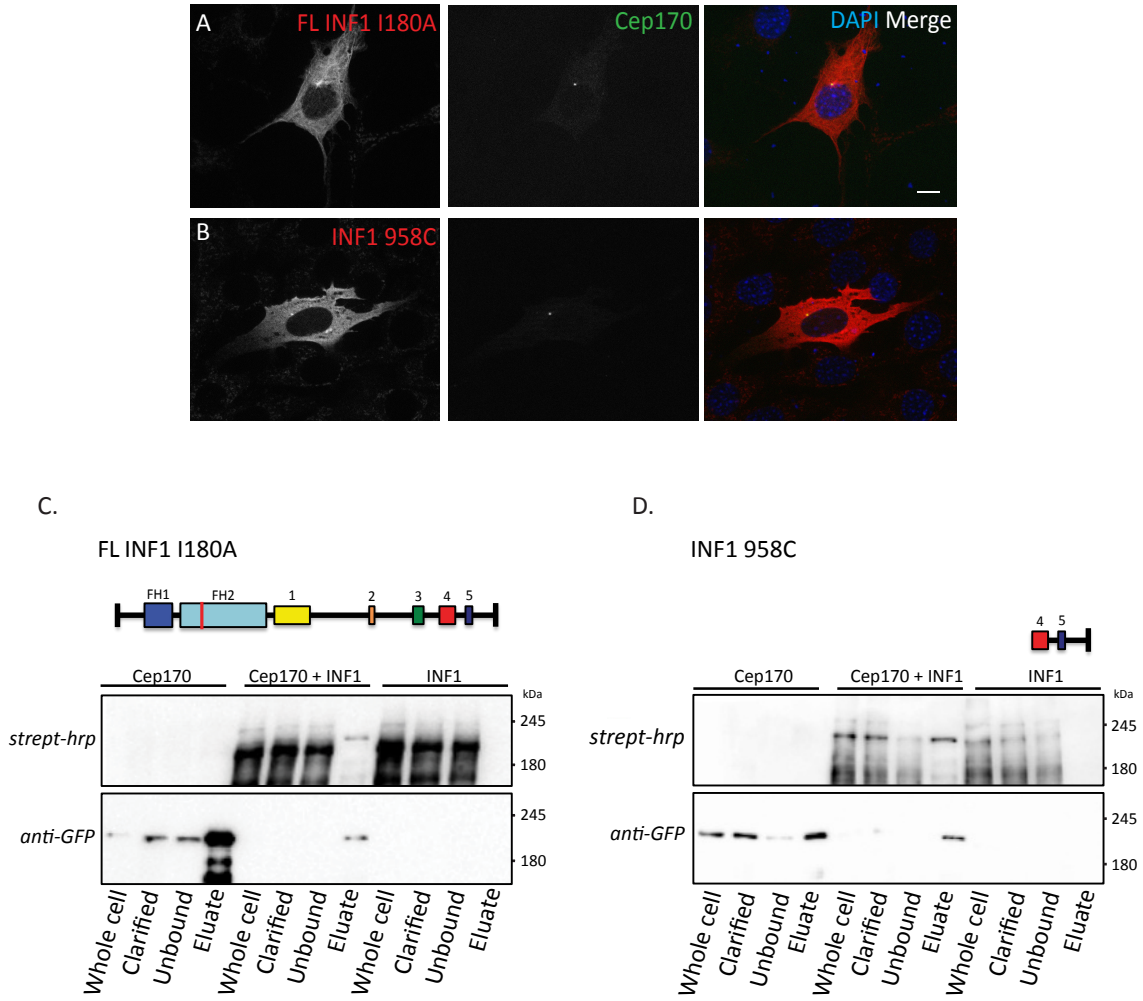

Figure 3.22. The MTBD and FH2 domain of INF1 are required for its proximal interaction with Cep170.

The interaction domain of BirA*-INF1 was mapped as in figure 3.5 using GFP-tagged Cep170 and various BirA*-INF1 point mutation and deletion derivatives. (A,B) BirA*-FL INF1 I180A, and -INF1 958C were co-expressed with GFP-Cep170 in NIH 3T3 cells. Post-biotin treatment cells were fixed and stained with fluorophore-tagged streptavidin (red). (C,D) Biotinylated GFP-Cep170 was present in the eluate from GFP-Cep170/BirA*-FL INF1 (C), and -INF1 ΔFH1 (D). (Bar=10µM)

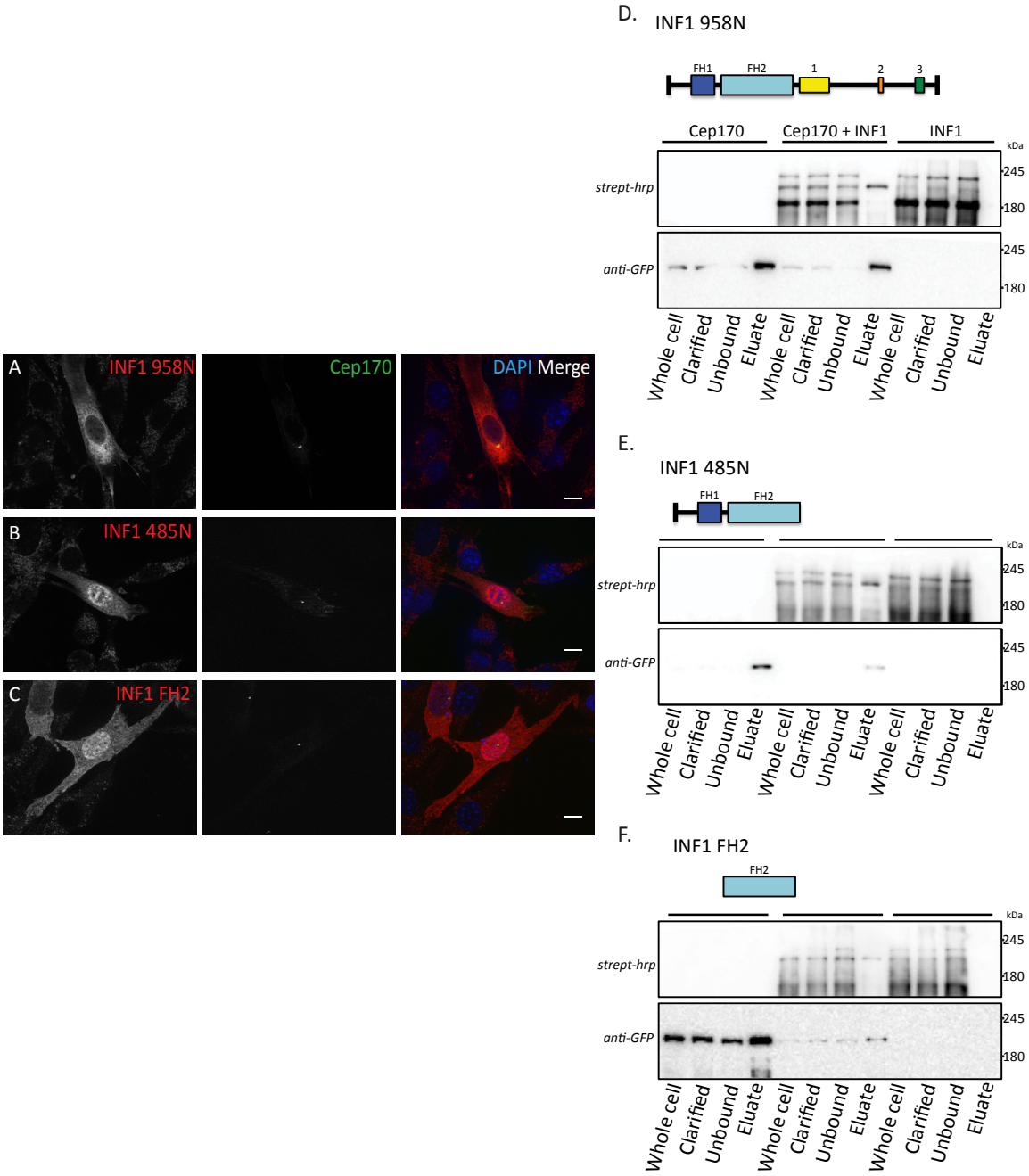

Figure 3.23. The MTBD and FH2 domain of INF1 are required for its proximal interaction with GFP-Cep170.

The interaction domain of BirA*-INF1 was mapped as in figure 3.5 using GFP-tagged Cep170 and various BirA*-INF1 point mutation and deletion derivatives. (A-C) BirA*-INF1 958N, -INF1 485N, and -INF1 FH2 were co-expressed with GFP-Cep170 in NIH 3T3 cells. Post-biotin treatment cells were fixed and stained with fluorophore-tagged streptavidin (red). (D-F) Biotinylated GFP-Cep170 was present in the eluate of GFP-Cep170/BirA*-INF1 958N (D). Weak biotinylated GFP-Cep170 was present in the eluate of GFP-Cep170/BirA*-INF1 485N (E), and -INF1 FH2 (F). (Bar=10µM)

GFP-Cep170 was co-expressed with epitope tagged FL INF1 under ciliogenic conditions. Flag-FL INF1 I180A and mCherry were co-expressed with GFP-Cep170 as controls. The percent of ciliated and non-ciliated cells were quantified in terms of the number of GFP-Cep170 puncta present per cell.

In the majority of control cells (FL INF1 I180A & mCherry) one Cep170 puncta localized to the base of the cilia as expected (Figure 3.24). It was also noted that FL INF1 I180A accumulated on a set of acetylated MTs that converge at the basal body (Figure 3.24 (B)). In contrast, the majority of FL INF1 over-expressing cells did not assemble cilia and no Cep170 puncta were detected in these cells. Where cilia were present, one Cep170 puncta was present at its base. Thus inhibition of cilia formation by INF1 correlates with the apparent loss of Cep170 from the basal body.

To confirm this result we also tested the effects of INF1 over-expression on the localization of the centriole marker, centrin2 (CENT2), that is present on both mother and daughter centrioles. Epitope-tagged FL INF1 was co-expressed with GFP-centrin2 under ciliogenic conditions for IFM analysis. In the majority of control cells (FL INF1 I180A & mCherry), two CETN2 puncta were present, with one puncta at the base of the cilia and the other in close proximity, typically <0.8µm away (Figure 3.25). In contrast, the majority of FL INF1 over-expressing cells did not assemble cilia and multiple CETN2 puncta, or two puncta >1.6µm apart were observed. Where cilia were present, the majority of cells had two centrioles >1.6µm apart with one centriole at the base of the elongated cilia.

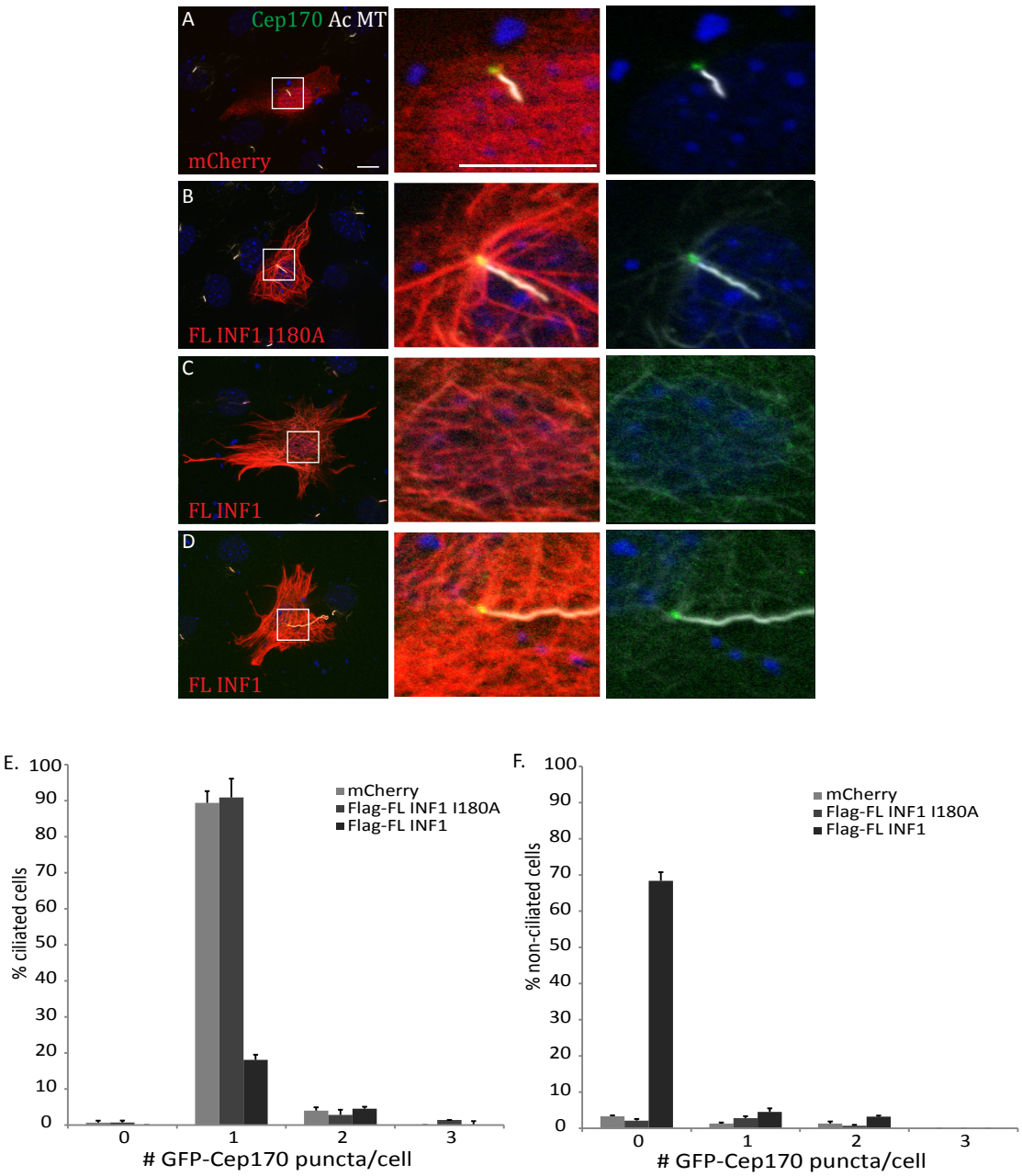

Figure 3.24. INF1 over-expression disrupts GFP-Cep170 sub-cellular localization. GFP-Cep170 was co-expressed with either flag-FL INF1, flag-FL INF1 I180A, or mCherry in NIH 3T3 cells under ciliogenic conditions. The cells were fixed and the cilia were stained with anti-acetylated tubulin (white), while anti-flag detected the flag epitope of the INF1 derivatives (red). (B) GFP-Cep170 was recruited to the basal body in control, FL INF1 I180A and mCherry expressing cells. Note the acetylated MTs bound by FL INF1 I180A that converge at the centrosome. (C) No GFP-Cep170 puncta were observed in cells co-expressing INF1 with no cilia present. Alternatively, Cep170 appears to be recruited to the cytoplasmic MTs. (D) A single GFP-Cep170 puncta was observed in ciliated INF1 over-expressing cells at the base of the cilia. The percent of ciliated (E) or non-ciliated (F) transfected cells with the number of GFP-Cep170 puncta present per cell were quantified. (N=3, 100 cells/experiment, error bars = SEM, scale bar = 10µM)

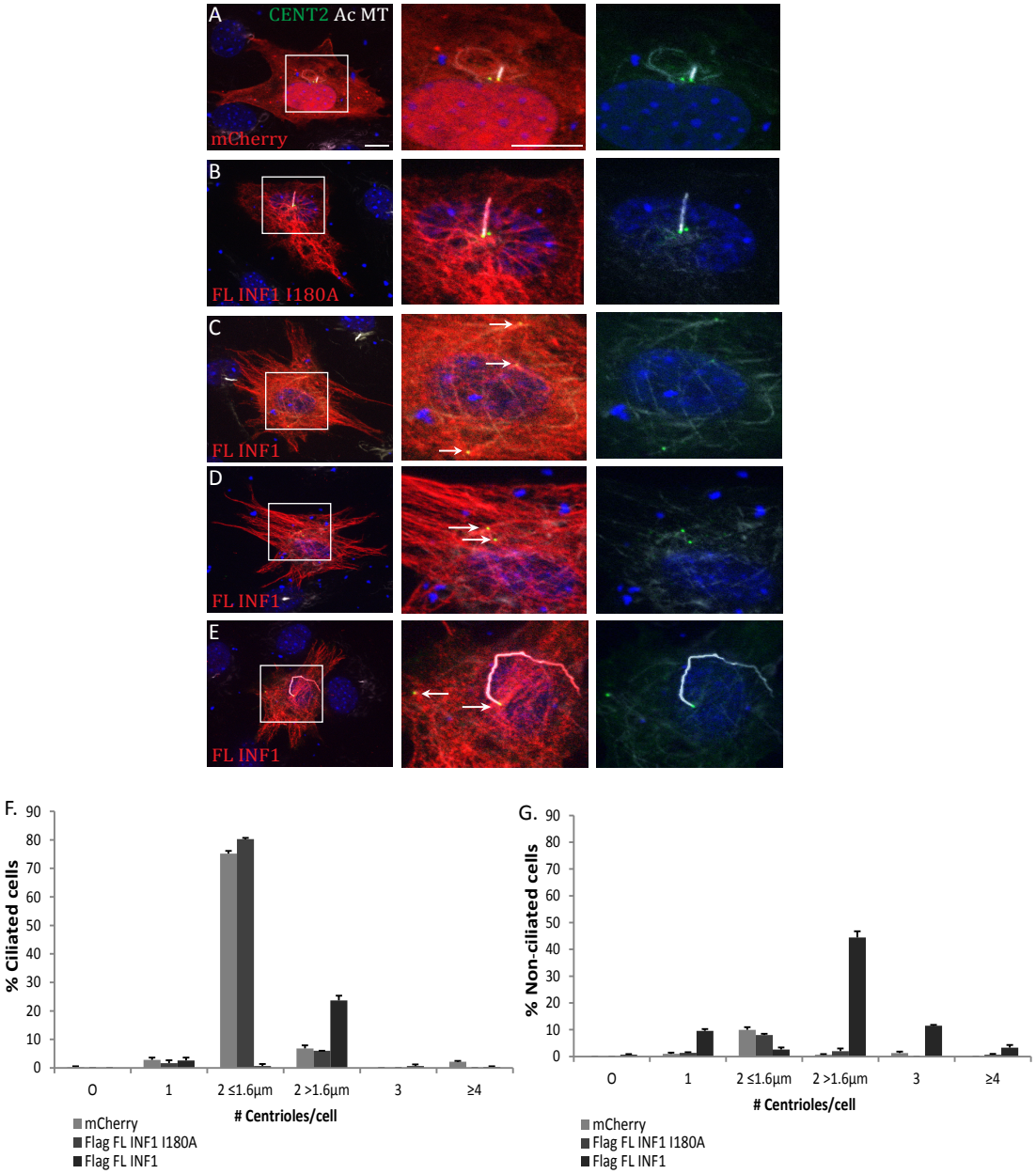

Figure 3.25. INF1 over-expression disrupts GFP-CENT2 sub-cellular localization. GFP-Centrin2 was co-expressed with either flag-FL INF1, flag-FL INF1 I180A, or mCherry in NIH 3T3 cells under ciliogenic conditions. The cells were fixed and the cilia were stained with anti-acetylated tubulin (white), while anti-flag detected the flag epitope of the INF1 derivatives (red). (A, B) In control, flag-FL INF1 I180A and mCherry expressing cells GFP-CETN2 was recruited to the daughter and mother centrioles in close proximity as expected. The CETN2 puncta of the mCherry expressing cells had an average distance of 0.8µM. (C) In cells over-expressing INF1 with no cilia present, CENT2 was recruited to both the centrioles >1.6µM apart. (D) In ciliated INF1 over-expressing cells one CENT2 puncta was recruited to the base of the cilia while the other was distanced. The percent of ciliated (E) and non-ciliated (F) transfected cells with the number of centrioles present per cell were quantified. (N=3, 100 cells/experiment, error bars = SEM, scale bar = 10µM)

Chapter 4: Discussion

INF1 plays a central role regulating cytoskeletal dynamics, Golgi morphology, and ciliogenesis. We hypothesized that, as part of its function, INF1 must interact with unknown targets that allow it to affect these diverse processes. The factors that mediate these effects of INF1 are unknown. Using a new proximity-labeling technique, BioID, I identified a number of putative INF1 binding proteins that likely mediate the effects of INF1 on ciliogenesis.

4.1 BioID SILAC AP/MS to Identify New INF1 Interacting Proteins

Previous attempts in our laboratory to affinity capture INF1 using gentle cell lysis had proven unsuccessful, perhaps due to its association with insoluble structures in the cell. This problem makes the BioID technique a particularly attractive approach. BioID labeling offers numerous advantages over traditional affinity purification/mass spectrometry approaches in that it is not reliant on preservation of fragile protein complexes during protein purification. Instead, once the covalent biotin tag is in place, harsh purification conditions can be used to isolate difficult to extract proteins (Roux, 2013). The promiscuous biotin ligase (BirA*) also facilitates the capture of transient, indirect, and direct protein interactions (Roux, 2013).

4.2 INF1 Proximally Interacts with Known Formin-Binding Proteins

The known formin-binding proteins, profilin2 and VASP, were identified by our BioID SILAC AP/MS screen and were validated as INF1 proximity interacting proteins

demonstrating the specificity and utility of the BioID technique. As expected, the INF1 proximity interaction with profilin2 required the FH1 domain, while VASP required the FH1/FH2 domains of INF1. Profilin is well established in the literature as a formin-binding protein that interacts specifically with the FH1 domain necessary for mediation of actin nucleation and elongation (Sagot et al., 2002). The interaction of the FH1/FH2 domains of INF1 with VASP is consistent with previous reports of Ena/VASP interactions with formin proteins (Barzik et al., 2014). In the future, it would be of interest to investigate the effects of the INF1 proximity interacting proteins, profilin2 and VASP, on INF1-regulated actin dynamics.

4.3 INF1 Acts at the SDAs of the Basal Body

Cep170 was identified and validated as an INF1 proximity interacting partner. INF1 over-expression disrupted GFP-Cep170 sub-cellular localization in non-ciliated cells suggesting that INF1 over-expression disrupts the SDAs (Guarguaglini et al., 2005). We also see over-expressed FL INF1 and FL INF1 I180A recruited to a subset of acetylated microtubules that converge on GFP-Cep170 and the basal body in ciliated cells. This suggests a model where INF1 acts as a part of a complex with Cep170 at the SDAs to anchor the basal body to the microtubule network (Figure 4.1). INF1 over-expression also disrupts the sub-cellular localization of GFP-centrin2. The distanced centrin2 puncta in non-ciliated and ciliated cells suggests that INF1 over-expression disrupts the link between the mother and daughter centrioles causing centriole disengagement that

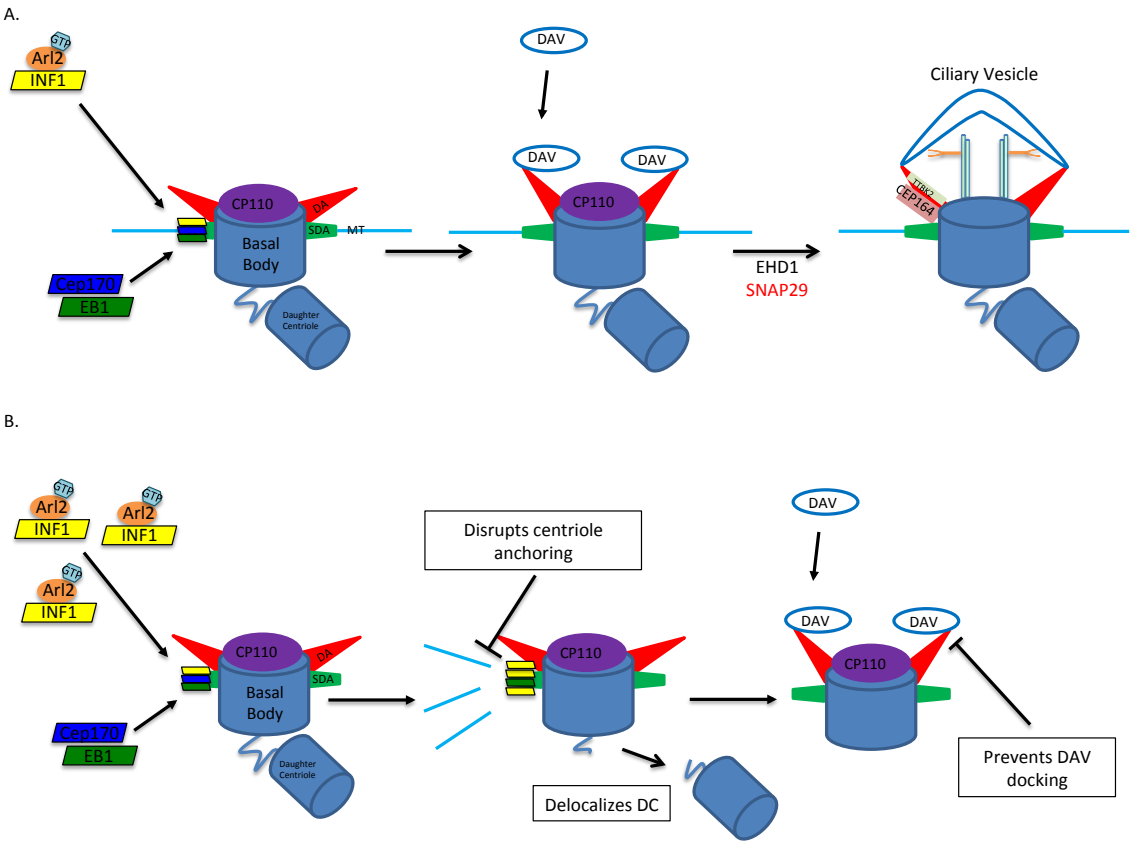

Adapted from Wei et al, Current Opinions Cell Biology, 2015

Figure 4.1. INF1 over-expression inhibits ciliogenesis.
(A) INF1 is recruited to the base of cilium by activated Arl2. INF1 acts as part of an EB1/INF1/Cep170 complex linking MTs to the SDA anchoring the basal body and permitting initiation of cilia biogenesis (B) INF1 over-expression disrupts the SDA complex inhibiting basal body anchoring. INF1 over-expression causes severing of the tight link between mother and daughter centrioles. INF1 over-expression also prevents DAV docking thus EHD1 and SNAP29 cannot shape and fuse the DAVs to form the ciliary vesicle essential to axoneme elongation and generation of the cilium. MTs, microtubules; SDA, sub-distal appendage; DAV, distal appendage vesicles.

The disruption of GFP-Cep170 and –centrin2 localization suggests that INF1 over-expression inhibits centrosome maturation.

EB1 was also validated as a proximity interacting protein of INF1. As with profilin and VASP, there is precedence in the literature for EB1/formin interactions, in this case mediated by the FH2 domain (Cheng and Mao, 2011). EB1 stabilizes microtubules and is required during primary cilium assembly to anchor the basal body to the cytoplasmic microtubules. This provides further support for our model where INF1 forms a complex with EB1 and Cep170 to bind and stabilize microtubules at the basal body (Figure 4.1) (Louie et al., 2004). The validation of EB1 also supports a role for INF1 over-expression in the disruption of the EB1/INF1/Cep170 complex and its function at the basal body.

Cep164 and SNAP29 were validated as INF1 proximity interaction partners. The weak INF1 proximity interaction with the DA protein, Cep164, supports INF1 localization to the base of the cilium (Graser et al., 2007). SNAP29 functions in ciliary vesicle assembly by fusing tubulated distal appendage vesicles suggesting a role for INF1 as a recruitment tool for SNAP29 to the DAs (Lu et al., 2015). INF1 over-expression may directly target or cause downstream disruption of the vesicle-docking site where SNAP29 helps form the ciliary vesicle (Figure 4.1) Alongside the localization of SNAP29 and INF1 to the base of the cilia, they are also known to localize to the Golgi, further supporting their proximal interaction (Lu et al., 2015; Copeland et al., 2015; Copeland et al., manuscript in prep). Interestingly, in SNAP29 deficient cells the Golgi acquires a dispersed morphology similar to that induced by knock down of INF1 (Rapaport et al.,

2010; Copeland et al., 2015). This suggests a role for SNAP29 as either a recruitment tool for INF1 or a target for INF1-induced Golgi dispersion.

The small GTPase, Arl2, was validated as an INF1 proximity interaction protein. Arl2 is known to recruit or anchor proteins to the base of the cilium, and depletion of Arl2 displaces proteins from the basal body (Davidson et al., 2013). This suggests a model where Arl2 acts to recruit INF1 to the base of the cilium, although we cannot rule out the possibility that INF1 acts upstream of Arl2 (Figure 4.1).

4.4 INF1 Extends the Axoneme of the Primary Cilium

The INF1 proximity interaction with Cep170 suggests that over-expressed INF1-induced inhibition of ciliogenesis is caused by disruption of basal body anchoring to the microtubules. Over-expressed INF1 also induces cilia elongation, likely by interfering with disassembly. EB1 is known to act at the basal body as well as inside the cilia, likely at the ciliary tip, binding and stabilizing microtubules (Schroder et al., 2011). This suggests a second model for the role of INF1 in ciliogenesis. Once assembly has begun INF1 may work with EB1 to promote axonemal extension by stabilizing the MTs and inhibiting disassembly of the axoneme (Figure 4.2).

The EB1 related protein, EB3 is also implicated in promotion of ciliogenesis likely facilitating vesicular trafficking to the base of the cilia, however EB3 is not present on the BioID SILAC AP/MS hit list (Schroder et al., 2011). In contrast, EB2 is an intermediate hit with 5 unique peptides, and a heavy-to-light ratio of 10.8, however, it has been identified as a BioID contaminant (Lambert et al., 2015). EB1 and EB2 interact with

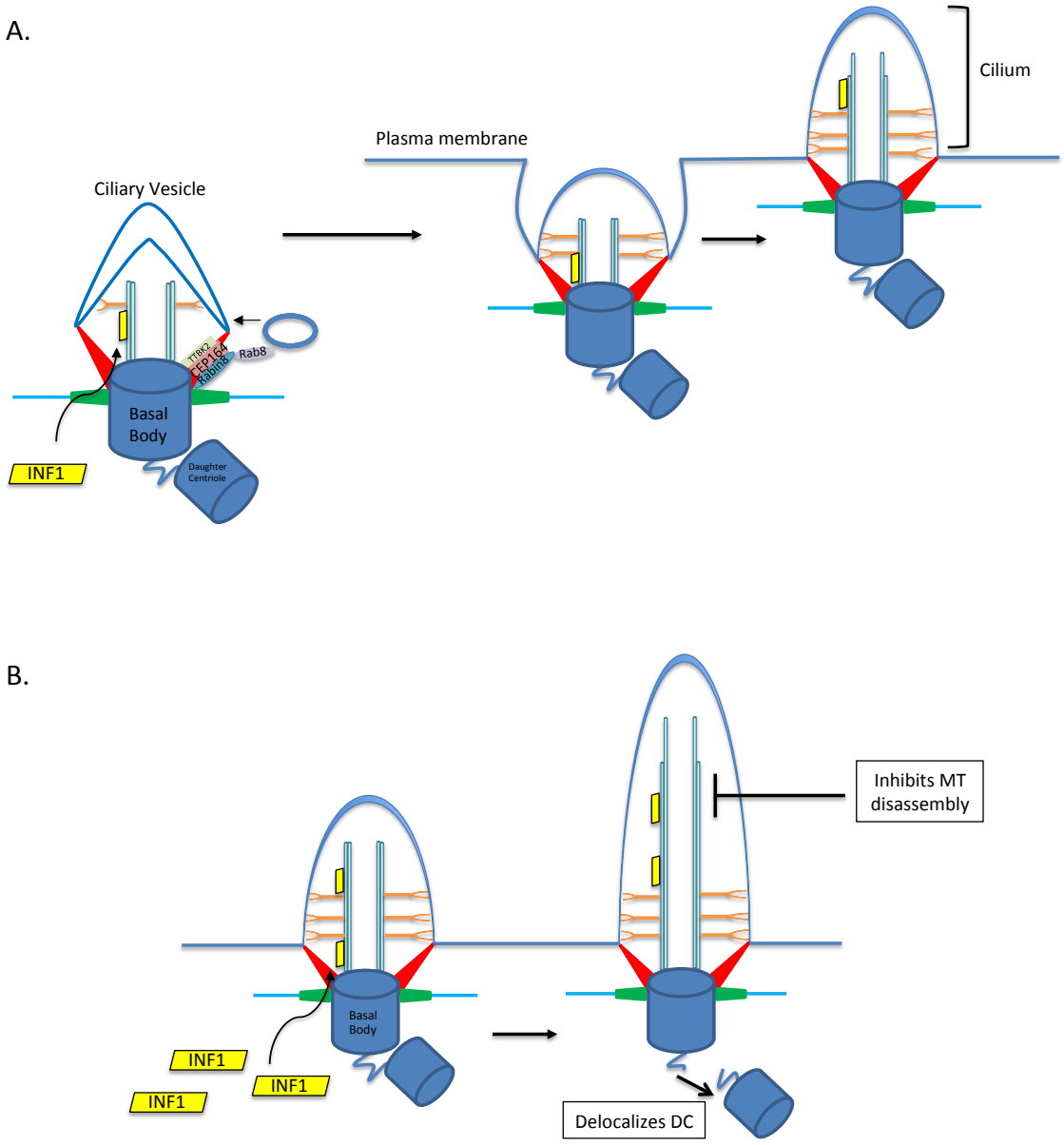

Adapted from Wei et al, Current Opinions Cell Biology, 2015

Figure 4.2. INF1 over-expression induces cilia elongation.
(A) INF1 enters the ciliary compartment and functions to bind and stabilize microtubules to promote axoneme elongation and generation of the cilium. (B) INF1 over-expression increases microtubule binding and stabilization inhibiting axonemal disassembly, severing the link between mother and daughter centrioles, and generating elongated cilia.

formins as part of their normal function, however, with opposite effects (Wen et al., 2004; Goldspink et al., 2013). EB1 cooperates with formins in MT-binding and stabilization while EB2 antagonizes this effect. It would be interesting to validate EB2 using the BioID pull-down technique and observe the effects of EB1 and EB2 expression on INF1-induced microtubule acetylation and stabilization.

4.5 INF1 Interacts with Trafficking-Associated Small GTPases

Arf1 was identified and validated as an INF1 proximity interacting protein. Interestingly, endogenous INF1 and Arf1 both localize to the cis-Golgi (Honda et al., 2005; Copeland et al., 2015). Arf1 promotes actin assembly and facilitates Arp2/3 complex-dependent actin polymerization necessary for assembly and release of transport vesicles from the Golgi (Heuvingh et al., 2007; Fucini et al., 2000). In future work it will be of interest to investigate Arf1-mediated recruitment of INF1 to the Golgi.

An unexpected validation is the proximity interaction between INF1 and Rab5A. Rab5A is primarily associated with early endosomes and currently there is no link between INF1 and recycling (Zhang et al., 2011). This validation may allude to a new function of INF1 in the endosomal-lysosomal pathway. A role for INF1 and Rab5A interaction may exist in the recycling of ciliary turnover products, such as inactive receptors, for degradation in the cytoplasm (Chen et al., 2009; Huang et al., 2009).

We were unable to validate the proximity interaction between INF1 and many small GTPases. Some, but not all, of these small GTPases are known agarose bead proteome contaminants (Trinkle-Mulcahy et al., 2008). The small GTPases may be

background, or the GFP tag may have interfered with the proximity interaction or the manner in which the POI folded. To fully explore the INF1 proximity interaction with these small GTPases a different tag or terminal location of the tag should be investigated using the BioID pull-down technique. It would also be beneficial to investigate the interaction between BirA*-INF1 and the endogenous proteins of interest.

4.6 Future Directions:

The work presented in this thesis identifies numerous INF1 proximity interacting proteins using BioID and SILAC-based quantitative AP/MS. The screen may be repeated in triplicate to lend confidence to the identified INF1 proximity interacting partners. The biotinylated proteins from the eluate of the BirA*-FL INF1 AP may also be separated using SDS-PAGE, blotted, and probed with antibodies corresponding to the endogenous proteins identified by the screen. To complement the BioID and SILAC-based quantitative AP/MS visualization of the protein-protein interaction between INF1 and the proximal interacting partners may be observed in living cells using Bimolecular fluorescence complementation (BiFC) assays.

It will also be of interest to observe the affects of depleted INF1 expression on the subcellular localization of the identified proximity interacting proteins. This may be observed using CRISPR knockout of INF1 and IFM staining for the endogenous proteins identified by the screen.

4.7 Conclusion

The validation of the cilia and centrosome associated proteins, Cep170, EB1, SNAP29, and Arl2, as INF1 proximity interaction partners, and the functional characterization of the Cep170/INF1 interaction suggests a mechanism for the effects of INF1 on ciliogenesis. These results suggest that INF1 plays a crucial role in connecting the actin and MT networks for the regulated assembly of the primary cilium by anchoring the basal body to the cytoplasmic MT network. Understanding the role of INF1 in ciliogenesis may lead to therapeutic treatments targeting defective ciliary signaling or assembly that are prevalent causes of Ciliopathies.

References:

Anderson, R.G. (1972). The three-dimensional structure of the basal body from the rhesus monkey oviduct. J Cell Biol *54*, 246-265.

Baker, K., and Beales, P.L. (2009). Making sense of cilia in disease: the human ciliopathies. Am J Med Genet C Semin Med Genet *151C*, 281-295.

Bartolini, F., and Gundersen, G.G. (2010). Formins and microtubules. Biochim Biophys Acta *1803*, 164-173.

Barzik, M., McClain, L.M., Gupton, S.L., and Gertler, F.B. (2014). Ena/VASP regulates mDia2-initiated filopodial length, dynamics, and function. Mol Biol Cell *25*, 2604-2619.

Bisel, B., Wang, Y., Wei, J.H., Xiang, Y., Tang, D., Miron-Mendoza, M., Yoshimura, S., Nakamura, N., and Seemann, J. (2008). ERK regulates Golgi and centrosome orientation towards the leading edge through GRASP65. J Cell Biol *182*, 837-843.

Bloodgood, R.A. (1992). Directed movements of ciliary and flagellar membrane components: a review. Biol Cell *76*, 291-301.

Bornens, M. (2002). Centrosome composition and microtubule anchoring mechanisms. Curr Opin Cell Biol *14*, 25-34.

Brown, J.M., and Witman, G.B. (2014). Cilia and Diseases. Bioscience *64*, 1126-1137.

Burke, M.C., Li, F.Q., Cyge, B., Arashiro, T., Brechbuhl, H.M., Chen, X., Siller, S.S., Weiss, M.A., O'Connell, C.B., Love, D.*, et al.* (2014). Chibby promotes ciliary vesicle formation and basal body docking during airway cell differentiation. J Cell Biol *207*, 123-137.

Cajanek, L., and Nigg, E.A. (2014). Cep164 triggers ciliogenesis by recruiting Tau tubulin kinase 2 to the mother centriole. Proc Natl Acad Sci U S A *111*, E2841-2850.

Chavrier, P., Parton, R.G., Hauri, H.P., Simons, K., and Zerial, M. (1990). Localization of low molecular weight GTP binding proteins to exocytic and endocytic compartments. Cell *62*, 317-329.

Chen, P.I., Kong, C., Su, X., and Stahl, P.D. (2009). Rab5 isoforms differentially regulate the trafficking and degradation of epidermal growth factor receptors. J Biol Chem *284*, 30328-30338.

Cheng, L., and Mao, Y. (2011). mDia3-EB1-APC: A connection between kinetochores and microtubule plus ends. Commun Integr Biol *4*, 480-482.

Chesarone, M.A., DuPage, A.G., and Goode, B.L. (2010). Unleashing formins to remodel the actin and microtubule cytoskeletons. Nat Rev Mol Cell Biol *11*, 62-74.

Choi-Rhee, E., Schulman, H., and Cronan, J.E. (2004). Promiscuous protein biotinylation by Escherichia coli biotin protein ligase. Protein Sci *13*, 3043-3050.

Cole, D.G., Diener, D.R., Himelblau, A.L., Beech, P.L., Fuster, J.C., and Rosenbaum, J.L. (1998). Chlamydomonas kinesin-II-dependent intraflagellar transport (IFT): IFT particles contain proteins required for ciliary assembly in Caenorhabditis elegans sensory neurons. J Cell Biol *141*, 993-1008.

Cooper, J.A., and Sept, D. (2008). New insights into mechanism and regulation of actin capping protein. Int Rev Cell Mol Biol *267*, 183-206.

Copeland, S.J., Tenneson, C., Kulacz, W., and Copeland, J.W. (Manuscript in prep). Effects of the novel formin INF1 on ciliogenesis.

Copeland, S.J., Thurston, S.F., and Copeland, J.W. (2015). Actin and Microtubule Dependent Regulation of Golgi Morphology by FHDC1. Mol Biol Cell.

Craige, B., Tsao, C.C., Diener, D.R., Hou, Y., Lechtreck, K.F., Rosenbaum, J.L., and Witman, G.B. (2010). CEP290 tethers flagellar transition zone microtubules to the membrane and regulates flagellar protein content. J Cell Biol *190*, 927-940.

Cronan, J.E. (2005). Targeted and proximity-dependent promiscuous protein biotinylation by a mutant Escherichia coli biotin protein ligase. J Nutr Biochem *16*, 416-418.

Crouse, J.A., Lopes, V.S., Sanagustin, J.T., Keady, B.T., Williams, D.S., and Pazour, G.J. (2014). Distinct functions for IFT140 and IFT20 in opsin transport. Cytoskeleton (Hoboken) *71*, 302-310.

Czarnecki, P.G., and Shah, J.V. (2012). The ciliary transition zone: from morphology and molecules to medicine. Trends Cell Biol *22*, 201-210.

D'Souza-Schorey, C., and Chavrier, P. (2006). ARF proteins: roles in membrane traffic and beyond. Nat Rev Mol Cell Biol *7*, 347-358.

Davidson, A.E., Schwarz, N., Zelinger, L., Stern-Schneider, G., Shoemark, A., Spitzbarth, B., Gross, M., Laxer, U., Sosna, J., Sergouniotis, P.I.*, et al.* (2013). Mutations in ARL2BP, encoding ADP-ribosylation-factor-like 2 binding protein, cause autosomal-recessive retinitis pigmentosa. Am J Hum Genet *93*, 321-329.

Dentler, W. (2005). Intraflagellar transport (IFT) during assembly and disassembly of Chlamydomonas flagella. J Cell Biol *170*, 649-659.

Deretic, D., Williams, A.H., Ransom, N., Morel, V., Hargrave, P.A., and Arendt, A. (2005). Rhodopsin C terminus, the site of mutations causing retinal disease, regulates trafficking by binding to ADP-ribosylation factor 4 (ARF4). Proc Natl Acad Sci U S A *102*, 3301-3306.

Donaldson, J.G., and Jackson, C.L. (2011). ARF family G proteins and their regulators: roles in membrane transport, development and disease. Nat Rev Mol Cell Biol *12*, 362-375.

Engel, B.D., Ludington, W.B., and Marshall, W.F. (2009). Intraflagellar transport particle size scales inversely with flagellar length: revisiting the balance-point length control model. J Cell Biol *187*, 81-89.

Fliegauf, M., Benzing, T., and Omran, H. (2007). When cilia go bad: cilia defects and ciliopathies. Nat Rev Mol Cell Biol *8*, 880-893.

Follit, J.A., Tuft, R.A., Fogarty, K.E., and Pazour, G.J. (2006). The intraflagellar transport protein IFT20 is associated with the Golgi complex and is required for cilia assembly. Mol Biol Cell *17*, 3781-3792.

Fuchs, E., and Weber, K. (1994). Intermediate filaments: structure, dynamics, function, and disease. Annu Rev Biochem *63*, 345-382.

Fucini, R.V., Navarrete, A., Vadakkan, C., Lacomis, L., Erdjument-Bromage, H., Tempst, P., and Stamnes, M. (2000). Activated ADP-ribosylation factor assembles distinct pools of actin on golgi membranes. J Biol Chem *275*, 18824-18829.

Gambaryan, S., Hauser, W., Kobsar, A., Glazova, M., and Walter, U. (2001). Distribution, cellular localization, and postnatal development of VASP and Mena expression in mouse tissues. Histochem Cell Biol *116*, 535-543.

Garcia-Gonzalo, F.R., Corbit, K.C., Sirerol-Piquer, M.S., Ramaswami, G., Otto, E.A., Noriega, T.R., Seol, A.D., Robinson, J.F., Bennett, C.L., Josifova, D.J.*, et al.* (2011). A transition zone complex regulates mammalian ciliogenesis and ciliary membrane composition. Nat Genet *43*, 776-784.

Garcia-Gonzalo, F.R., and Reiter, J.F. (2012). Scoring a backstage pass: mechanisms of ciliogenesis and ciliary access. J Cell Biol *197*, 697-709.

Gillingham, A.K., and Munro, S. (2007). The small G proteins of the Arf family and their regulators. Annu Rev Cell Dev Biol *23*, 579-611.

Gilula, N.B., and Satir, P. (1972). The ciliary necklace. A ciliary membrane specialization. J Cell Biol *53*, 494-509.

Goetz, S.C., and Anderson, K.V. (2010). The primary cilium: a signalling centre during vertebrate development. Nat Rev Genet *11*, 331-344.

Goetz, S.C., Liem, K.F., Jr., and Anderson, K.V. (2012). The spinocerebellar ataxia-associated gene Tau tubulin kinase 2 controls the initiation of ciliogenesis. Cell *151*, 847-858.

Goldman, R.D., Grin, B., Mendez, M.G., and Kuczmarski, E.R. (2008). Intermediate filaments: versatile building blocks of cell structure. Curr Opin Cell Biol *20*, 28-34.

Goldspink, D.A., Gadsby, J.R., Bellett, G., Keynton, J., Tyrrell, B.J., Lund, E.K., Powell, P.P., Thomas, P., and Mogensen, M.M. (2013). The microtubule end-binding protein EB2 is a central regulator of microtubule reorganisation in apico-basal epithelial differentiation. J Cell Sci *126*, 4000-4014.

Goley, E.D., and Welch, M.D. (2006). The ARP2/3 complex: an actin nucleator comes of age. Nat Rev Mol Cell Biol *7*, 713-726.

Goode, B.L., and Eck, M.J. (2007). Mechanism and function of formins in the control of actin assembly. Annu Rev Biochem *76*, 593-627.

Graser, S., Stierhof, Y.D., Lavoie, S.B., Gassner, O.S., Lamla, S., Le Clech, M., and Nigg, E.A. (2007). Cep164, a novel centriole appendage protein required for primary cilium formation. J Cell Biol *179*, 321-330.

Greer, Y.E., Westlake, C.J., Gao, B., Bharti, K., Shiba, Y., Xavier, C.P., Pazour, G.J., Yang, Y., and Rubin, J.S. (2014). Casein kinase 1delta functions at the centrosome and Golgi to promote ciliogenesis. Mol Biol Cell *25*, 1629-1640.

Grosse, R., Copeland, J.W., Newsome, T.P., Way, M., and Treisman, R. (2003). A role for VASP in RhoA-Diaphanous signalling to actin dynamics and SRF activity. EMBO J *22*, 3050-3061.

Guarguaglini, G., Duncan, P.I., Stierhof, Y.D., Holmstrom, T., Duensing, S., and Nigg, E.A. (2005). The forkhead-associated domain protein Cep170 interacts with Polo-like kinase 1 and serves as a marker for mature centrioles. Mol Biol Cell *16*, 1095-1107.

Gurel, P.S., Hatch, A.L., and Higgs, H.N. (2014). Connecting the cytoskeleton to the endoplasmic reticulum and Golgi. Curr Biol *24*, R660-672.

Hammond, J.W., Cai, D., and Verhey, K.J. (2008). Tubulin modifications and their cellular functions. Curr Opin Cell Biol *20*, 71-76.

Hao, L., Thein, M., Brust-Mascher, I., Civelekoglu-Scholey, G., Lu, Y., Acar, S., Prevo, B., Shaham, S., and Scholey, J.M. (2011). Intraflagellar transport delivers tubulin isotypes to sensory cilium middle and distal segments. Nat Cell Biol *13*, 790-798.

Harris, E.S., Li, F., and Higgs, H.N. (2004). The mouse formin, FRLalpha, slows actin filament barbed end elongation, competes with capping protein, accelerates polymerization from monomers, and severs filaments. J Biol Chem *279*, 20076-20087.

Haycraft, C.J., Schafer, J.C., Zhang, Q., Taulman, P.D., and Yoder, B.K. (2003). Identification of CHE-13, a novel intraflagellar transport protein required for cilia formation. Exp Cell Res *284*, 251-263.

Heuvingh, J., Franco, M., Chavrier, P., and Sykes, C. (2007). ARF1-mediated actin polymerization produces movement of artificial vesicles. Proc Natl Acad Sci U S A *104*, 16928-16933.

Higgs, H.N. (2005). Formin proteins: a domain-based approach. Trends Biochem Sci *30*, 342-353.

Higgs, H.N., and Peterson, K.J. (2005). Phylogenetic analysis of the formin homology 2 domain. Mol Biol Cell *16*, 1-13.

Honda, A., Al-Awar, O.S., Hay, J.C., and Donaldson, J.G. (2005). Targeting of Arf-1 to the early Golgi by membrin, an ER-Golgi SNARE. J Cell Biol *168*, 1039-1051.

Howard, J., and Hyman, A.A. (2009). Growth, fluctuation and switching at microtubule plus ends. Nat Rev Mol Cell Biol *10*, 569-574.

Huang, K., Diener, D.R., and Rosenbaum, J.L. (2009). The ubiquitin conjugation system is involved in the disassembly of cilia and flagella. J Cell Biol *186*, 601-613.

Hubbert, C., Guardiola, A., Shao, R., Kawaguchi, Y., Ito, A., Nixon, A., Yoshida, M., Wang, X.F., and Yao, T.P. (2002). HDAC6 is a microtubule-associated deacetylase. Nature *417*, 455-458.

Hunkapiller, J., Singla, V., Seol, A., and Reiter, J.F. (2011). The ciliogenic protein Oral-Facial-Digital 1 regulates the neuronal differentiation of embryonic stem cells. Stem Cells Dev *20*, 831-841.

Hurtado, L., Caballero, C., Gavilan, M.P., Cardenas, J., Bornens, M., and Rios, R.M. (2011). Disconnecting the Golgi ribbon from the centrosome prevents directional cell migration and ciliogenesis. J Cell Biol *193*, 917-933.

Iomini, C., Li, L., Esparza, J.M., and Dutcher, S.K. (2009). Retrograde intraflagellar transport mutants identify complex A proteins with multiple genetic interactions in Chlamydomonas reinhardtii. Genetics *183*, 885-896.

Ishikawa, H., and Marshall, W.F. (2011). Ciliogenesis: building the cell's antenna. Nat Rev Mol Cell Biol *12*, 222-234.

Jenkins, P.M., McEwen, D.P., and Martens, J.R. (2009). Olfactory cilia: linking sensory cilia function and human disease. Chem Senses *34*, 451-464.

Jin, H., White, S.R., Shida, T., Schulz, S., Aguiar, M., Gygi, S.P., Bazan, J.F., and Nachury, M.V. (2010). The conserved Bardet-Biedl syndrome proteins assemble a coat that traffics membrane proteins to cilia. Cell *141*, 1208-1219.

Johnson, K.A., and Rosenbaum, J.L. (1992). Polarity of flagellar assembly in Chlamydomonas. J Cell Biol *119*, 1605-1611.

Jones, J., Bentas, W., Blaheta, R.A., Makarevic, J., Hudak, L., Wedel, S., Probst, M., Jonas, D., and Juengel, E. (2008). Modulation of adhesion and growth of colon and pancreatic cancer cells by the histone deacetylase inhibitor valproic acid. Int J Mol Med *22*, 293-299.

Joo, K., Kim, C.G., Lee, M.S., Moon, H.Y., Lee, S.H., Kim, M.J., Kweon, H.S., Park, W.Y., Kim, C.H., Gleeson, J.G*., et al.* (2013). CCDC41 is required for ciliary vesicle docking to the mother centriole. Proc Natl Acad Sci U S A *110*, 5987-5992.

Kim, D.I., Birendra, K.C., Zhu, W., Motamedchaboki, K., Doye, V., and Roux, K.J. (2014). Probing nuclear pore complex architecture with proximity-dependent biotinylation. Proc Natl Acad Sci U S A *111*, E2453-2461.

Kinzel, D., Boldt, K., Davis, E.E., Burtscher, I., Trumbach, D., Diplas, B., Attie-Bitach, T., Wurst, W., Katsanis, N., Ueffing, M.*, et al.* (2010). Pitchfork regulates primary cilia disassembly and left-right asymmetry. Dev Cell *19*, 66-77.

Kodani, A., Kristensen, I., Huang, L., and Sutterlin, C. (2009). GM130-dependent control of Cdc42 activity at the Golgi regulates centrosome organization. Mol Biol Cell *20*, 1192-1200.

Kodani, A., Salome Sirerol-Piquer, M., Seol, A., Garcia-Verdugo, J.M., and Reiter, J.F. (2013). Kif3a interacts with Dynactin subunit p150 Glued to organize centriole subdistal appendages. EMBO J *32*, 597-607.

Kodani, A., and Sutterlin, C. (2009). A new function for an old organelle: microtubule nucleation at the Golgi apparatus. EMBO J *28*, 995-996.

Kovar, D.R. (2006). Molecular details of formin-mediated actin assembly. Curr Opin Cell Biol *18*, 11-17.

Kovar, D.R., Harris, E.S., Mahaffy, R., Higgs, H.N., and Pollard, T.D. (2006). Control of the assembly of ATP- and ADP-actin by formins and profilin. Cell *124*, 423-435.

Kwiatkowski, D.J., Aklog, L., Ledbetter, D.H., and Morton, C.C. (1990). Identification of the functional profilin gene, its localization to chromosome subband 17p13.3, and demonstration of its deletion in some patients with Miller-Dieker syndrome. Am J Hum Genet *46*, 559-567.

Lambert, J.P., Tucholska, M., Go, C., Knight, J.D., and Gingras, A.C. (2015). Proximity biotinylation and affinity purification are complementary approaches for the interactome mapping of chromatin-associated protein complexes. J Proteomics *118*, 81-94.

Lechtreck, K.F., Johnson, E.C., Sakai, T., Cochran, D., Ballif, B.A., Rush, J., Pazour, G.J., Ikebe, M., and Witman, G.B. (2009). The Chlamydomonas reinhardtii BBSome is an IFT cargo required for export of specific signaling proteins from flagella. J Cell Biol *187*, 1117-1132.

Lee, K.H., Johmura, Y., Yu, L.R., Park, J.E., Gao, Y., Bang, J.K., Zhou, M., Veenstra, T.D., Yeon Kim, B., and Lee, K.S. (2012). Identification of a novel Wnt5a-CK1varepsilon-Dvl2-Plk1-mediated primary cilia disassembly pathway. EMBO J *31*, 3104-3117.

Loktev, A.V., Zhang, Q., Beck, J.S., Searby, C.C., Scheetz, T.E., Bazan, J.F., Slusarski, D.C., Sheffield, V.C., Jackson, P.K., and Nachury, M.V. (2008). A BBSome subunit links ciliogenesis, microtubule stability, and acetylation. Dev Cell *15*, 854-865.

Louie, R.K., Bahmanyar, S., Siemers, K.A., Votin, V., Chang, P., Stearns, T., Nelson, W.J., and Barth, A.I. (2004). Adenomatous polyposis coli and EB1 localize in close proximity of the mother centriole and EB1 is a functional component of centrosomes. J Cell Sci *117*, 1117-1128.

Lowery, J., Kuczmarski, E.R., Herrmann, H., and Goldman, R.D. (2015). Intermediate Filaments Play a Pivotal Role in Regulating Cell Architecture and Function. J Biol Chem *290*, 17145-17153.

Lu, Q., Insinna, C., Ott, C., Stauffer, J., Pintado, P.A., Rahajeng, J., Baxa, U., Walia, V., Cuenca, A., Hwang, Y.S.*, et al.* (2015). Early steps in primary cilium assembly require EHD1/EHD3-dependent ciliary vesicle formation. Nat Cell Biol *17*, 228-240.

Luders, J., and Stearns, T. (2007). Microtubule-organizing centres: a re-evaluation. Nat Rev Mol Cell Biol *8*, 161-167.

Manolea, F., Chun, J., Chen, D.W., Clarke, I., Summerfeldt, N., Dacks, J.B., and Melancon, P. (2010). Arf3 is activated uniquely at the trans-Golgi network by brefeldin A-inhibited guanine nucleotide exchange factors. Mol Biol Cell *21*, 1836-1849.

Miller, P.M., Folkmann, A.W., Maia, A.R., Efimova, N., Efimov, A., and Kaverina, I. (2009). Golgi-derived CLASP-dependent microtubules control Golgi organization and polarized trafficking in motile cells. Nat Cell Biol *11*, 1069-1080.

Molla-Herman, A., Ghossoub, R., Blisnick, T., Meunier, A., Serres, C., Silbermann, F., Emmerson, C., Romeo, K., Bourdoncle, P., Schmitt, A.*, et al.* (2010). The ciliary pocket: an endocytic membrane domain at the base of primary and motile cilia. J Cell Sci *123*, 1785-1795.

Moseley, J.B., Sagot, I., Manning, A.L., Xu, Y., Eck, M.J., Pellman, D., and Goode, B.L. (2004). A conserved mechanism for Bni1- and mDia1-induced actin assembly and dual regulation of Bni1 by Bud6 and profilin. Mol Biol Cell *15*, 896-907.

Mukhopadhyay, S., Lu, Y., Qin, H., Lanjuin, A., Shaham, S., and Sengupta, P. (2007). Distinct IFT mechanisms contribute to the generation of ciliary structural diversity in C. elegans. EMBO J *26*, 2966-2980.

Nachury, M.V., Loktev, A.V., Zhang, Q., Westlake, C.J., Peranen, J., Merdes, A., Slusarski, D.C., Scheller, R.H., Bazan, J.F., Sheffield, V.C.*, et al.* (2007). A core complex of BBS proteins cooperates with the GTPase Rab8 to promote ciliary membrane biogenesis. Cell *129*, 1201-1213.

Nagae, S., Meng, W., and Takeichi, M. (2013). Non-centrosomal microtubules regulate F-actin organization through the suppression of GEF-H1 activity. Genes Cells *18*, 387-396.

Nigg, E.A., and Raff, J.W. (2009). Centrioles, centrosomes, and cilia in health and disease. Cell *139*, 663-678.

Nigg, E.A., and Stearns, T. (2011). The centrosome cycle: Centriole biogenesis, duplication and inherent asymmetries. Nat Cell Biol *13*, 1154-1160.

Paintrand, M., Moudjou, M., Delacroix, H., and Bornens, M. (1992). Centrosome organization and centriole architecture: their sensitivity to divalent cations. J Struct Biol *108*, 107-128.

Palazzo, A.F., Joseph, H.L., Chen, Y.J., Dujardin, D.L., Alberts, A.S., Pfister, K.K., Vallee, R.B., and Gundersen, G.G. (2001). Cdc42, dynein, and dynactin regulate MTOC reorientation independent of Rho-regulated microtubule stabilization. Curr Biol *11*, 1536-1541.

Pan, J., Wang, Q., and Snell, W.J. (2004). An aurora kinase is essential for flagellar disassembly in Chlamydomonas. Dev Cell *6*, 445-451.

Pan, X., Ou, G., Civelekoglu-Scholey, G., Blacque, O.E., Endres, N.F., Tao, L., Mogilner, A., Leroux, M.R., Vale, R.D., and Scholey, J.M. (2006). Mechanism of transport of IFT particles in C. elegans cilia by the concerted action of kinesin-II and OSM-3 motors. J Cell Biol *174*, 1035-1045.

Papanikou, E., and Glick, B.S. (2014). Golgi compartmentation and identity. Curr Opin Cell Biol *29*, 74-81.

Pazour, G.J., and Rosenbaum, J.L. (2002). Intraflagellar transport and cilia-dependent diseases. Trends Cell Biol *12*, 551-555.

Pedersen, L.B., and Rosenbaum, J.L. (2008). Intraflagellar transport (IFT) role in ciliary assembly, resorption and signalling. Curr Top Dev Biol *85*, 23-61.

Piperno, G., and Mead, K. (1997). Transport of a novel complex in the cytoplasmic matrix of Chlamydomonas flagella. Proc Natl Acad Sci U S A *94*, 4457-4462.

Pitaval, A., Tseng, Q., Bornens, M., and Thery, M. (2010). Cell shape and contractility regulate ciliogenesis in cell cycle-arrested cells. J Cell Biol *191*, 303-312.

Pring, M., Evangelista, M., Boone, C., Yang, C., and Zigmond, S.H. (2003). Mechanism of formin-induced nucleation of actin filaments. Biochemistry *42*, 486-496.

Pruyne, D., Evangelista, M., Yang, C., Bi, E., Zigmond, S., Bretscher, A., and Boone, C. (2002). Role of formins in actin assembly: nucleation and barbed-end association. Science *297*, 612-615.

Pugacheva, E.N., Jablonski, S.A., Hartman, T.R., Henske, E.P., and Golemis, E.A. (2007). HEF1-dependent Aurora A activation induces disassembly of the primary cilium. Cell *129*, 1351-1363.

Rapaport, D., Lugassy, Y., Sprecher, E., and Horowitz, M. (2010). Loss of SNAP29 impairs endocytic recycling and cell motility. PLoS One *5*, e9759.

Rivero, S., Cardenas, J., Bornens, M., and Rios, R.M. (2009). Microtubule nucleation at the cis-side of the Golgi apparatus requires AKAP450 and GM130. EMBO J *28*, 1016-1028.

Rohatgi, R., Milenkovic, L., and Scott, M.P. (2007). Patched1 regulates hedgehog signaling at the primary cilium. Science *317*, 372-376.

Roux, K.J. (2013). Marked by association: techniques for proximity-dependent labeling of proteins in eukaryotic cells. Cell Mol Life Sci *70*, 3657-3664.

Roux, K.J., Kim, D.I., Raida, M., and Burke, B. (2012). A promiscuous biotin ligase fusion protein identifies proximal and interacting proteins in mammalian cells. J Cell Biol *196*, 801-810.

Sagot, I., Rodal, A.A., Moseley, J., Goode, B.L., and Pellman, D. (2002). An actin nucleation mechanism mediated by Bni1 and profilin. Nat Cell Biol *4*, 626-631.

Satir, P., and Christensen, S.T. (2007). Overview of structure and function of mammalian cilia. Annu Rev Physiol *69*, 377-400.

Schirenbeck, A., Arasada, R., Bretschneider, T., Stradal, T.E., Schleicher, M., and Faix, J. (2006). The bundling activity of vasodilator-stimulated phosphoprotein is required for filopodium formation. Proc Natl Acad Sci U S A *103*, 7694-7699.

Schirenbeck, A., Bretschneider, T., Arasada, R., Schleicher, M., and Faix, J. (2005). The Diaphanous-related formin dDia2 is required for the formation and maintenance of filopodia. Nat Cell Biol *7*, 619-625.

Schroder, J.M., Larsen, J., Komarova, Y., Akhmanova, A., Thorsteinsson, R.I., Grigoriev, I., Manguso, R., Christensen, S.T., Pedersen, S.F., Geimer, S*., et al.* (2011). EB1 and EB3 promote cilia biogenesis by several centrosome-related mechanisms. J Cell Sci *124*, 2539-2551.

Signor, D., Wedaman, K.P., Rose, L.S., and Scholey, J.M. (1999). Two heteromeric kinesin complexes in chemosensory neurons and sensory cilia of Caenorhabditis elegans. Mol Biol Cell *10*, 345-360.

Sillibourne, J.E., Specht, C.G., Izeddin, I., Hurbain, I., Tran, P., Triller, A., Darzacq, X., Dahan, M., and Bornens, M. (2011). Assessing the localization of centrosomal proteins by PALM/STORM nanoscopy. Cytoskeleton (Hoboken) *68*, 619-627.

Sorokin, S. (1962). Centrioles and the formation of rudimentary cilia by fibroblasts and smooth muscle cells. J Cell Biol *15*, 363-377.

Sorokin, S.P. (1968). Reconstructions of centriole formation and ciliogenesis in mammalian lungs. J Cell Sci *3*, 207-230.

Sui, H., and Downing, K.H. (2006). Molecular architecture of axonemal microtubule doublets revealed by cryo-electron tomography. Nature *442*, 475-478.

Tanos, B.E., Yang, H.J., Soni, R., Wang, W.J., Macaluso, F.P., Asara, J.M., and Tsou, M.F. (2013). Centriole distal appendages promote membrane docking, leading to cilia initiation. Genes Dev *27*, 163-168.

Tateishi, K., Yamazaki, Y., Nishida, T., Watanabe, S., Kunimoto, K., Ishikawa, H., and Tsukita, S. (2013). Two appendages homologous between basal bodies and centrioles are formed using distinct Odf2 domains. J Cell Biol *203*, 417-425.

Thurston, S.F., Kulacz, W.A., Shaikh, S., Lee, J.M., and Copeland, J.W. (2012). The ability to induce microtubule acetylation is a general feature of formin proteins. PLoS One *7*, e48041.

Trinkle-Mulcahy, L., Boulon, S., Lam, Y.W., Urcia, R., Boisvert, F.M., Vandermoere, F., Morrice, N.A., Swift, S., Rothbauer, U., Leonhardt, H.*, et al.* (2008). Identifying specific protein interaction partners using quantitative mass spectrometry and bead proteomes. J Cell Biol *183*, 223-239.

Vinogradova, T., Paul, R., Grimaldi, A.D., Loncarek, J., Miller, P.M., Yampolsky, D., Magidson, V., Khodjakov, A., Mogilner, A., and Kaverina, I. (2012). Concerted effort of centrosomal and Golgi-derived microtubules is required for proper Golgi complex assembly but not for maintenance. Mol Biol Cell *23*, 820-833.

Wade, R.H., and Hyman, A.A. (1997). Microtubule structure and dynamics. Curr Opin Cell Biol *9*, 12-17.

Wang, C., Low, W.C., Liu, A., and Wang, B. (2013). Centrosomal protein DZIP1 regulates Hedgehog signaling by promoting cytoplasmic retention of transcription factor GLI3 and affecting ciliogenesis. J Biol Chem *288*, 29518-29529.

Wen, Y., Eng, C.H., Schmoranzer, J., Cabrera-Poch, N., Morris, E.J., Chen, M., Wallar, B.J., Alberts, A.S., and Gundersen, G.G. (2004). EB1 and APC bind to mDia to stabilize microtubules downstream of Rho and promote cell migration. Nat Cell Biol *6*, 820-830.

Wheway, G., Parry, D.A., and Johnson, C.A. (2014). The role of primary cilia in the development and disease of the retina. Organogenesis *10*, 69-85.

Williams, C.L., Li, C., Kida, K., Inglis, P.N., Mohan, S., Semenec, L., Bialas, N.J., Stupay, R.M., Chen, N., Blacque, O.E.*, et al.* (2011). MKS and NPHP modules cooperate to establish basal body/transition zone membrane associations and ciliary gate function during ciliogenesis. J Cell Biol *192*, 1023-1041.

Yadav, S., Puri, S., and Linstedt, A.D. (2009). A primary role for Golgi positioning in directed secretion, cell polarity, and wound healing. Mol Biol Cell *20*, 1728-1736.

Ye, X., Zeng, H., Ning, G., Reiter, J.F., and Liu, A. (2014). C2cd3 is critical for centriolar distal appendage assembly and ciliary vesicle docking in mammals. Proc Natl Acad Sci U S A *111*, 2164-2169.

Young, K.G., Thurston, S.F., Copeland, S., Smallwood, C., and Copeland, J.W. (2008). INF1 is a novel microtubule-associated formin. Mol Biol Cell *19*, 5168-5180.

Zhang, C., Li, A., Zhang, X., and Xiao, H. (2011). A novel TIP30 protein complex regulates EGF receptor signaling and endocytic degradation. J Biol Chem *286*, 9373-9381.

Zigmond, S.H., Evangelista, M., Boone, C., Yang, C., Dar, A.C., Sicheri, F., Forkey, J., and Pring, M. (2003). Formin leaky cap allows elongation in the presence of tight capping proteins. Curr Biol *13*, 1820-1823.

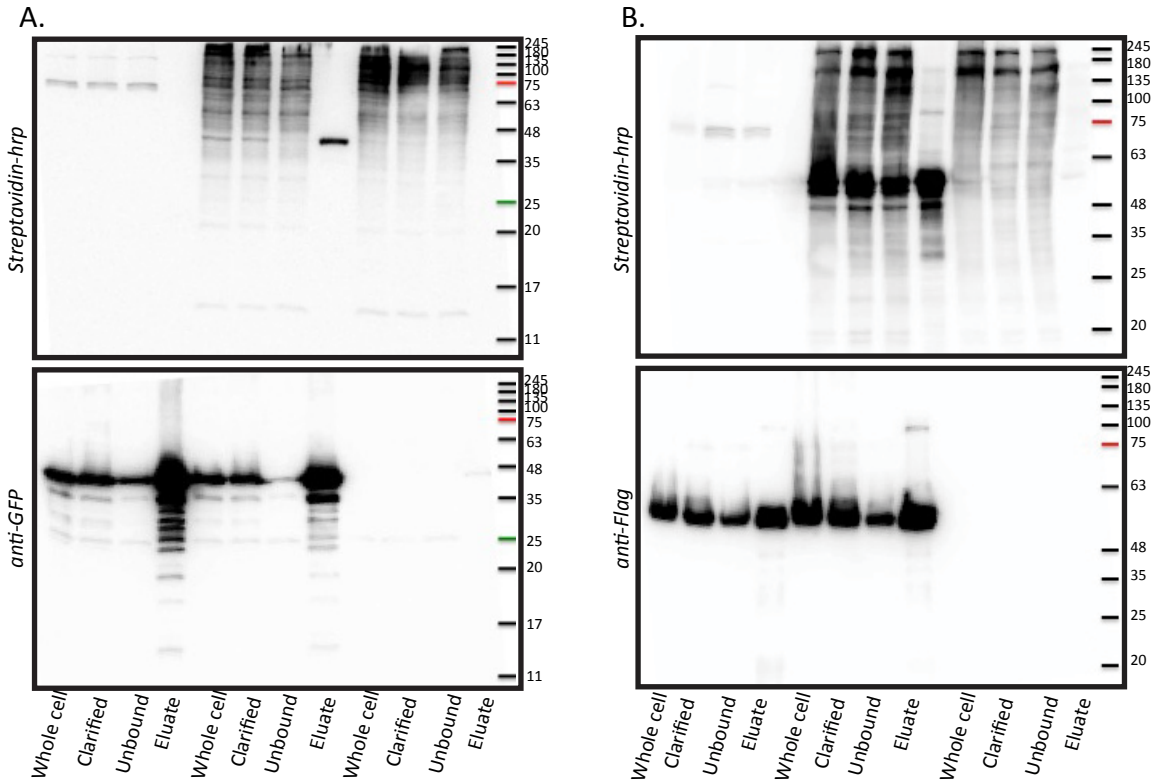

Figure A1. INF1 proximally interacts with formin-associated proteins Profilin2 & VASP. Putative INF1 interacting protein PFN2 was expressed as GFP-tagged protein in HEK-293T/17 cells with or without BirA*-INF1. BirA*-INF1 was expressed alone as an additional negative control. The transfected cells were incubated with biotin for 24hrs, the cells were lysed and the GFP/Flag-tagged proteins were affinity purified with GFP Trap beads or anti-flag affinity gel. Samples of the whole cell lysate, clarified lysate, unbound fraction, and bead eluate were subjected to SDS-PAGE and duplicate blots were probed with streptavidin-HRP (top box) or, anti-GFP or -flag (bottom box). Specific biotinylation of the GFP-tagged protein by co-expression with BirA*-INF1 confirmed the interaction between INF1 and the protein of interest. (A) Biotinylated GFP-PFN2 was detected in the eluate from GFP-PFN2/BirA*-INF1 expressing cells but not in eluates from cells expressing GFP-PFN2 or BirA*-INF1 alone. The bands below the expected 48kDa molecular weight (MW) of GFP-PFN2 were likely degradation products. (B) Flag-VASP also proximally interacted with BirA*-INF1 in this assay with an anticipated MW of 55kDa.

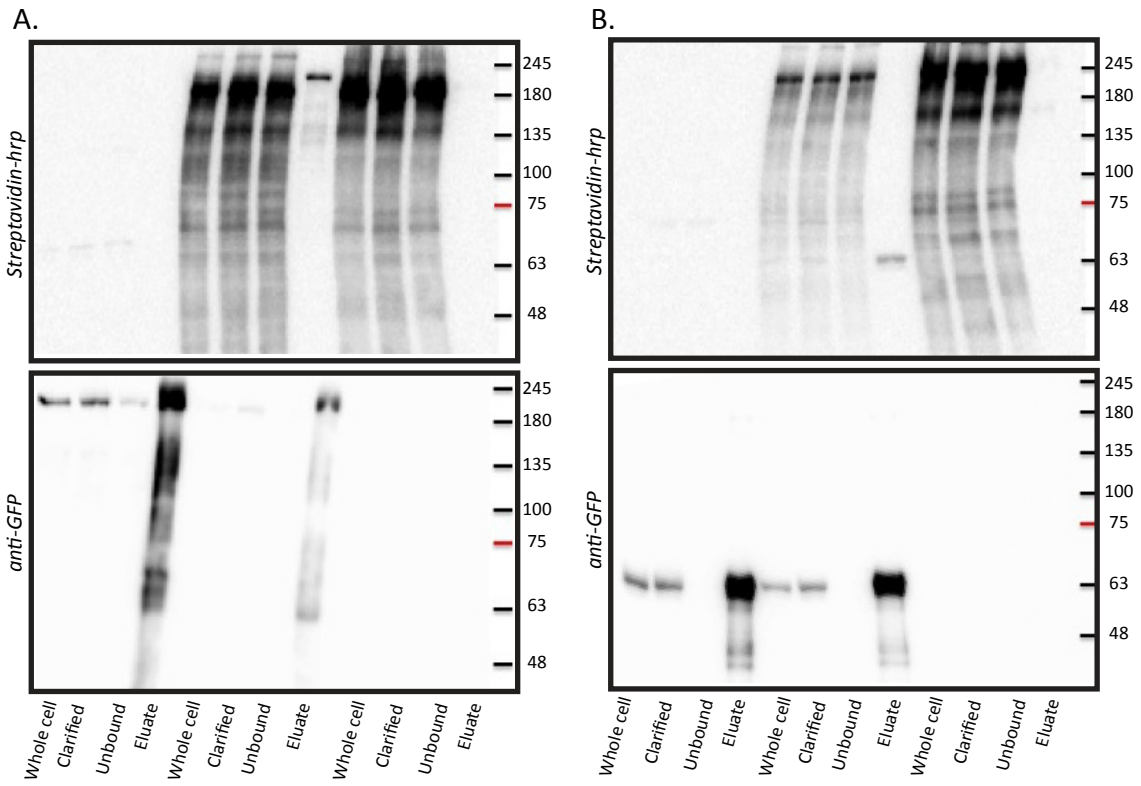

Figure A2. INF1 proximally interacts with Cep170 & EB1.
Putative INF1 interacting protein Cep170 was expressed as GFP-tagged protein in HEK-293T/17 cells with or without BirA*-INF1. BirA*-INF1 was expressed alone as an additional negative control. The transfected cells were incubated with biotin for 24hrs, the cells were lysed and the GFP-tagged proteins were affinity purified with GFP Trap beads. Samples of the whole cell lysate, clarified lysate, unbound fraction, and bead eluate were subjected to SDS-PAGE and duplicate blots were probed with streptavidin-HRP (top box) or, anti-GFP (bottom box). Specific biotinylation of the GFP-tagged protein by co-expression with BirA*-INF1 confirmed the interaction between INF1 and the protein of interest. (A) Biotinylated GFP-Cep170 was detected in the eluate from GFP-Cep170/BirA*-INF1 expressing cells but not in eluates from cells expressing GFP-Cep170 or BirA*-INF1 alone. The bands below the expected 200kDa molecular weight (MW) of GFP-Cep170 were likely degradation products. (B) GFP-EB1 also proximally interacted with BirA*-INF1 in this assay with an expected MW of 63kDa.

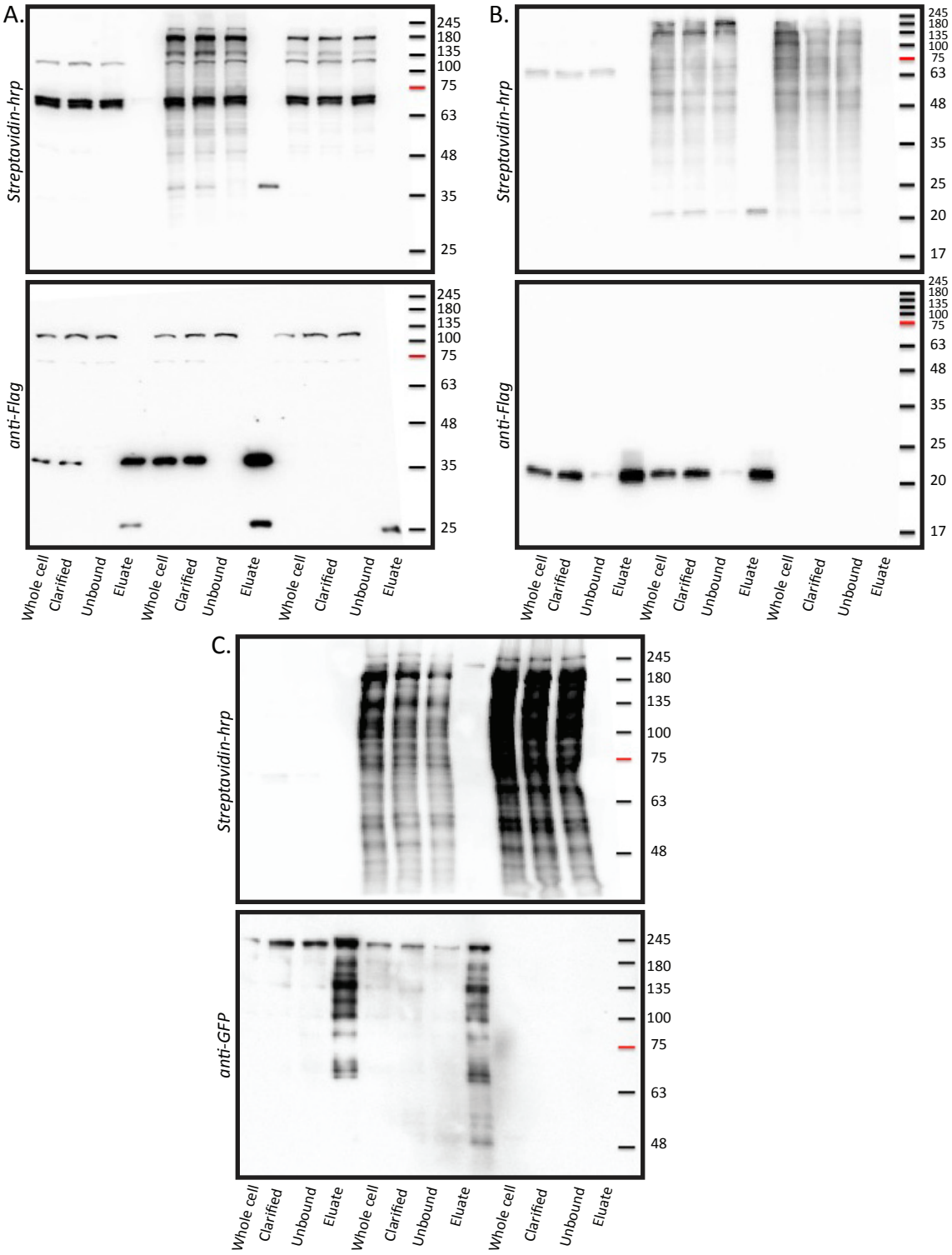

Figure A3. SNAP29, Arl2, and Cep164 proximally interact with INF1.
The interaction between BirA*-INF1 and the indicated proteins were tested as in figure A1. (A) Biotinylated flag-SNAP29, with an expected MW of 44kDa, was detected in the eluate from flag-SNAP29/BirA*-INF1 expressing cells but not in eluates from cells expressing flag-SNAP29 or BirA*-INF1 alone. (B,C) Flag-Arl2, with an expected MW of 21kDa, and GFP-Cep164 (MW 200kDa) proximally interacted with INF1 in this assay.

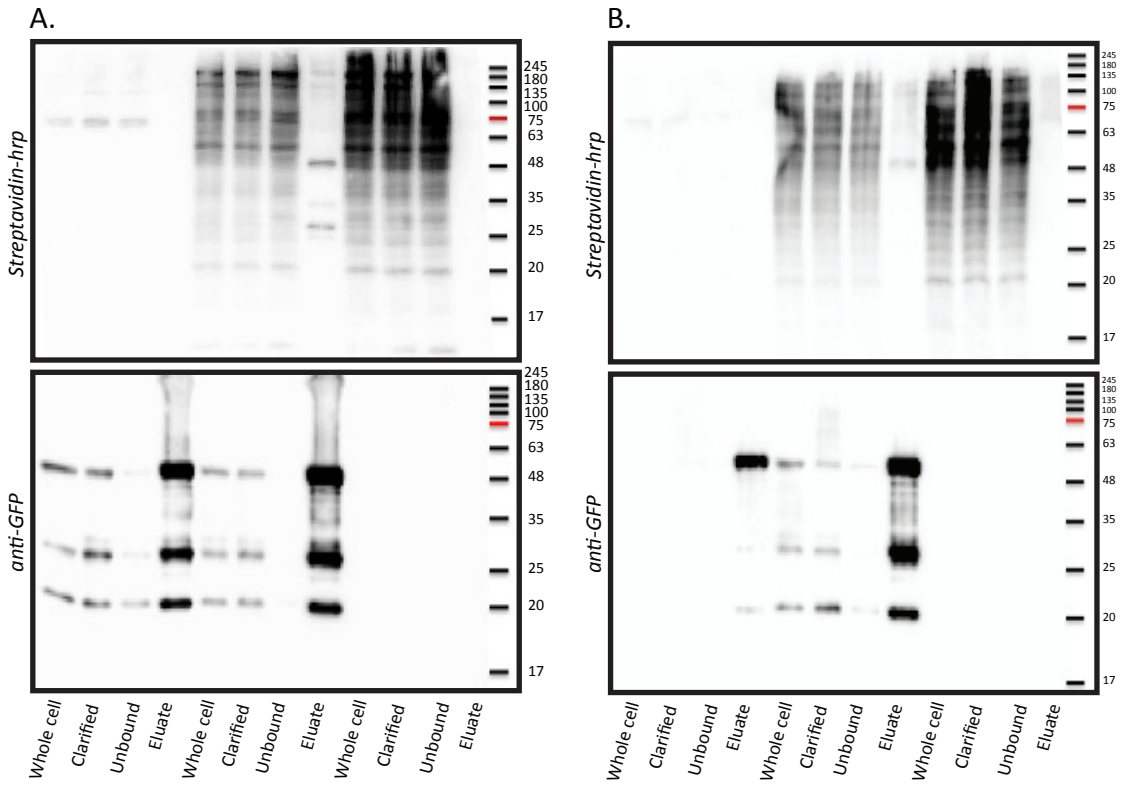

Figure A4. The small GTPase, Arf1, is an INF1 proximal interacting protein.
The interaction between BirA*-INF1 and the indicated proteins was tested as in figure A1. (A) Biotinylated GFP-Arf1 had an expected MW of 54kDa and was detected in the eluate from GFP-Arf1/BirA*-INF1 expressing cells but not in eluates from cells expressing GFP-Arf1 or BirA*-INF1 alone. (B) A faint biotinylated band was present for GFP-Arf3 with an expected MW of 54kDa.

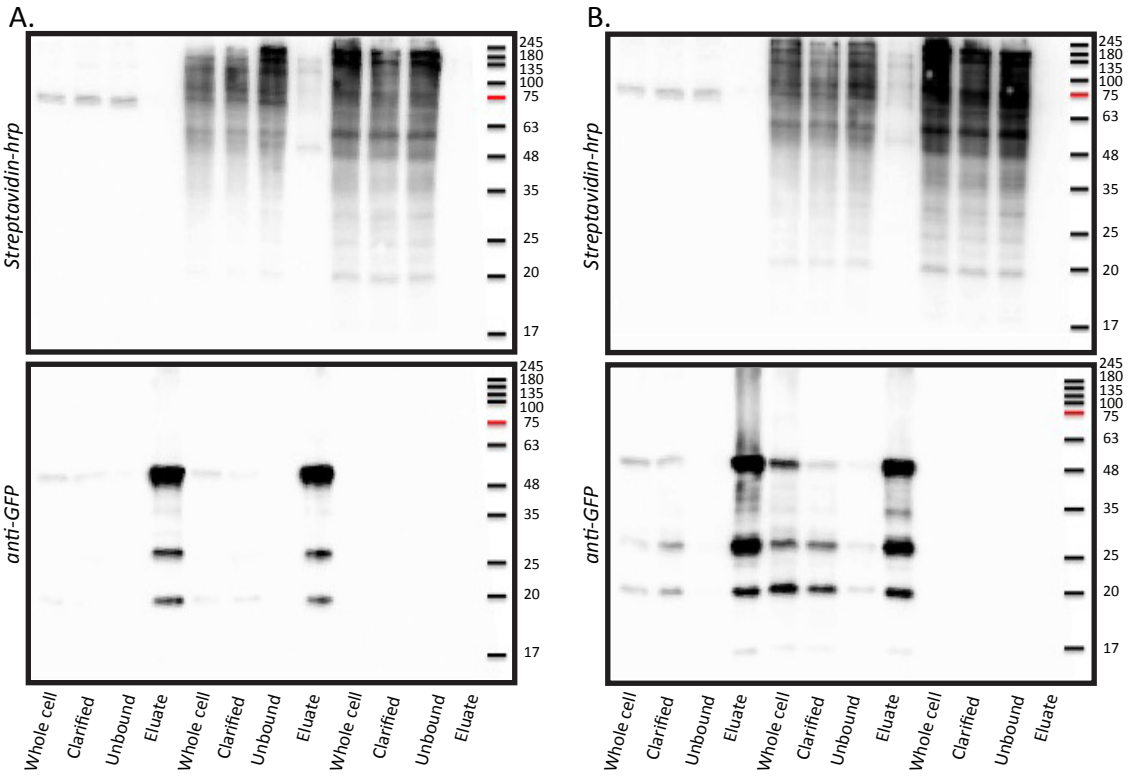

Figure A5. The small GTPases Arf4 and Arf5 are not INF1 proximal interacting proteins. The interaction between BirA*-INF1 and the indicated proteins was tested as in figure A1. (A) Weak biotinylated GFP-Arf4 was faintly detected in the eluate at the expected MW of 51kDa from GFP-Arf4/BirA*-INF1 expressing cells but not in eluates from cells expressing GFP-Arf4 or BirA*-INF1 alone. (B) A faint biotinylated band was also present for GFP-Arf5 at the anticipated MW of 51kDa in the eluate lane from GFP-Arf5/ BirA*-INF1 expressing cells.

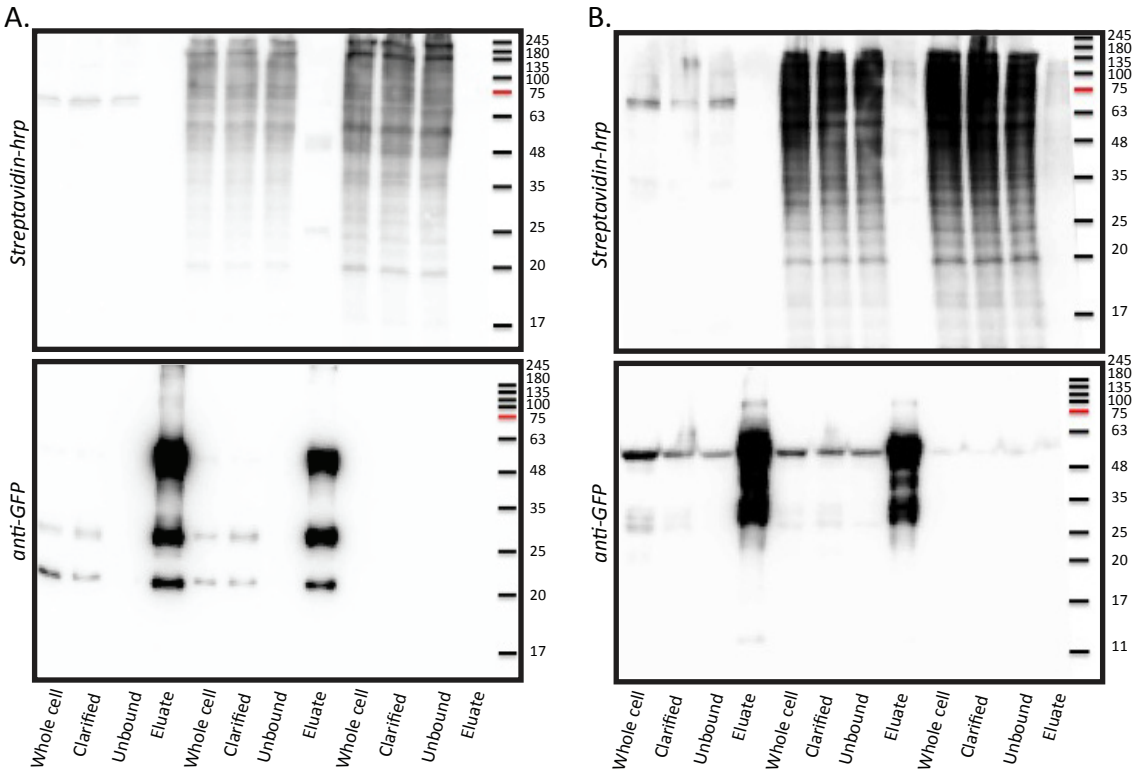

Figure A6. The small GTPase, Rab5A, is an INF1 proximal interacting protein.
The interaction between BirA*-INF1 and the indicated proteins was tested as in figure A1 (A,B) Strong positive results were obtained for GFP-Rab5A with an anticipated MW of 57kDa, while a weak band was present for GFP-Arl8A with an expected MW of 51kDa.

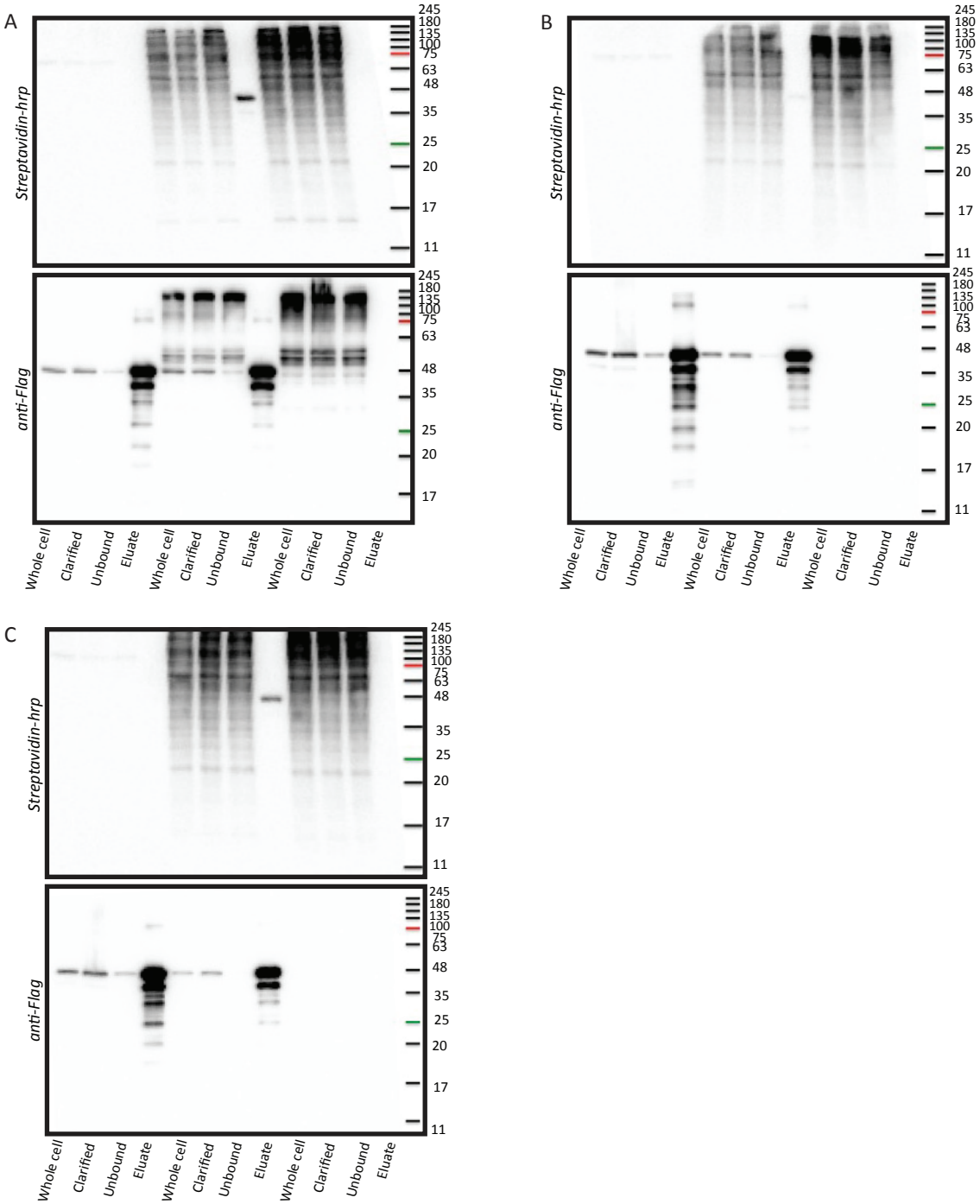

Figure A7. INF1 proximity interaction domain mapping with PFN2.
The interaction domain of BirA*-INF1 was mapped as in figure A1. Biotinylated GFP-PFN2 was detected in the eluate from GFP-PFN2/BirA*-FL INF1 (A), and -FL INF1 I180A (C), but not in the eluate of -INF1 ΔFH1 (B).

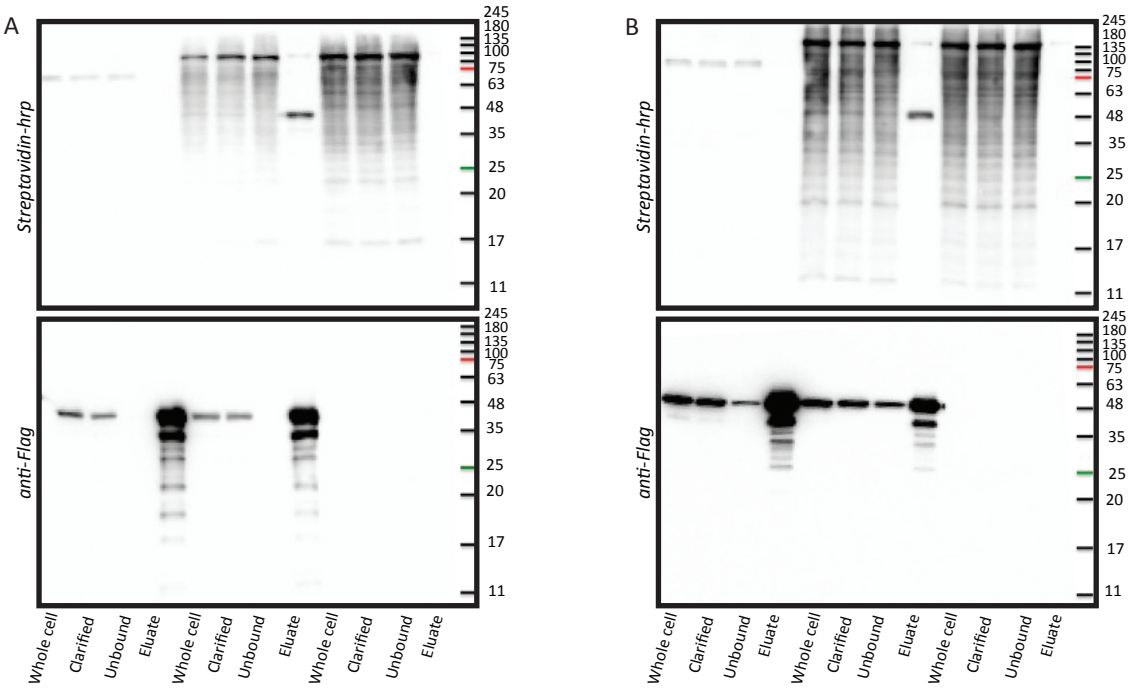

Figure A8. INF1 proximity interaction domain mapping with PFN2.
The interaction domain of BirA*-INF1 was mapped as in figure A1. Biotinylated GFP-PFN2 was detected in the eluate from GFP-PFN2/BirA*-INF1 485N (A), and -INF1 485N I180A (B).

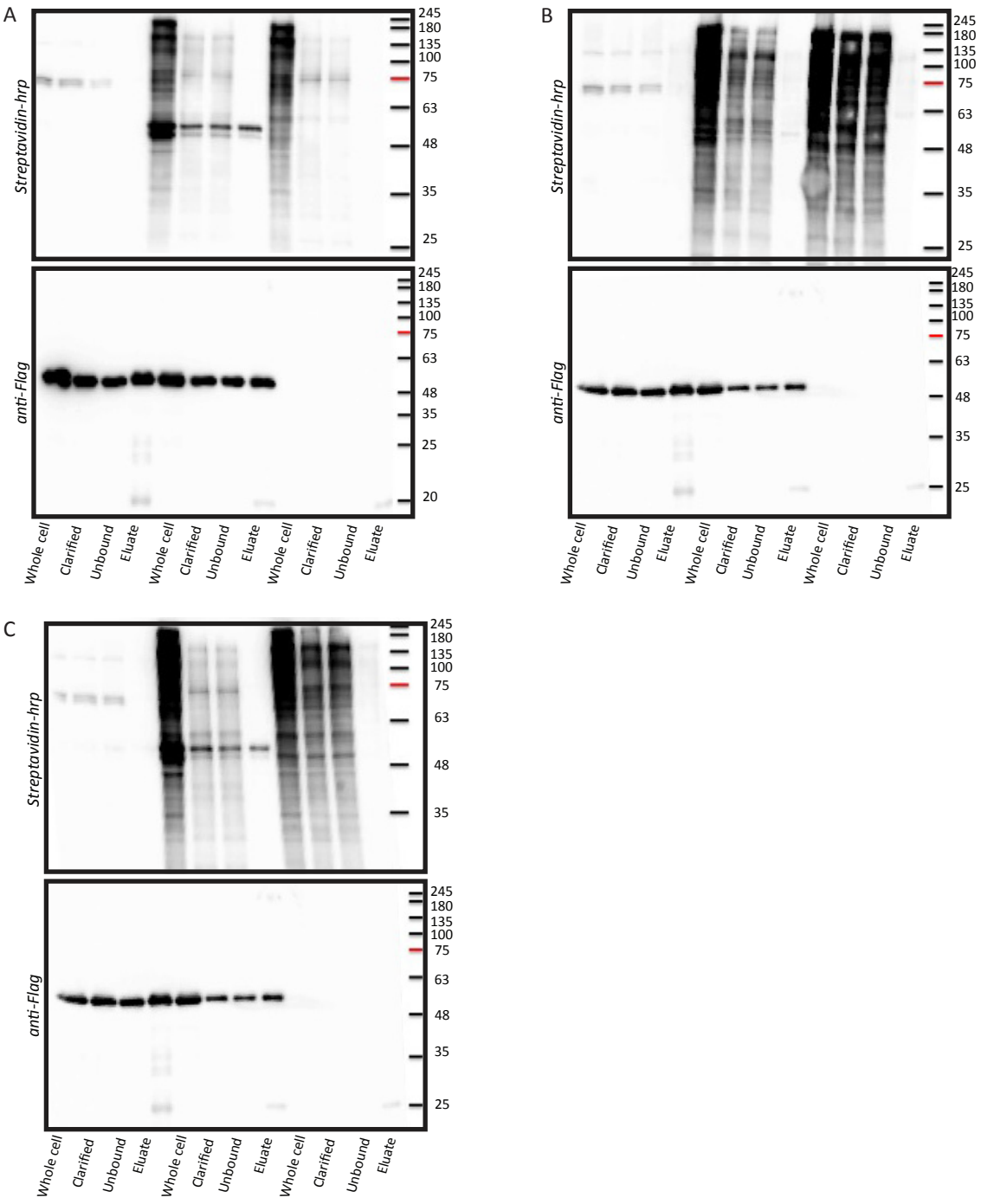

Figure A9. INF1 proximity interaction domain mapping with VASP.
The interaction domain of BirA*-INF1 was mapped as in figure A1. Biotinylated Flag-VASP was detected in the eluate from Flag-Snap29/BirA*-FL INF1 (A), -INF1 Δ FH1(B), and -FL INF1 I180A (C).

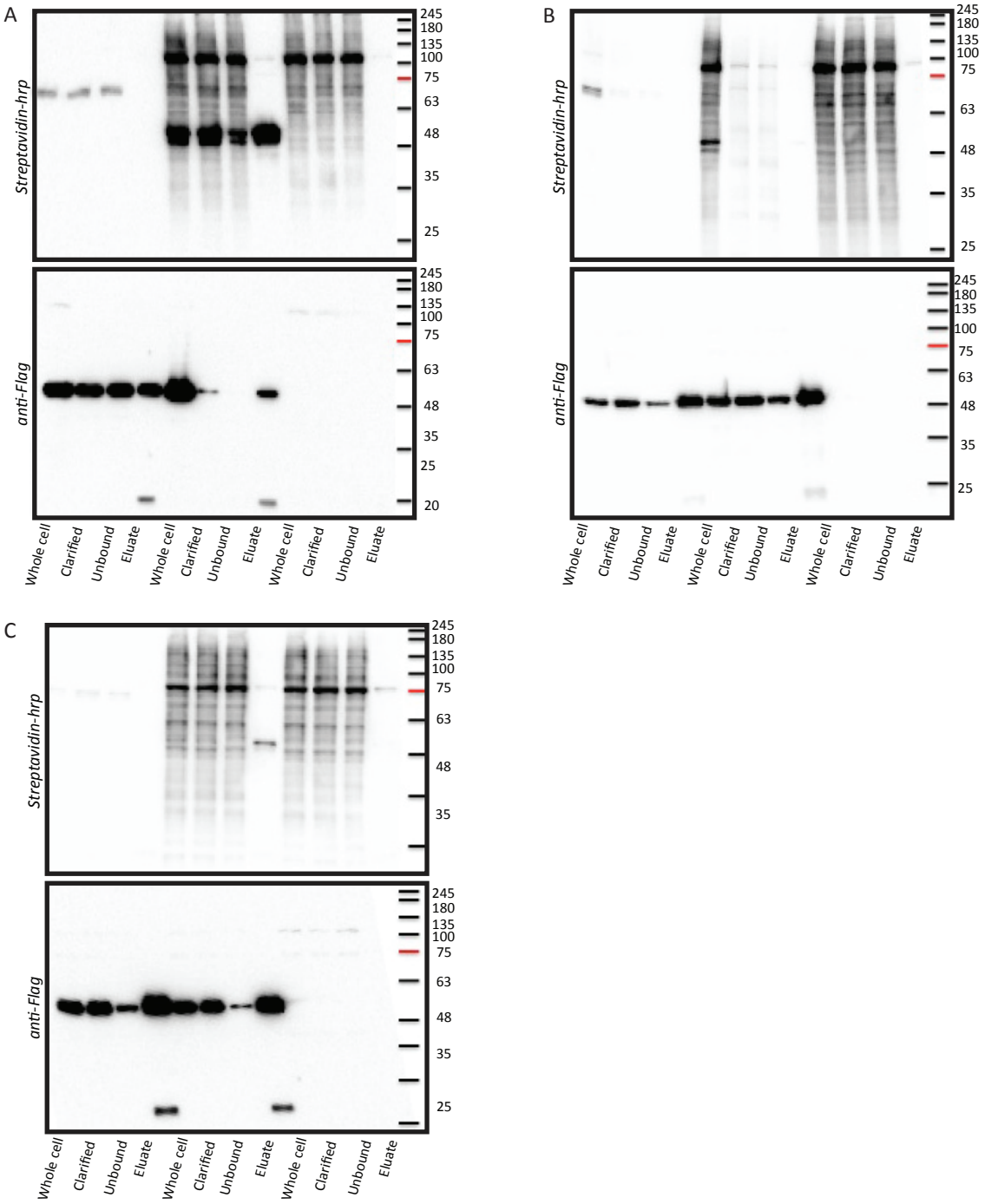

Figure A10. INF1 proximity interaction domain mapping with VASP.
The interaction domain of BirA*-INF1 was mapped as in figure A11. Biotinylated Flag-VASP was detected in the eluate from Flag-Snap29/BirA*-485N (A), -INF1 485N I180A (B), and -INF1 FH2 (C).

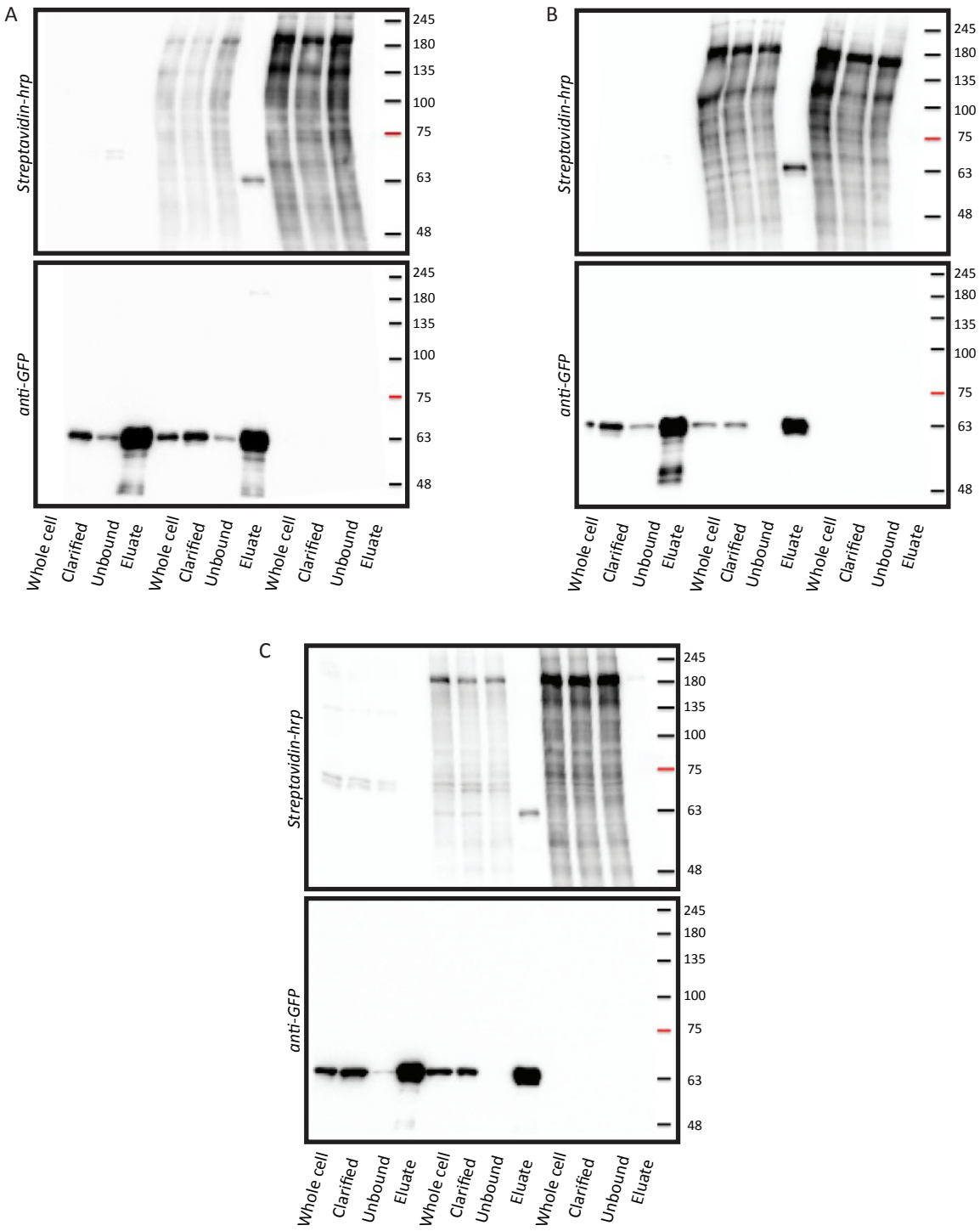

Figure A11. INF1 proximity interaction domain mapping with EB1.
The interaction domain of BirA*-INF1 was mapped as in figure A1. Biotinylated GFP-EB1 was detected in the eluate from GFP-EB1/BirA*-FL INF1 (A), -INF1 ΔFH1 (B), and -INF1 958N (C).

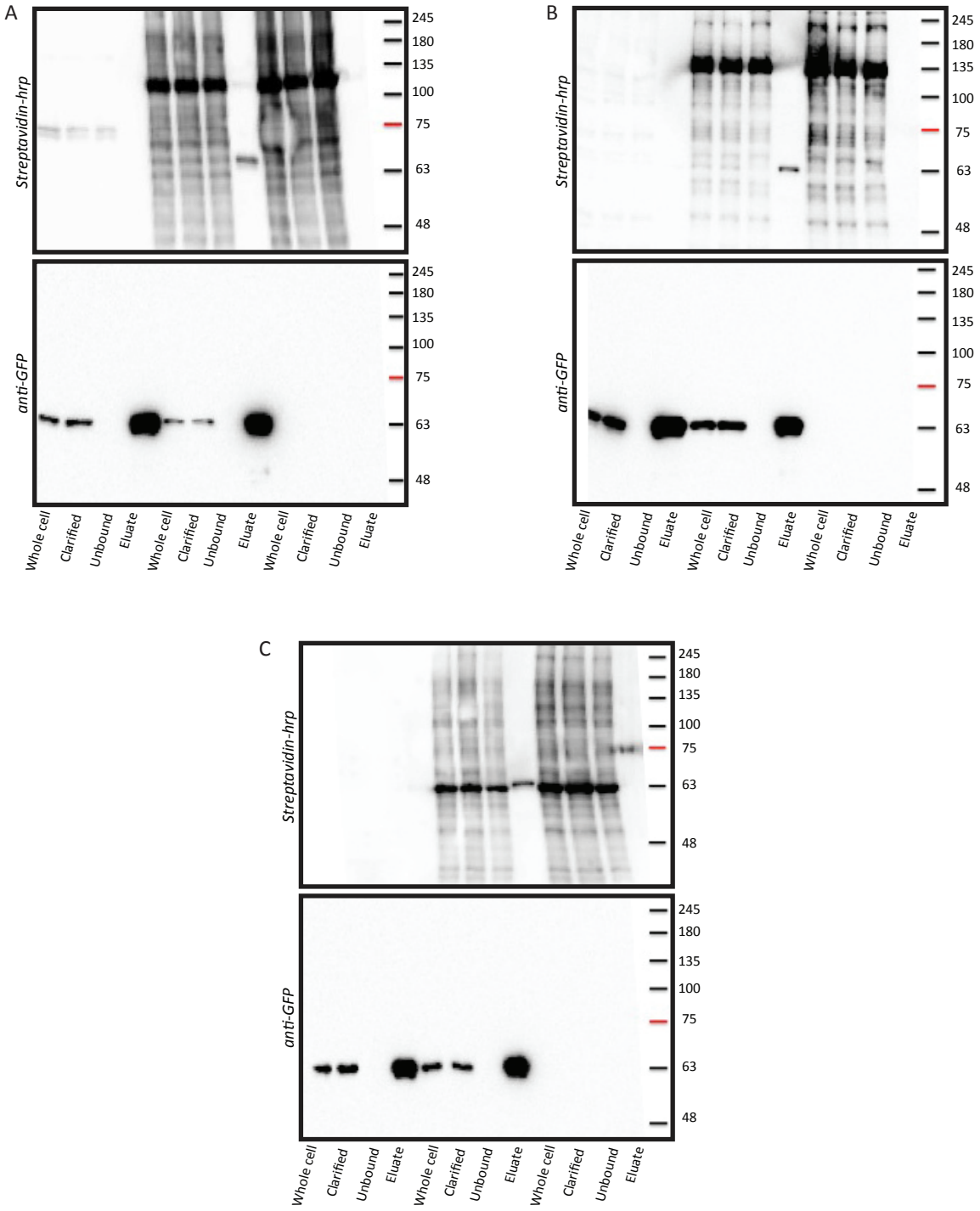

Figure A12. INF1 proximity interaction domain mapping with EB1.
The interaction domain of BirA*-INF1 was mapped as in figure A1. Biotinylated GFP-EB1 was detected in the eluate from GFP-EB1/BirA*-INF1 485N (A), -INF1 486C (B), and -INF1 958C (C).

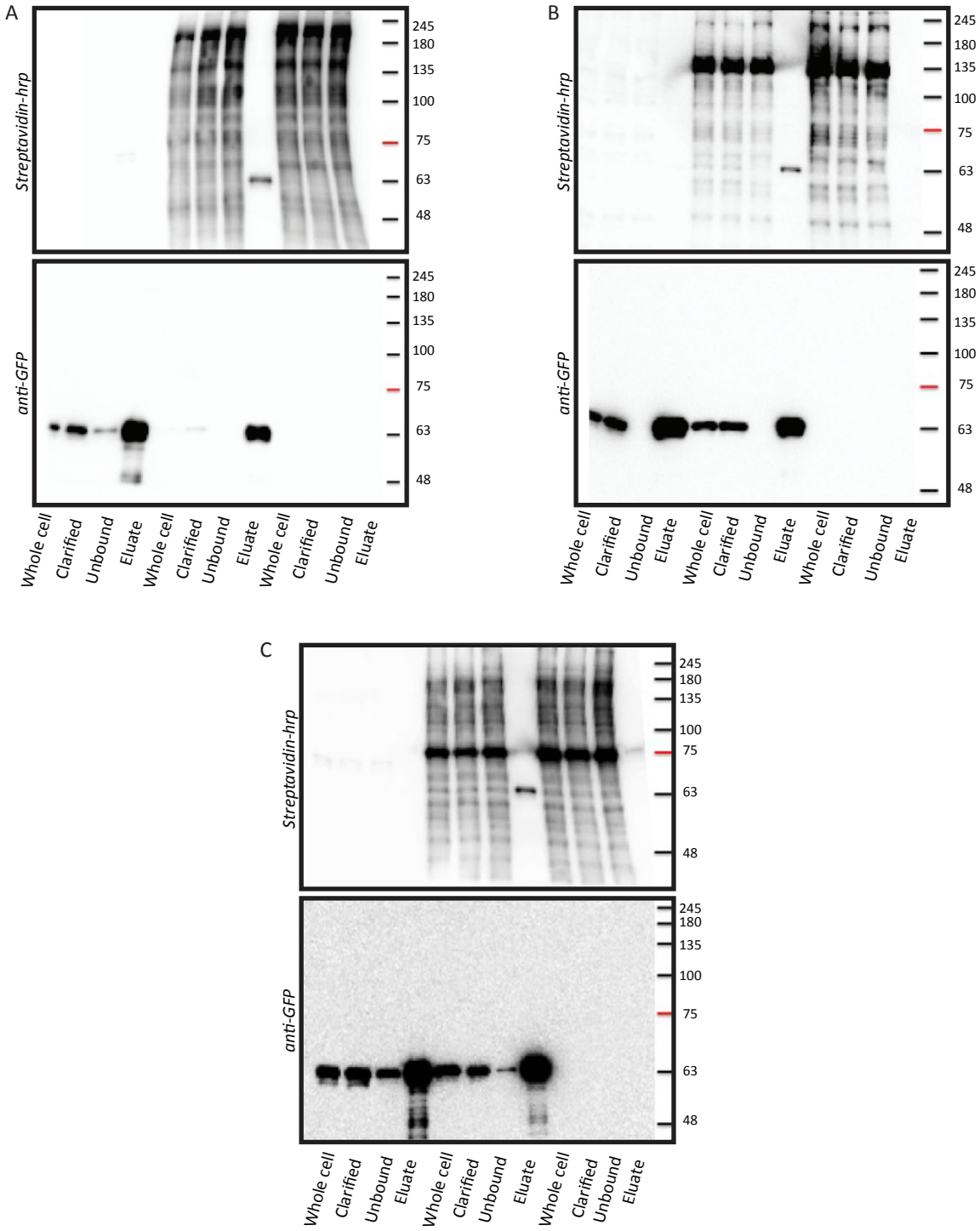

Figure A13. INF1 proximity interaction domain mapping with EB1.
The interaction domain of BirA*-INF1 was mapped as in figure A1. Biotinylated GFP-EB1 was detected in the eluate from GFP-EB1/BirA*-FL INF1 I180A (A), -INF1 485N I180A (B), and -INF1 FH2 (C).

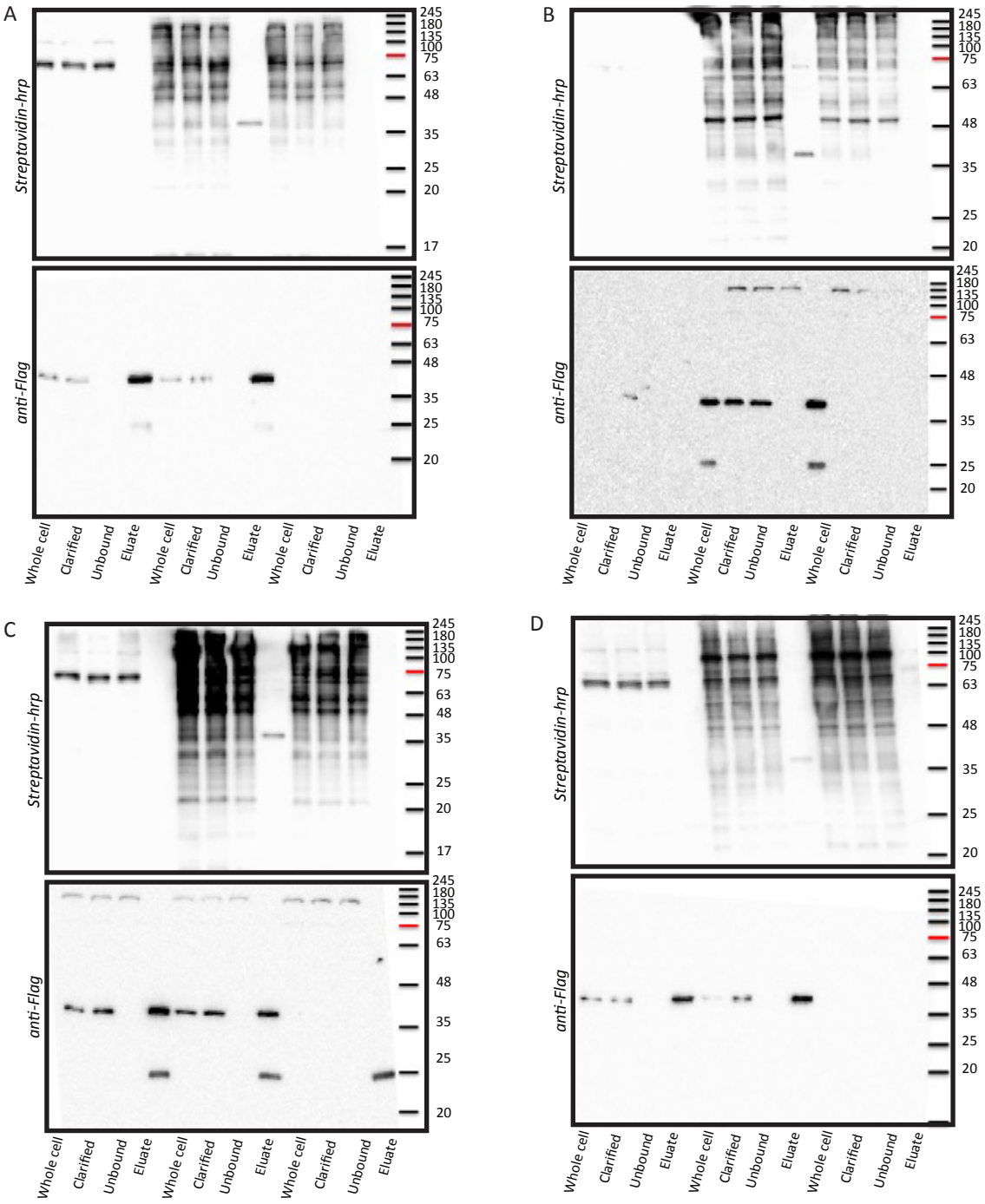

Figure A14. INF1 proximity interaction domain mapping with SNAP29.
The interaction domain of BirA*-INF1 was mapped as in figure A1. Biotinylated Flag-Snap29 was detected in the eluate from Flag-Snap29/BirA*-FL INF1 (A), -INF1 Δ FH1(B), -FL INF1 I180A (C), and -INF1 485N (D).

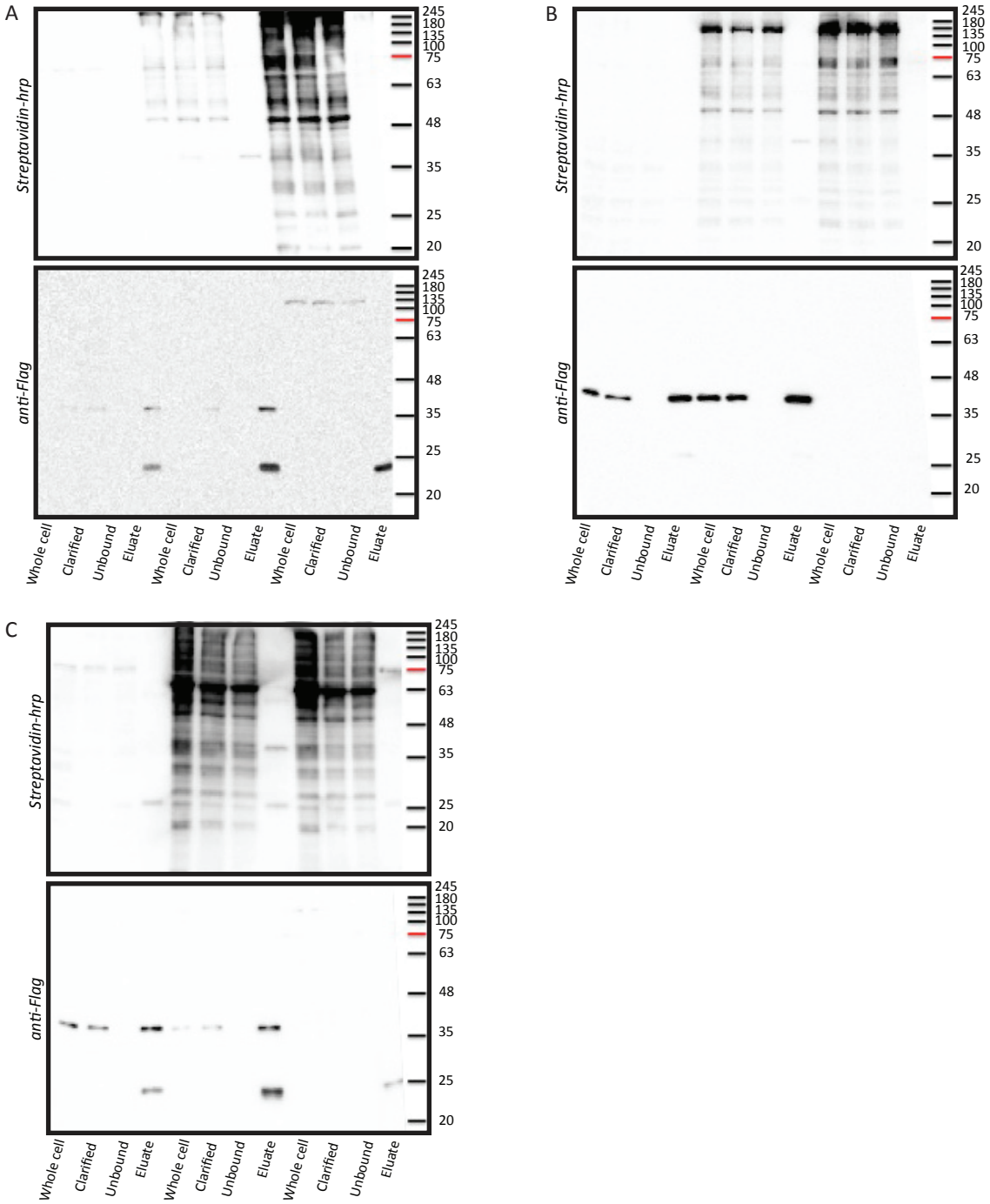

Figure A15. INF1 proximity interaction domain mapping with SNAP29.
The interaction domain of BirA*-INF1 was mapped as in figure A1. Biotinylated Flag-Snap29 was detected in the eluate from Flag-Snap29/BirA*-INF1 958N (A), -INF1 486C (B), and -INF1 958C(C).

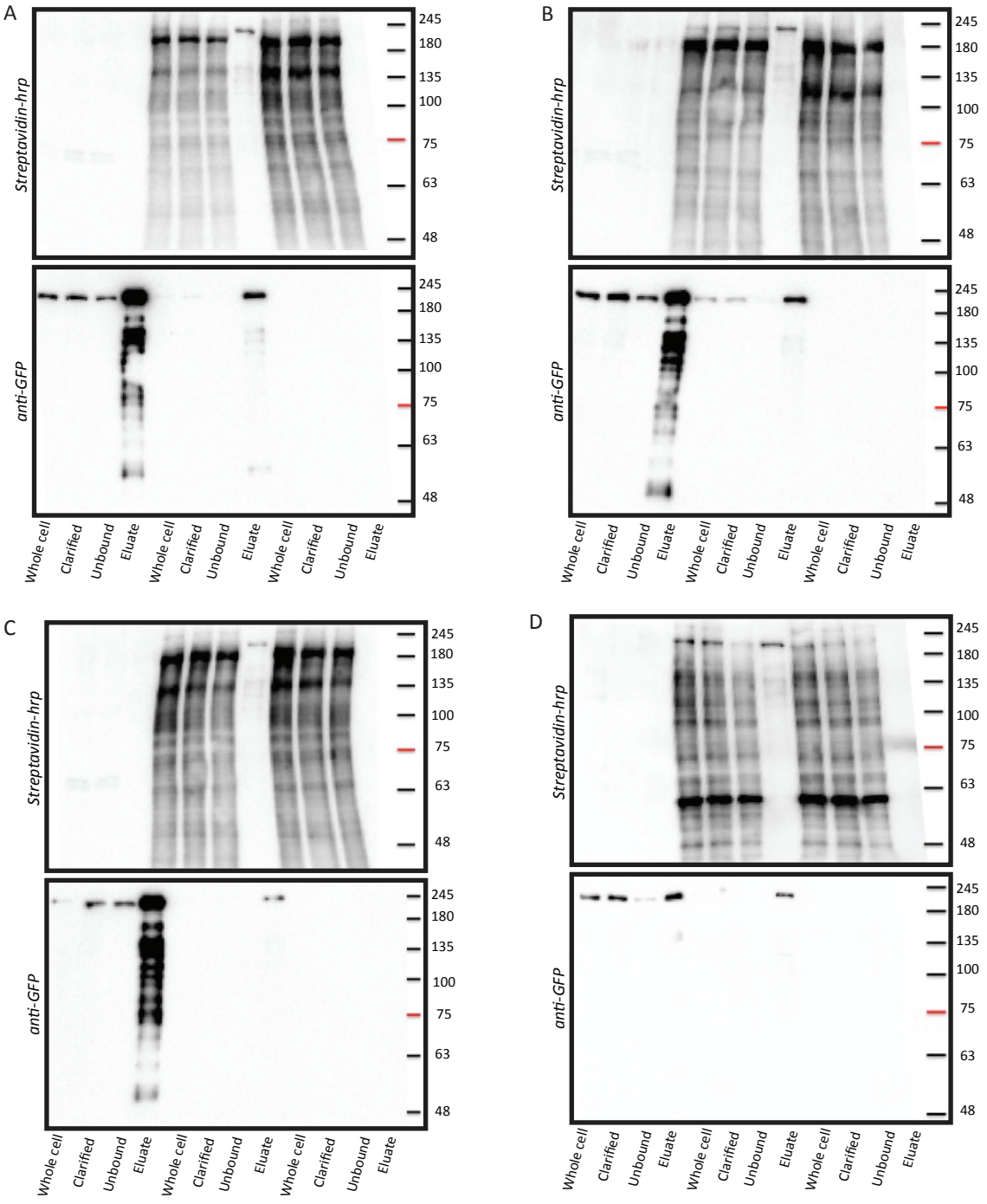

Figure A16. INF1 proximity interaction domain mapping with Cep170.
The interaction domain of BirA*-INF1 was mapped as in figure A11. Biotinylated GFP-Cep170 was detected in the eluate from GFP-EB1/BirA*-FL INF1 (A), -INF1 ΔFH1(B), -FL INF1 I180A(C), and -INF1 958C (D).

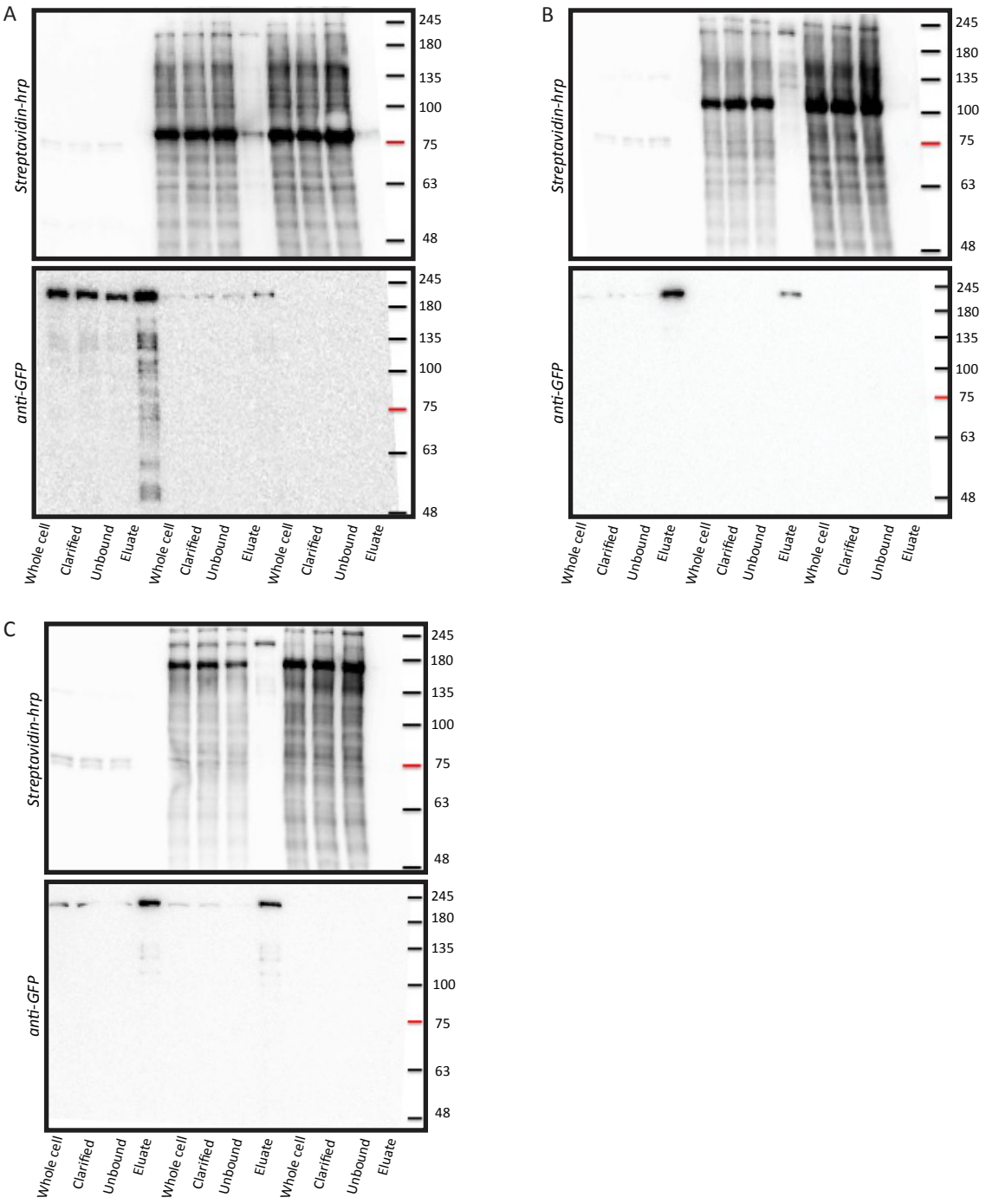

Figure A17. INF1 proximity interaction domain mapping with Cep170.
The interaction domain of BirA*-INF1 was mapped as in figure A11. Biotinylated GFP-Cep170 was detected in the eluate from GFP-EB1/BirA*-INF1 958N (A), -INF1 485N (B), and -INF1 FH2 (C).